PHYSICS REPORTS (Section C of Physics Letters) 23, No. 1 (1976) 1--121. NORTH-HOLLAND PUBLISHING COMPANY

LARGE TRANSVERSE MOMENTUM PROCESSES *

Dennis SIVERS, Stanley J. BRODSKY and Richard BLANKENBECLER

Stanford Linear Accelerator Center, Stanford University, Stanford, Calif. 94305, USA

Received 17 June 1975

Contents:

* Work supported by the U.S. Energy Research and Development Administration.

LARGE TRANSVERSE MOMENTUM PROCESSES

Dennis SIVERS, Stanley J.BRODSKY and Richard BLANKENBECLER

Stanford Linear Accelerator Center, Stanford University, Stanford, Calif. 94305, USA

NORTH-HOLLAND PUBLISHING COMPANY – AMSTERDAM

Abstract:

We present a comprehensive survey of experimental and theoretical work on large transverse momentum processes. Exclusive data and single particle inclusive measurements are summarized and some discussion of multiparticle inclusive data is included. We review many of the predictions of nonparton models including the geometrical, statistical, eikonal and bootstrap approaches. A more detailed discussion is given of the structure of models based on the hard scattering of constituents. The predictions for hadronic and electromagnetic processes based on quark counting rules and the constituent interchange model (CIM) are summarized. We present numerous comparisons with experiment and indicate the framework for the comparison with new experimental data. Recent theoretical progress in the problem of relating short distance structure of hadrons with the asymptotic behavior of form factors and fixed angle amplitudes is also reviewed. We include a brief discussion of the possible influence of new hadronic degrees of freedom on large-p_T phenomena. Finally, we attempt to anticipate the type of experiments which will prove decisive in the understanding of this subject.

1. Introduction

1.1. Large transverse momentum reactions and the structure of hadrons

It has long been known that the average hadron–hadron collision produces particles with low transverse momentum. A few years ago, early experiments at the CERN–ISR indicated that the probability of producing a particle with large transverse momentum, though quite small, is actually several orders of magnitude higher than might have been expected on the basis of a simple extrapolation of the low transverse momentum data. While these experimental results were not as dramatic as the famous Rutherford α-particle scattering experiments [205], they may have the same sort of significance. It is apparent that it is not feasible to conceive of hadronic collision processes as occurring between structureless matter distributions, but that there is an effective nonuniformity characterized by a small distance scale or perhaps by pointlike constituents.

In the past decade, the observation of scale-invariant electron and muon scattering at large momentum transfer has demonstrated that hadrons have an effective pointlike constituent structure. These experimental data have been well-explained in terms of the quark–parton model, in which the carriers of the currents are structureless but yet carry a finite fraction of the hadron's momentum. Thus one expects that hadrons can scatter to large transverse momentum via hard, large angle scattering processes involving their constituents. The possibility that the large transverse momentum processes involving only hadrons are directly related to the deep inelastic lepton induced reactions has attracted a great deal of attention. We will devote the major portion of this review exploring and pursuing the consequences of this type of connection.

In contrast, there have been numerous attempts to explain the large transverse momentum processes without invoking partons. These models lack some of the attractive features of quark–parton models in that they do not make the kind of unification between hadron spectroscopy, electroproduction and hadronic scattering possible in the quark model. They are important, however, in order to see how far we can go without invoking quarks and in order to define what constitutes a definitive test of the application of quark–parton ideas to hadronic scattering.

Even if granted the basic postulates of the quark–parton picture of hadronic structure, one must still admit that the violent collision of hadrons is a more difficult way to probe that structure than deep inelastic lepton–hadron since both the beam and target particles possess unknown complexity. To use an analogy due to Feynman, studying hadron–hadron collisions is like smashing two watches together and watching the gears fly out! Pursuing this analogy we see that the production of large p_T hadrons in such a collision provides a unique way to studying the, possibly funda-

mental, "gear–gear" interaction. The ultimate goal is to understand both lepton and hadron-induced reactions within the same basic framework and to unravel the essential dynamical degrees of freedom of the hadrons. The variety of information on violent hadronic interactions which is experimentally accessible is large and there are many opportunities for testing and refining our theoretical ideas. The extra complexity in the hadron–hadron interaction, if it can be handled, offers the possibility of a richer lode of information. Conceivably, such information could help illuminate the central mystery of quark–parton models: the mechanism of confinement which prevents quarks from being observed singly.

In this review we will attempt to summarize what is known experimentally about large transverse momentum reactions as well as to examine the current theoretical speculations. This summary will be as current as possible but the nature of the field is such that there may be substantial new information and possible "surprises" from new experiments that we have not been able to cover. The cutoff date on experimental information is roughly January 1, 1975 *.

Our review is organized as follows. The remainder of the introduction will present some general theoretical concepts and should serve to warn the careful reader of our personal prejudices. We also outline here the main implications of the data for various theories, the connection between small-p_T and large-p_T phenomena, and the interrelation between large p_T inclusive production and exclusive large-angle scattering. In section 2 we discuss in further detail the main experiments and try to extract the phenomenological features of the data. In section 3 we review model approaches to large transverse momentum which do not involve partons, including eikonal, bootstrap, fireball and thermodynamic models. Interestingly enough, we find that many features of the data can be understood in these purely hadronic terms. In section 4 we return to a more careful treatment of hard collision models. Particular emphasis is placed on the separation of short-distance and large-distance phenomena, the dimensional counting ansatz and specific features of the constituent interchange model. We also include a review of recent theoretical treatments of the elastic form factor. In section 5 we conclude with a discussion of how experiments may be able to discriminate between models. The appendices include a derivation of the basic equation of the hard scattering model and a comparison of different techniques for calculations. We also discuss areas ripe for more theoretical work. Large transverse momentum physics is just at its infancy and this review can only be a small step toward illuminating a crucial new area of hadronic physics.

1.2. Implications of power-law scaling for inclusive cross sections

The fact that the observed inclusive spectrum of hadrons produced at large transverse momentum at the CERN–ISR was much larger than an extrapolation of the form $\exp(-6p_T)$ based on the Hagedorn thermodynamic model suggests that the data can be explained in a hard scattering model. In these models, because of the assumed structureless nature of the constituents the general form of the invariant cross section for A + B → C + anything is predicted to be

$$\frac{d^3\sigma}{d^3p/E}(s,t,\mathcal{M}^2) \xrightarrow[p_T^2 \gg m^2]{} \frac{1}{(p_T^2)^N} f(t/s, \mathcal{M}^2/s)\,, \tag{1.2.1}$$

where $p_T^2 \cong tu/s$ and $\mathcal{M}$ is the missing mass. We call this factorization of the cross section into a

* Another review, with emphasis on the experimental aspects of large transverse momentum phenomena, is now in preparation (P. Darriulat). It should review this fast moving field as of the end of 1975. (Editorial note.)

power times a function of the dimensionless "scaling" parameters *power law scaling*. For two-body exclusive processes A + B → C + D at fixed θ_{CM} the analogous scaling form is

$$\frac{d\sigma}{dt}(s,t) \xrightarrow[p_T^2 \gg m^2]{} \frac{1}{(p_T^2)^N} f(t/s) . \tag{1.2.2}$$

This latter scaling law also implies the power law falloff for the electromagnetic form factors of hadrons. In general, the value of N in (1.2.1) and (1.2.2) depends on the particles involved.

There is substantial experimental evidence for the approximate validity of (1.2.1) and (1.2.2) which we will examine in more detail later. The one thing we want to note here is that a simple parametrization of the inclusive cross section pp → π^o anything (see fig. 1.1), can be written (Busser et al., [66])

$$\frac{d^3\sigma}{d^3p/E}(pp \to \pi^o X) \cong \frac{120\ \text{mb/GeV}^2}{[p_T^2 + 1\ \text{GeV}^2]^4} \exp(-13x_T) , \qquad 0.1 < x_T < 0.4 \tag{1.2.3}$$

where $x_T = p_T/p_T\ \text{max} \cong 2p_T/\sqrt{s}$. Charged pion data at FNAL (for $0.3 < x_T < 0.7$) seems to fall even more rapidly with p_T, roughly as p_T^{-12} (Cronin et al. [93]).

It is interesting to compare this empirical formula with the observation of Bjorken scaling for deep inelastic lepton production. We can write the invariant cross section as

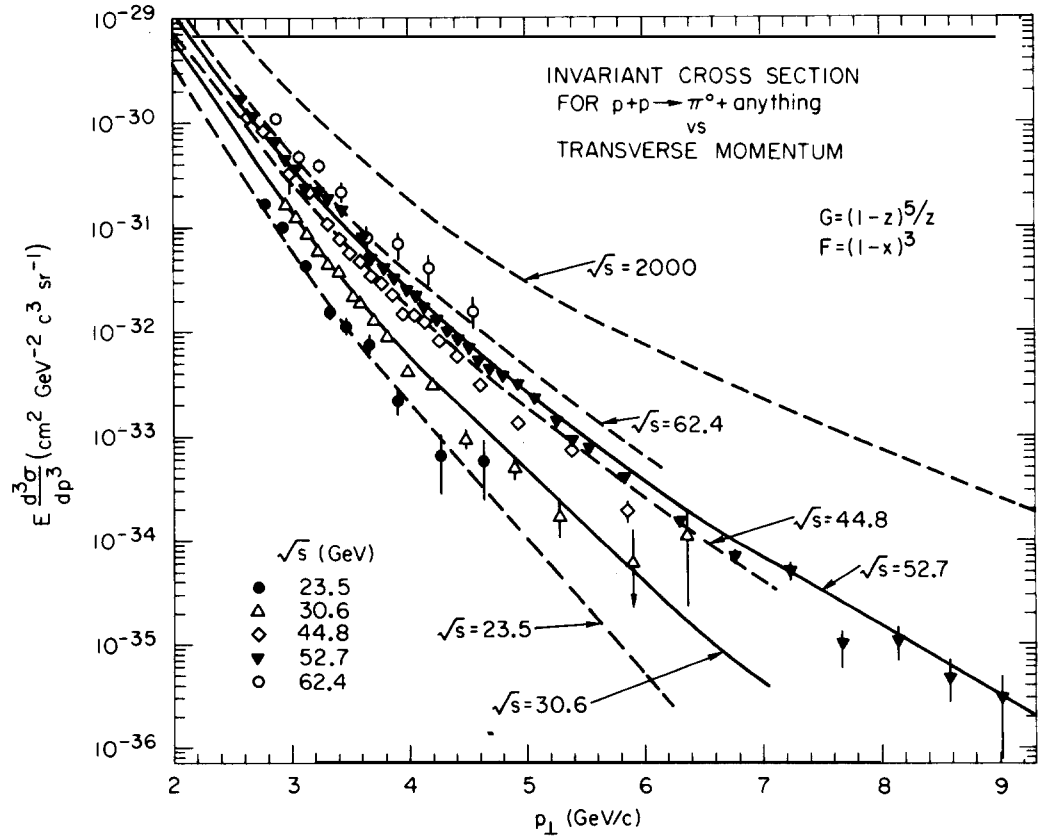

Fig. 1.1. The inclusive cross section pp → π^o + X versus transverse momentum. The data are from the CCR collaboration [66].

$$\frac{d^3\sigma}{d^3p/E}(ep \to eX) = \frac{4\pi\alpha^2}{t^2} f(t/s, \mathcal{M}^2/s), \qquad s \gg m^2, \quad \mathcal{M}^2/s, \quad t/s \text{ fixed} \tag{1.2.4}$$

which is equivalent to

$$\frac{d^3\sigma}{d^3p/E}(ep \to eX) \propto \frac{1}{p_T^4} \tilde{f}(\theta_{cm}, \mathcal{M}^2/s). \tag{1.2.5}$$

This formula displays the scale-invariance of the lepton inclusive cross section. There is apparently no relevant mass involved in this reaction. To the extent that scale invariance is valid experimentally, we can deduce (in the one-photon approximation) that the usual structure functions $W_1(p\cdot q, q^2)$ and $\nu W_2(p\cdot q, q^2)$ are functions only of the variable $x = -t/(\mathcal{M}^2 - t)$.

Since the data now imply that the electromagnetic interactions within hadrons are essentially scale-invariant, it is evident that the exchange of one photon will lead to a scale invariant cross section for hadron–hadron collisions. This fact has been emphasized by Berman, Bjorken and Kogut [28]. The cross section for one-photon exchange for hadrons is, however, everywhere more than four orders of magnitude smaller than the current data (see fig. 1.2). Using (1.2.3) to extrapolate, we can surmise that one-photon exchange may be important at $\sqrt{s} \cong 2000$ GeV and $p_T \cong 45$ GeV/c which is near the upper limits of the range of possible future Isabelle experiments. At very high p_T we might also have a contribution from the weak interactions of hadrons. The kinematic range where all three types of interactions are potentially important is likely to be full of surprises.

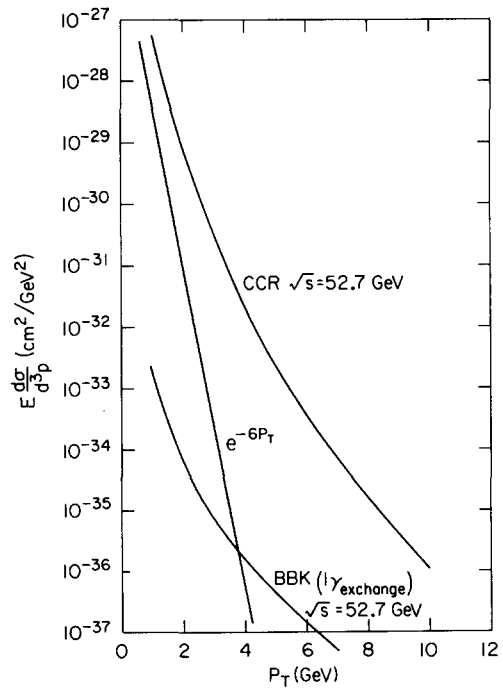

Fig. 1.2. The extrapolation of the Hagedorn exp ($-6p_T$) and the contribution of 1γ exchange from BBK are compared with CCR data.

In view of the form predicted for one-photon exchange, a natural ansatz for violent hadron–hadron collisions proposed by Berman, Bjorken and Kogut [28] and in a different form by Berman and Jacob [29] is that there is a contribution due to the carriers of the electromagnetic current interacting through vector gluon exchange. It is conventional to assume that the coupling constant which characterizes this interaction is dimensionless, as in QED, in order to have a renormalizable theory. This, in turn, leads to a scale-invariant cross section $E\mathrm{d}^3\sigma/\mathrm{d}^3p \propto p_T^{-4} f(t/s, \mathcal{M}^2/s)$ in contrast to the parametrization (1.2.3). Within the context of this model, however, the observed p_T behavior might be interpreted as implying that the matrix element is not dimensionless.

One of the major problems in understanding the relevance of quark–parton ideas to violent hadron–hadron collisions is then the apparent absence of this p_T^{-4} contribution. One simple possibility is just to assume a super-renormalizable theory such as an underlying $g\phi^3$ theory in order that the coupling constant possesses units of mass. As discussed in ref. [10] scalar exchange will give the observed p_T^{-8} behavior. Another possibility is that, due to kinematic requirements and the absence of observable quarks, a particle with form factor $F(t) \sim (1-t/m^2)^{-1}$ is always involved in the interaction. This contribution is important in the Constituent Interchange Model (CIM) of Blankenbecler, Brodsky and Gunion [41, 42], the related model of Landshoff and Polkinghorne [174], and, as discussed by Ellis [107, 108] contributes to a "semi-inclusive" mode of the parton gluon model.

It is not clear, however, that merely removing the possible p_T^{-4} term solves all the problems. Data from the Chicago–Princeton group on $pp \to \pi^{\pm}X$ and Fermilab indicates the situation is more complicated in that a single term of the form (1.2.1) apparently cannot fit all the data since the effective power of N in (1.2.1) is different in different kinematic regions. The most natural ways of reconciling all the data is to assume that a sum of power law scaling terms is needed or that N depends on x_T. Correlation experiments can tell these options apart, as we shall see.

A sum of terms is actually predicted in the constituent interchange model (CIM) of Blankenbecler, Brodsky and Gunion and in the massive quark model of Preparata [199, 200]. One finds that different terms with different powers of p_T dominate in different parts of the CP experiment. A quite acceptable fit to the FNAL and ISR data can be achieved with a two-term parametrization although, in principle, there is no reason to exclude more terms. The soft gluon model of Fried, Gaisser and Kirby [129, 130] predicts that N increases with x_T (Fried [124]).

In the former vein, Bander, Barnett and Silverman [22] and Ellis [107] suggest that three types of mechanisms can be important – each dominant within its own regime in x_T. At small x_T quark–quark scattering is important, at intermediate x_T quark–hadron processes become more important, and as one moves toward the exclusive boundary only hadron–hadron contributions may be important. Experimentally, this is still very much a possibility as long as the p_T^{-4} contribution is small. Within the context of asymptotically free gauge theories there might be some reasons for this type of suppression (Cahalan, Geer, Kogut and Susskind [68]).

As noted by Ellis [107] the production of "jets", many hadrons with a total transverse momentum of p_T, may show a p_T^{-4} scaling law even though the production of a single hadron, at ISR energies, falls off more rapidly. Similarly, in a model due to Preparata [199, 200], a scale invariant form will not arise until $q\bar{q} \to$ two "fireballs" becomes possible. We will discuss the predictions of all these distinct models for inclusive spectra in more detail and see to what extent current or projected experimental data will allow us to distinguish models. In any event the apparent absence of a scale-invariant quark–quark contribution in current data is of enormous theoretical importance from a quark–parton viewpoint and is one of the most striking indications that there are important

aspects of hadron structure not seen in deep inelastic lepton scattering but which can be studied in large-p_T hadronic collisions.

1.3. Further implications of the large-transverse-momentum data – Feynman scaling

The different kinematic regions of the inclusive process AB → C + anything are defined in the Peyrou plot shown in fig. 1.3. The invariant cross section is described in terms of the center-of-mass variables, p_T, θ_{CM} and ϵ,

$$\begin{aligned} & p_T^2 = tu/s \\ & -t/s \cong \tfrac{1}{2}(1-\cos\theta_{CM}) \\ & -u/s \cong \tfrac{1}{2}(1+\cos\theta_{CM}) \\ & \epsilon = \mathcal{M}^2/s \cong 1 - x_R = 1 - (x_T^2 + x_L^2)^{1/2} , \end{aligned} \tag{1.3.1}$$

where $\mathcal{M}$ is the missing mass, $x_T = p_T/p_{CM}^{max}$ and $x_L = p_L/p_{CM}^{max}$. The radial distance from the perimeter of the Peyrou plot is measured by ϵ.

The small-p_T region where $x_T \cong 0$ contains the bulk of the data. By convention it is further subdivided at high energy into the "central" region, $x_L \cong 0$, the "triple-Regge" region, $x_L \cong 1$, and the "fragmentation" region consisting of all intermediate values of x_L. The large-p_T or "deep" region is the one in which we are primarily interested here. It extends from $p_T > 2$–3 GeV/c right out to $\epsilon = 0$, the exclusive limit. Since the deep region shares boundaries with each of the others, important constraints on hadronic theories can be obtained by requiring a smooth connection between this and the other kinematic regions.

One important feature of the inclusive cross section data is the approximate validity of Feynman scaling. For small transverse momentum this means we can write

$$\frac{d^3\sigma}{d^3p/E}(s, p_T, x_L) \sim f(p_T, x_L) . \tag{1.3.2}$$

This approximate asymptotic energy independence is expected theoretically to be valid to within logarithmic factors. These factors are important in the discussion of the asymptotic behavior of total cross sections but they will be neglected here.

As one continues out into the deep region, Feynman scaling is expected to generalize. One

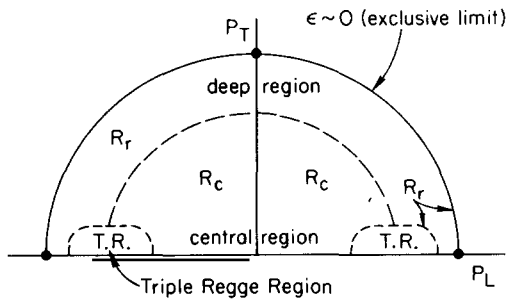

Fig. 1.3. A Peyrou plot for the process AB → C + anything showing the different kinematic regions.

possible simple generalization is to write

$$\frac{d^3\sigma}{d^3p/E}(s, p_T, x_R) \sim f(p_T, x_R) . \tag{1.3.3}$$

At fixed p_T, $x_T \cong 2p_T/\sqrt{s}$ goes to zero as $s \to \infty$ and we expect some energy dependence of the cross section associated with this fact. This does not mean that Feynman scaling fails at large p_T, it merely means that correction terms depend on p_T so that scaling is approached more slowly at large p_T. One can argue that the approach to scaling is largely kinematic in that the energy behavior of $pp \to \bar{p}$ and the energy behavior of $pp \to \pi$ are very similar if they are compared at the same value of "effective mass", $\sqrt{m^2 + p_T^2}$. This point is emphasized in fig. 1.4 taken from the review of Walker [225].

If we view hadrons as composite or complex systems, it is interesting to ask what the effective energy of the fundamental interactions in a collision might be. For ordinary production processes most of the energy is radiated as hadronic "bremsstrahlung" down the beam direction. High energy alone is not sufficient to study high-energy interactions since, for example, in a multiperipheral chain we can go to high total energy without any subenergies becoming large. When we observe a high-p_T particle, however, we are guaranteed that there is a violent subprocess which occurs at a minimum effective energy squared of

$$s_{\text{eff}} \gtrsim 4p_T^2 . \tag{1.3.5}$$

The structure of an interaction with a hard component is illustrated schematically in fig. 1.5. In much of the discussion of this review we are investigating the possibility that this hard component may represent a simple or even a fundamental interaction. If we can find a prescription for stripping away the effects of the outer bremsstrahlung, then we can see whether we can *fairly* compare this core subprocess with some annihilation cross section, such as, for example, $\sigma_{e^+e^-} \to$ hadrons at $s_{e^+e^-} \gtrsim 4p_T^2$. The division of the process illustrated in the diagram of fig. 1.5 is quite universal; virtually all the models which have been proposed turn out to have this structure in common. If we assume the absence of important interference effects, the inclusive cross section corresponding to fig. 1.5 can be written in a simple form involving probabilities. We define the distribution

$$G_{b/B}(x) = dN_{b/B}/dx ; \qquad 0 \leqslant x \leqslant 1 \tag{1.3.6}$$

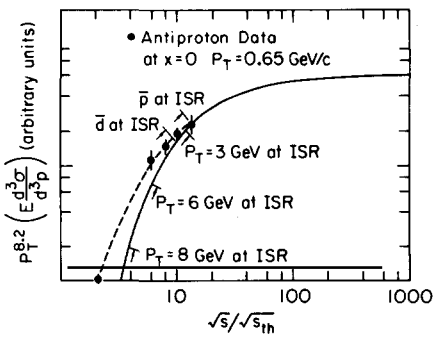

Fig. 1.4. Figure taken from Walker [225] comparing the approach to scaling of large-p_T pion data with antiproton data.

for hadron B to contain an offshell fragment b with the longitudinal fraction $x = p_L^b/p_L^B$ of the initial momentum. There is an implied integration over the transverse momentum which is assumed to be rapidly convergent. The conservation of momentum implies the constraint

$$1 = \sum_b \int_0^1 x\,dx\,G_{b/B}(x) \tag{1.3.7}$$

Notice that there is a term in $G_{b/B}(x)$ which corresponds to the "elastic" propagation of B without bremsstrahlung

$$G_{B/B}(x) \simeq Z\delta(1-x)\,. \tag{1.3.8}$$

The quark–parton model for deep inelastic scattering gives the familiar relation

$$F_{2B}(x) = \nu W_2(x) = \sum_a \lambda_a^2 x\, G_{q_a/B}(x)\,, \tag{1.3.9}$$

where $G_{q_a/B}$ is now the infinite momentum frame probability function for a quark–parton of charge λ_a within hadron B. Within the same spirit, the inclusive hadron–hadron reactions can, at large-p_T, be written in the form

$$\frac{d^3\sigma}{d^3p/E}(AB \to CX) = \sum_{\substack{a\in A\\ b\in B}} \int_0^1 dx_a \int_0^1 dx_b\, G_{a/A}(x_a)\, G_{b/B}(x_b)\, \frac{d^3\sigma^I}{d^3p/E}(ab \to CX)\,, \tag{1.3.10}$$

where $d^3\sigma^I/(d^3p/E)(ab \to CX)$ is hadron irreducible since the initial bremsstrahlung is contained in the G's. A derivation of (1.3.10) is given in Appendix A. The "violent" subprocess, $ab \to CX$ occurs at reduced $s_{eff} = x_a x_b s \gtrsim 4p_T^2$. If the integration over transverse momentum (which is implied in eq. (1.3.10)) is not performed, for example, we can study azimuthal correlations in two-particle inclusives. With a specific choice of elementary scattering, eq. (1.3.10) and fig. 1.5 were originally given by Berman, Bjorken and Kogut [28]. It has been rederived and generalized in various forms using infinite momentum frame techniques (Blankenbecler et al. [41,42]), Sudakov variables (Landshoff and Polkinghorne [174,175,176]) and an analysis of the multiperipheral model (Amati, Caneschi and Testa [10]; Levin and Ryskin [180]). The interrelations between these approaches are discussed in Appendix B. Possible off-shell effects in the hard subprocess $d^3\sigma^I/(d^3p/E)(ab \to CX)$ are not explicitly included in eq. (1.3.10). The fact that $G_{b/B}(x)$ becomes a function independent of $|\boldsymbol{p}_B|$ for $|\boldsymbol{p}_B| \to \infty$, can be derived in super-renormalizable elementary field theories and bound state calculations.

Other examples of reactions which have the same general form as eq. (1.3.10) include the Drell–Yan formula [102] for the process $hh \to \mu^+\mu^- X$ via $\bar{q}q$ annihilation and the two-photon process $ee \to ee$ + hadrons.

It is important to note the connection between the behavior of $G(x)$ near $x = 0$ and the Regge behavior of total cross sections. If $\sigma_{\bar{a}A} \sim s^{\alpha-1}$ one readily finds (modulo logarithmic factors) (Feynman [119]; Landshoff, Polkinghorne and Short [178]; Abarbanel et al. [1])

$$G_{a/A}(x) \sim Cx^{-\alpha}\,. \tag{1.3.11}$$

Inserting this into (1.3.10) we see that Pomeron exchange, $\alpha = 1$, gives Feynman scaling for the inclusive cross section, eq. (1.3.4).

1.4. Relations among cross sections in hard scattering models

It is interesting to note that many of the properties of cross sections in hard-scattering models can be determined directly from the underlying basic assumption. Consider any model in which we can write in the limit $s, t, u \gg$ (masses)^2 the exclusive cross section as

$$\frac{d\sigma}{dt}(AB \to CD) = (F^b_{BD}(t))^2 K^c_{Ab}(s,t,u) \tag{1.4.1}$$

and the inclusive cross section in the triple-Regge region as

$$\frac{E d^3\sigma}{d^3p}(AB \to CX)|_{T.R.} = \frac{s}{s+u} F_{b/B}(x) K^c_{Ab}(xs, t, xu) , \tag{1.4.2}$$

where $x = -t/(s+u) = -t/\mathcal{M}^2 - t$ is the Bjorken scaling variable. The hadronic form factor $F^b_{BD}(t)$ reflects the probability of the transition B → D with D remaining intact and $F_{b/B}(x)$ is the generalized structure function describing the breakup of the target B due to the projectile b. These equations are the analogs of the usual electron scattering formulae and include the assumption that the large momentum transfer is achieved in a single factorizable impulse. A sum over the internal index b of such separable terms can be considered as well but we will not write this sum explicitly.

The expressions (1.4.1) and (1.4.2) are connected in the limit of small missing mass by a relation of the Drell–Yan–West type [101, 226]. The $x \to 1$ limit of the inclusive cross section can be written

$$\lim_{x\to 1} \frac{d^3\sigma}{dt\, d\mathcal{M}^2} = \frac{1}{\mathcal{M}^2} [(1-x)F_{b/B}(x)] K^c_{Ab}(s,t,u) . \tag{1.4.3}$$

If this is to join smoothly onto exclusive scattering for $\mathcal{M}^2 = m_D^2$, then for $(1-x) \cong m_D^2/(m_D^2 - t)$ we must have

$$(1-x)F_{b/B}(x) \propto (F^b_{BD}(t))^2 . \tag{1.4.4}$$

Hence,

$$F^b_{BD}(t) \sim (-t)^{-n} \Longleftrightarrow F_{b/B}(x) \sim (1-x)^{2n-1} . \tag{1.4.5}$$

This is a simple extension of the Drell–Yan–West relation but one has not assumed that the hadronic form factors have the same t-behavior of the electromagnetic form factor.

From (1.4.1), we see that in general the function K falls off less rapidly at fixed angle than the exclusive cross section itself. Furthermore, if

$$\frac{d\sigma}{dt}(AB \to CD)|_{\text{fixed } t} \sim \beta^2(t) s^{2\alpha(t)-2} , \tag{1.4.6}$$

then

$$K^c_{Ab}(s,t,u)|_{\text{fixed } t} \sim \bar{\beta}^2(t) s^{2\alpha(t)-2} \tag{1.4.7}$$

with

$$\beta(t) = F^b_{BD}(t)\, \bar{\beta}(t) . \tag{1.4.8}$$

Therefore, in the limit $s \gg \mathcal{M}^2 \gg |t|$ (the triple-Regge region with $x \cong 0$) the inclusive cross section can be written

$$\frac{E\mathrm{d}^3\sigma}{\mathrm{d}^3p}(\mathrm{AB}\to\mathrm{CX}) \sim (-t)^{2\alpha(t)-2}\,\bar{\beta}^2(t)\,F_{\mathrm{b/B}}(0)\left(\frac{\mathcal{M}^2-t}{s}\right)^{1-2\alpha(t)}. \tag{1.4.9}$$

If this term is to contribute to Feynman scaling we must require $F_{\mathrm{b/B}}(0) \neq 0$. A more general parametrization of $F_{\mathrm{b/B}}(x)$ near $x = 0$

$$F_{\mathrm{b/B}}(x) \sim f_{\mathrm{b/B}}x^a \tag{1.4.10}$$

results in the behavior

$$\frac{E\mathrm{d}^3\sigma}{\mathrm{d}^3p}(\mathrm{AB}\to\mathrm{CX}) \sim (-t)^{2\alpha(t)-2}\,\bar{\beta}^2(t)\,f_{\mathrm{b/B}}(-t/s)^a\left(\frac{\mathcal{M}^2-t}{s}\right)^{1-a-2\alpha(t)}. \tag{1.4.11}$$

The usual triple-Regge formula is independent of the $x \to 1$ behavior of $F_{\mathrm{b/B}}(x)$, however, if we want to guarantee that it connects smoothly onto the exclusive limit it is important that we continue away from $x = 0$ with the appropriate form of $F_{\mathrm{b/B}}(x)$ obeying (1.4.4). This simple correction to the triple-Regge formula becomes important for decreasing missing mass.

If we want to generalize the expression (1.4.2) to describe the inclusive cross section in the central region we must consider the fragmentation of the projectile A. If we write the probability of finding fragment a of particle A with longitudinal momentum fraction x_a as $G_{\mathrm{a/A}}(x_\mathrm{a}) = x_\mathrm{a}^{-1}F_{\mathrm{a/A}}(x_\mathrm{a})$ it is suggestive to write the cross section in the explicitly symmetric form

$$\frac{E\mathrm{d}^3\sigma}{\mathrm{d}^3p}(\mathrm{AB}\to\mathrm{CX}) = \int \mathrm{d}x_\mathrm{a}\,\mathrm{d}x_\mathrm{b}\,\delta(x_\mathrm{a}x_\mathrm{b}s + x_\mathrm{a}t + x_\mathrm{b}u - m_\mathrm{a}^2 - m_\mathrm{b}^2 - m_\mathrm{c}^2 - m_\mathrm{d}^2)$$

$$\times F_{\mathrm{a/A}}(x_\mathrm{a})\,F_{\mathrm{b/B}}(x_\mathrm{b})\,K_{\mathrm{ab}}^{\mathrm{c}}(x_\mathrm{a}x_\mathrm{b}s, x_\mathrm{a}t, x_\mathrm{b}u)\,, \tag{1.4.12}$$

where a sum over a and b is again understood. Comparing this form with eq. (1.3.10) we see we have isolated a restricted subset of possible internal processes in the most general hard scattering model where the internal sub-process is a 2–2 scattering leading to particle c.

By a simple change of variable, eq. (1.4.12) can be rewritten as an angular integral of the form

$$\frac{E\mathrm{d}\sigma}{\mathrm{d}^3p} \simeq \int_{-(1-2x_1)}^{(1-2x_2)} \frac{\mathrm{d}z}{(1-z^2)}\,F_{\mathrm{a/A}}\left(\frac{2x_1}{1+z}\right)F_{\mathrm{b/B}}\left(\frac{2x_2}{1-z}\right)K_{\mathrm{ab}}^{\mathrm{c}}\left(s=\frac{4p_\mathrm{T}^2}{1-z^2}, z\right), \tag{1.4.13}$$

where K can be identified with $(2/\pi)\,\mathrm{d}\sigma/\mathrm{d}t$ (ab → cd). In the limit of large p_T^2 at fixed x_1 and x_2, the dependence on p_T^2 is given in terms of the fixed angle behavior of the basic process described by $K_{\mathrm{ab}}^{\mathrm{c}}$. For example, for the process $\mathrm{pp}\to\pi\mathrm{X}$, an estimate of the contribution from the pion intermediate state can be made by using the empirical result that $\pi\mathrm{p}\to\pi\mathrm{p}$ varies as s^{-8} at fixed angle $F_\mathrm{p}(t) \sim (-t)^{-2}$, and hence $K \sim s^{-4}$. This contribution to the inclusive cross section therefore varies as $(p_\mathrm{T}^2)^{-4}$. It is possible to make a much better estimate by a more detailed estimate of $K(s,t,u)$ but this will be postponed until specific models are discussed. We see that many different models will yield formulas of the above structure; they must be judged, therefore, on their detailed predictions for $F_{\mathrm{BD}}(t)$, $F_{\mathrm{b/B}}(x)$, and $K(s,b,u)$, on their range of applicability, and their simplicity. A further generalization of (1.4.13) allows for final state fragmentation of c into C.

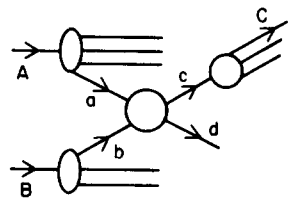

Fig. 1.5. The structure of an inclusive process in a hard-collision model where there is a underlying 2–2 subprocess.

1.5. What are the important internal mechanisms?

Given that the underlying structure of current models is roughly determined by the form of the diagram shown in fig. 1.5, the differences between the various approaches consist of assumptions concerning the question of what the important internal mechanisms, ab → CX in eq. (1.3.10), can be. The possibilities include the following.

1.5.1. Quark–quark scattering

This is the mechanism originally discussed by Berman and Jacob [29] and made explicit in the pioneering paper of BBK. The large-angle quark–quark scattering is followed by the scale-invariant fragmentation of one of the quarks into the hadron C. If the fundamental quark–quark interaction is scale-invariant this leads to $E\,d\sigma/d^3p$ scaling as p_T^{-4} as discussed earlier. The implications of this model for particle ratios and for two-particle production have been explored by Ellis and Kislinger [110] and by Bjorken [32, 33, 34]. More complicated phenomenological forms for the quark–quark cross section, constrained to agree with fixed-angle exclusive hadronic processes, are used in the calculations of Horn and Moshe [148].

Quark–quark scattering is in many senses, the most attractive hard collision model because of its simple connection with ideas found useful in deep inelastic lepton production and the amount of work done on the many alternatives is due largely to the apparent absence of the p_T^{-4} behavior. The specific predictions for the phase-space structure of events and for particle ratios are important predictions which merit testing in spite of this failure.

1.5.2. Quark–hadron scattering

These are the dominant contributions of the constituent interchange model of BBG. The basic hypothesis is that the quark–quark scattering contributions are suppressed leaving other types of internal subprocesses involving quarks and hadrons (perhaps because the dominant interaction is between quarks and their containers). One important example of such a contribution is qM → qM (quark–meson scattering). Here we can either detect the hard-scattering meson directly or the quark or meson can fragment into a hadron. Since the fragmentation functions are assumed scale invariant, the power of p_T in the power law scaling, eq. (1.2.1), directly reflects the fixed angle energy dependence of the subprocess. A simple ansatz for the scaling laws of exclusive processes is given by the dimensional counting rules of Brodsky and Farrar [62] and Matveev, Muradyan and Tavkhelidze [183]. We will discuss in considerable detail in section 4.3 how these rules are derived and their implications for several processes. The nontrivial extension to the general case and to inclusive scattering was given by Blankenbecler and Brodsky [40] and will also be covered in considerable detail.

The quark–hadron mechanism has also been discussed in detail by Landshoff and Polkinghorne [174–177] where there is special emphasis on the fusion mechanism $q\bar{q} \to MM$. A related approach can also be found in the work of Kinoshita [160] and collaborators.

1.5.3. Hadron–hadron scattering

In the multiperipheral model of Amati, Caneschi and Testa [10] and Levin and Ryskin [180], the diagram of fig. 1.5 is still relevant if we think of the central collision as the two-body process $MM \to MM$ where the M is the elementary scalar in a $g\phi^3$ field theory. This model has been thoroughly discussed by Levin and Ryskin [180]. It leads asymptotically to a strict p_T^{-8} scaling law for the inclusive cross section but there are serious difficulties in making connections with deep inelastic reactions and large angle exclusive processes. In its simplest form the model predicts limited multiplicities in the recoil system opposite a high-p_T hadron.

A more general approach has been discussed by Teper [221] who merely assumes that the violent subprocess is a purely hadronic large angle scattering process. Quarks or partons are thus never explicitly mentioned. If we adopt either the constituent counting rules or empirical fits for various exclusive large-angle processes this can provide interesting lower bounds on the behavior of the inclusive cross section. Experimentally, exclusive meson–baryon scattering is roughly consistent with the scaling law

$$\frac{d\sigma}{dt}(MB \to MB) \sim \frac{1}{s^8} f(\theta_{CM}) . \tag{1.5.1}$$

Thus, using eq. (1.3.10), we see that we must have a contribution proportional to

$$\frac{E d^3\sigma}{d^3p} \gtrsim \frac{1}{p_T^{16}} f(\theta_{CM}, \epsilon) \tag{1.5.2}$$

both for $pp \to BX$ and $pp \to \pi X$. These contributions are also present in the CIM but they are usually assumed to be dominated by terms involving quarks at sufficiently large values of p_T (at fixed x_T). Similarly, the assumed behavior

$$\frac{d\sigma}{dt}(MM \to MM) \sim \frac{1}{s^6} f(\theta_{CM}) \tag{1.5.3}$$

given by the dimensional counting rules can lead to a contribution

$$\frac{E d\sigma}{d^3p}(pp \to \pi X) \geq \frac{1}{p_T^{12}} f(\theta_{CM}, \epsilon) . \tag{1.5.4}$$

It is a virtue of the assumption that the violent subprocess involves hadrons that it allows us to use the structure of eq. (1.3.10) directly with experimental data on large-angle exclusive scattering in order to calculate inclusive cross sections. *To the extent* that we can neglect off-mass-shell effects and coherence, this should provide important normalization checks. The approach should also predict simply particle ratios for small x_T where the fragmentation functions are proportional to total cross sections. Since it is not clear whether a point-like power-law falloff or an exponential falloff associated with a mass scale is required for large-angle exclusive cross sections, the advantage of dealing directly with data is obvious.

If we discuss the violent subprocesses in fig. 1.5 in purely hadronic terms the notion of a "fireball" or high-mass excited hadronic state becomes important. For example, in the early model

of Berman and Jacob [29] the internal heavy vector gluon exchange leads to the excitation of baryonic fireballs. A version of this model was discussed by Berger and Branson [27]. In its direct form, the model requires that a baryon be found with large transverse momentum on each side of the collision axis along the direction of the scattered fireballs. There may also be problems with Feynman scaling or crossing symmetry in the particular versions of the model discussed so far.

Another approach to diagram 1.5 is to assume the core subprocess consists of the production of a single heavy fireball. In order to be different from the fireballs in the statistical bootstrap approach of Hagedorn [137] and Frautschi [122], this new heavy fireball must have some unusual characteristics associated with it. If it possessed the usual cascade decay mode found in bootstrap models, then the invariant cross section would be approximately given by a Boltzmann factor $\exp(-p_T/kT_0)$ although Bouquet, Letessier and Tounsi [54] have shown that modifications due to a large recoil momentum building up after several decays can broaden the p_T distribution. With one or more new mass scales in addition to the usual $kT_0 \cong m_\pi$ of the statistical bootstrap theory we can obviously reproduce single particle distributions but there may be some problems in getting reasonable two-particle distributions and multiplicities from a cascade decay mode. Within the context of one fireball model, it is difficult to treat quantum number constraints correctly so that, for example, a nontrivial K^+/K^- particle ratio can be obtained.

Another possibility is that this new type of heavy fireball possesses a non-negligible fission decay mode, $F^*(M) \to F^*(M/2)\,F^*(M/2)$, in order to give the final state a distribution in phase space more like the jet structure of the parton model. Obviously, to a certain accuracy, we can then reproduce many parton-model results.

1.6. The structure of high-p_T events

One of the potentially most interesting pieces of information that can be obtained concerning large transverse momentum phenomena is the structure of events in phase space. When a high-p_T particle is produced we would like to know how many other particles are produced and what regions of phase-space they populate. A spectacular possibility is that completely new and unexpected types of matter, such as colored or charmed hadrons, weak bosons, or heavy leptons, may be preferentially produced in association with large transverse momentum particles. In any case, the measurement of correlations and associated multiplicities can provide severe restraints on models for the underlying production mechanism.

An essential characteristic of hard-collision models typified by fig. 1.6 is the development of some sort of jet structure. It is easy to see how this arises within the context of these models. The fragmentation of the initial hadrons and possible fragmentation of the scattered constituents is assumed to be a gentle process which preserves the direction of all hadronic momenta within fluctuations of typical size $\langle p_T \rangle \sim 0.3 - 0.4$ GeV/c. In the case that one of the scattered particles is a quark parton, this entails a belief that as in models for deep inelastic scattering the final state interactions which neutralize quark quantum numbers are of this same gentle nature. The coplanarity of the internal hard-scattering process is therefore approximately maintained in the regions of phase space in which final state hadrons are found. Event-by-event there will be fragmentation products along both beam directions and along the direction of the scattered large-p_T constituents. This structure is shown in fig. 1.6. The fact that the two large-p_T jets emerge approximately coplanar but not collinear is due to the center-of-mass motion of a and b.

The observation of jet structure would be a success for hard-scattering models while the measure-

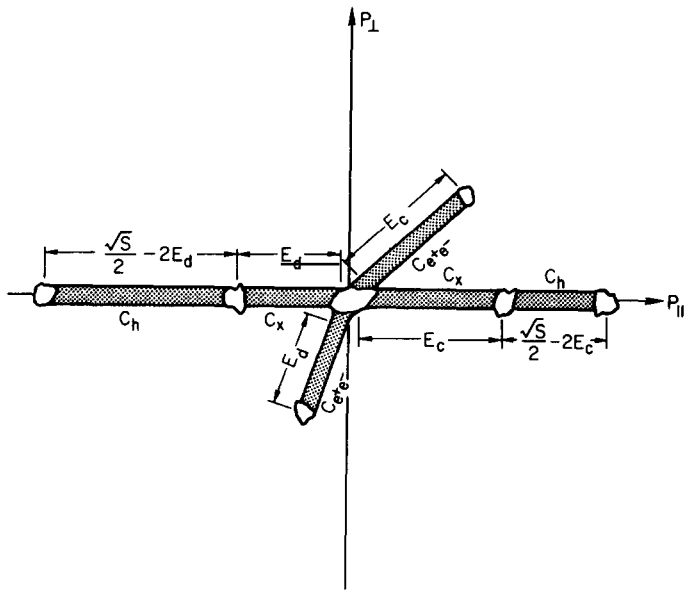

Fig. 1.6. Figure taken from Savit [208] demonstrates the regions of phase space populated by hadrons in hard-collision models. The underlying 2–2 subprocess leads to jet structure.

ment of jet–jet cross sections would offer the potential of looking back "inside" an event and deducing the fundamental quark–quark or quark–hadron cross section. However, there is some evidence from recent measurements of azimuthal correlations associated with large-p_T by the CCR group that the deviations from coplanarity in large-p_T events are significantly greater than what is expected on the basis of the simple arguments (Bjorken [35]). The spread in hadron momenta around a jet axis is more like 1.2 GeV/c than 0.35 GeV/c. It may be possible that hard-scattering models, since they prefer p_T distributions that fall rather slowly (as powers), will be able to accommodate this fact but the situation is not as clear as it might have been (Gunion [135,136]).

An important point to remember is that if one of the scattered constituents is a quark, the multiplicity and distribution of hadrons in the jet associated with that quark should be identical to that of the system which balances the transverse momentum of a deeply-inelastic-scattered lepton. This connection, involving particle ratios, etc., can be tested experimentally in order to quantify our presumption that quarks represent an important dynamical degree of freedom in large-p_T hadronic processes.

If the basic hard process is quark–quark scattering, the usual assumption is that in a given event all the available phase space regions shaded in fig. 1.6 are approximately uniformly populated. However, if the quarks scatter through a single elementary exchange then the middle regions will usually be empty of hadrons: Further details on multiplicities and the phase space-geography of the parton model are discussed by Bjorken [35], Savit [208], and by Ellis and Kislinger [110].

Let us briefly compare several models. In the hadronic multiperipheral model, the active process is just meson–meson scattering and the average high-p_T jets consist of only a limited number of particles. The fusion process $q\bar{q} \to MM$ is assumed to dominate in the covariant parton model of Landshoff and Polkinghorne [177]. In the simplest version of this model we would again expect

a typical jet to contain a fixed number of particles. In the CIM another important process is qM → qM which leads to an asymmetric situation where the average multiplicity on the quark side grows with increasing p_T while the multiplicity on the other side stays fixed. Since there are potentially many different processes important in the CIM and each can have different characteristics, the average phase space population is probably more like the simple parton model.

An important prediction in the fireball model of Berman and Jacob [29] and Berger and Branson [27] is that one expects baryon number one in each jet.

2. Experimental summary

The production of particles with large transverse momentum in hadronic collisions is a subject of intrinsic experimental interest. Even if it were clear that the results could be fit by mundane extensions of ideas valid at small transverse momentums, the experiments would be valuable in order to explore and define the short-distance boundary of the strong interactions. Of course, the experiments done so far have not been mundane but have produced some big surprises. This make physics interesting and it is the interest generated by those surprises which triggered the large amount of work which now justifies this review.

In this section we attempt to summarize the available experimental data with a minimum of theoretical input. Theoretical prejudice will not be absent since it will influence what subjects we include and since it has a large effect on how we or the original authors of the papers reviewed here choose to plot data. We hope that this summary of those data which bear directly or indirectly on the nature of hadronic interactions at short distance may prove valuable a source material to those with new untried-theoretical ideas or that it can provide an entry into the original literature for those interested in more details of the experimental situation.

The data we review here includes two-body exclusive scattering through large angles, single-particle inclusive spectra, and two-or-more particle inclusive correlations. We conclude with a partial list of experiments which have been proposed and which may produce results in the near future.

Previous reviews or experimental summary talks which can be consulted for more data include Lundby [182], Walker [225], Ellis and Thun [111], Brodsky [58, 59, 60], Landshoff [169, 170], Cronin [92], Darriulat et al. [97] and Jacob [154].

2.1. Exclusive scattering at large angles

Data on exclusive 2–2 scattering processes have accumulated steadily over the years. In the forward and backward directions differential cross sections can be described by Regge parametrizations of the form

$$\frac{\mathrm{d}\sigma}{\mathrm{d}t}\,(\mathrm{AB}\to\mathrm{CD})\big|_{s\to\infty} \sim \beta(w)\, s^{2\alpha(w)-2}\,, \tag{2.1.1}$$

where $w = t$ or u. The size and energy dependence of these peripheral peaks is correlated dramatically with the quantum numbers exchanged in the t or the u channel. Fig. 2.1.1, taken from Chiu [78], indicates one aspect of this correlation which supports (2.1.1). The bulk of the existing data lies within the peripheral peaks and it is therefore not surprising that most of the theoretical

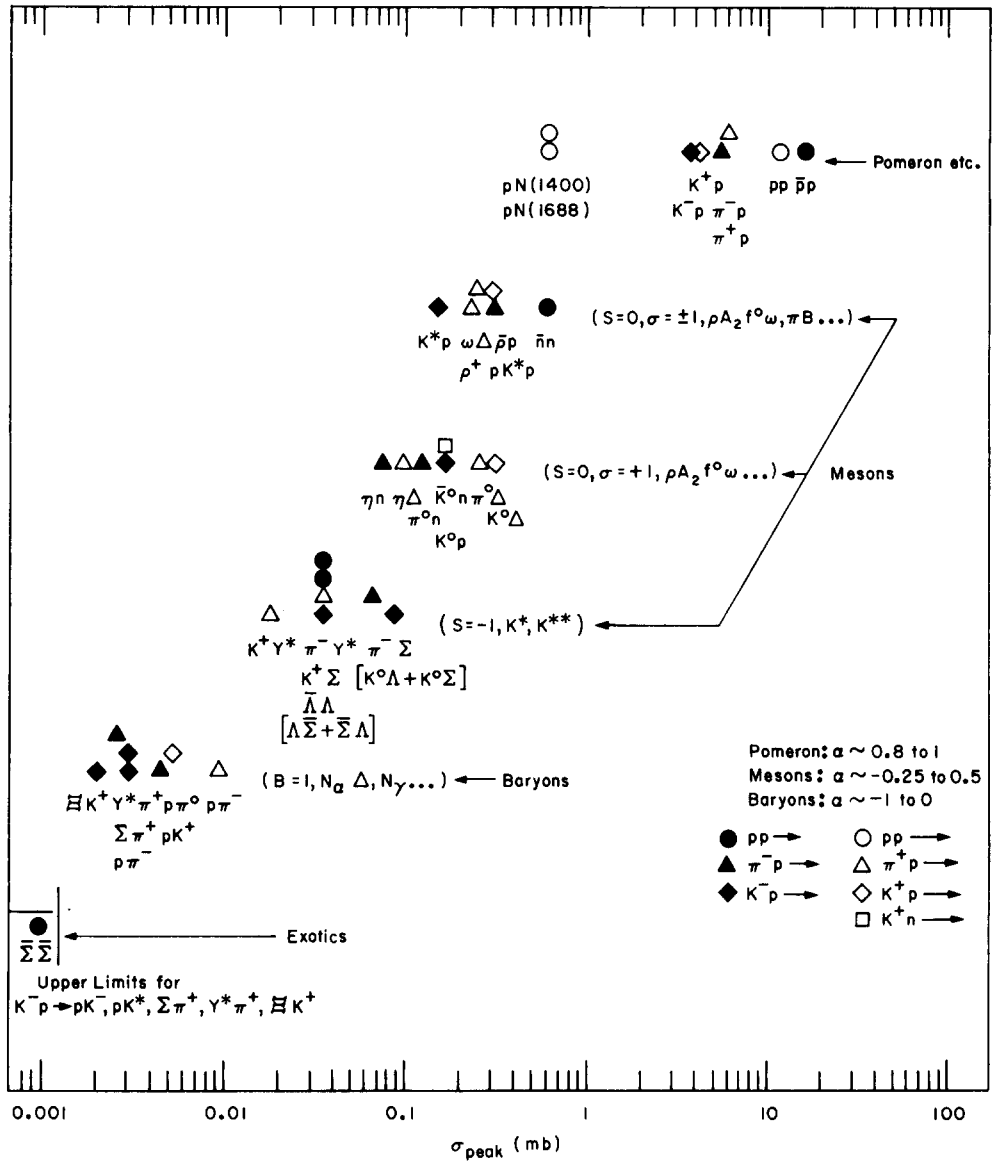

Fig. 2.1.1. Taken from Chiu [78]. The cross section of peripheral peaks at $p_{LAB} = 5$ GeV/c is correlated with the exchanged quantum numbers. The systematics of this correlation is support for the basic features of Regge theory.

attention has been directed towards this Regge region.

We are primarily interested here in the scattering of hadrons through large angles. Away from the peripheral peaks, the one thing common to all reactions is that the differential cross sections fall rapidly with energy, requiring experiments with high beam intensity and/or long running time. The kinematic range in which measurements have been made reflects this counting-rate restriction but accentuated theoretical interest in the topic may help justify the considerable experimental effort and machine time necessary to extend the coverage of this kinematic region.

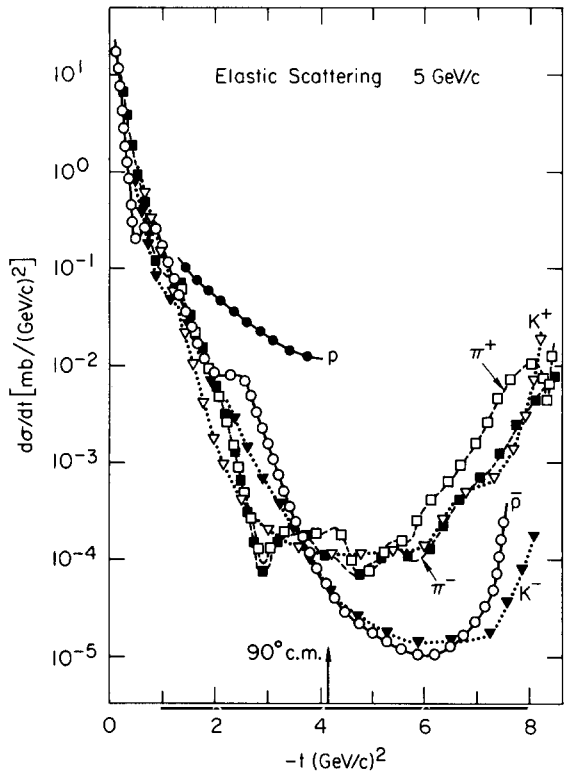

Fig. 2.1.2. Figure from Eide et al. [104] showing the elastic differential cross sections at 5 GeV/c for pp, π^+p, π^-p, K^+p, K^-p and $\bar{p}$p.

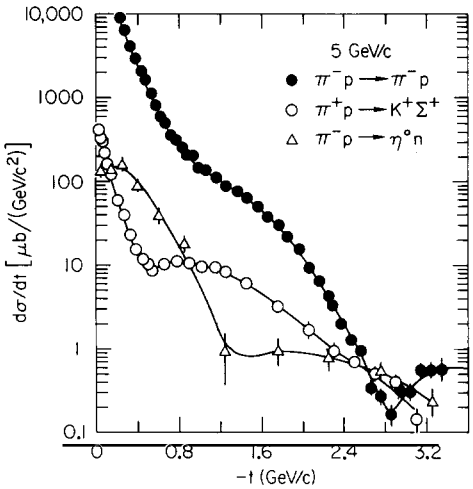

Fig. 2.1.3. The π^-p elastic cross section at 5.0 GeV/c is compared with $\pi^+p \to K^+\Sigma^+$ and $\pi^-p \to \eta^0 n$ at large t.

Differential cross sections at p_{LAB} = 5 GeV/c for pp, $\bar{p}$p, $\pi^{\pm}$p, $K^{\pm}$p elastic scattering are shown in fig. 2.1.2. In fig. 2.1.3 π^-p elastic scattering is compared with $\pi^+p \to K^+\Sigma^+$ and $\pi^-p \to \eta^0 n$. Except for pp scattering, all the other large angle cross sections are remarkably similar in magnitude at this energy. There appears to be no solid explanation for the special role of pp but the striking similarity in size of the other cross sections at 90° compared with the large differences in the size of the peripheral peaks indicated in fig. 2.1.1 is worth noting. Evidence discussed below suggests that the pp cross section falls with energy more rapidly than the others so there may be an energy regime where they are all comparable.

When considering the energy dependence of the large-angle differential cross sections, it is important to note the fact that *low-energy* non-diffractive cross sections in the forward and backward regions exhibit a rapid falloff with energy before the emergence of the peripheral peaks. This fact has been emphasized by Lundby [182]. Fig. 2.1.4 shows backward $K^{\pm}$p elastic cross sections as a function of laboratory momentum. Both reactions initially exhibit a rapid falloff at low energies which, for K^+p, is replaced above s = 4 GeV^2 by a slower energy dependence as the peripheral peak emerges. No backward peak is observed in K^-p scattering until even higher energies and for this reaction the initial energy dependence is maintained much longer. Fig. 2.1.5 demonstrates this same point. The data for backward $\bar{p}$p scattering show another reaction where, in an exotic-

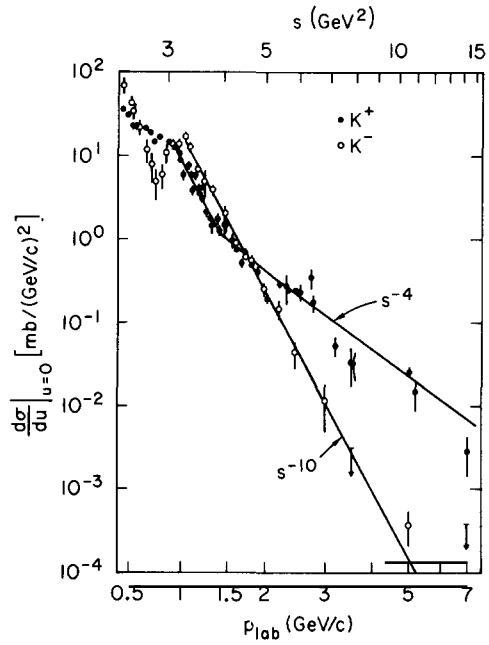

Fig. 2.1.4. Energy dependence of backward K^+p and K^-p elastic scattering.

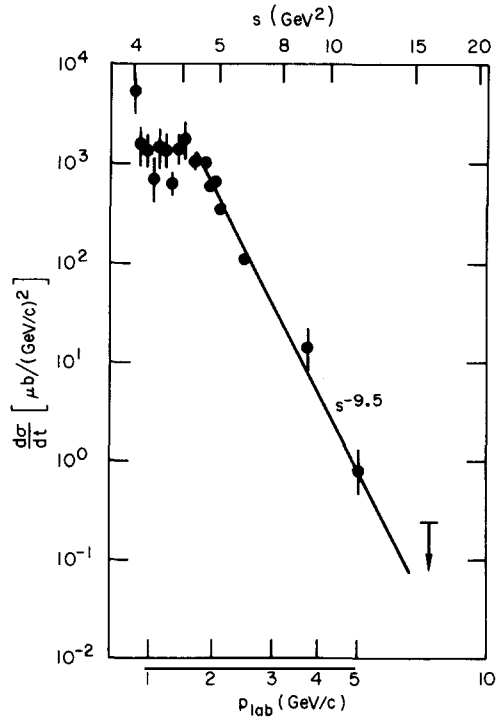

Fig. 2.1.5. Backward elastic $\bar{p}p$ scattering.

exchange channel, the typically rapid low-energy falloff of the cross section continues to a fairly high energy. A possible connection of the low-energy mechanism which is responsible for this rapid falloff with the dynamic mechanism responsible for the high-energy fixed-angle cross section will be discussed in section 4.5. This may be an interesting point to explore further since behavior of the low-energy cross sections is usually attributed to specific properties of the low-lying direct channel resonances.

One corollary of this observation is that it is possible to extrapolate the large-angle cross sections from low energies to high energies without encounting the type of dramatic break observed in fig. 2.1.4 for backward K^+p. As an example the K^+p elastic cross section as measured by Baglin et al. [19, 20], Danysz et al. [96], Akerlof et al. [3] and Yuta et al. [229] is shown in fig. 2.1.6.

Of course, the best reaction for a detailed study of the energy dependence of the differential cross section at large angles is $pp \to pp$ where we have good data over a large range of energy. The pp differential cross section at 60°, 70°, 80°, and 90° is shown as a function of $\ln s$ in fig. 2.1.7. The lines drawn through the data indicate the possibility of dip structure in the cross section at these large angles. This structure, as well as fits to the data based on current models will be discussed in more detail later. One feature in the data which is notable is the absence of any large shrinkage effects – the cross section at different angles is falling at approximately the same rate. This indicates the possibility of approximately factorizing the cross section at large angles into a form

$$\frac{d\sigma}{dt}(s, \cos\theta)\Big|_{\cos\theta \neq \pm 1} \cong f(s)\, g(\cos\theta)\,. \qquad (2.1.2)$$

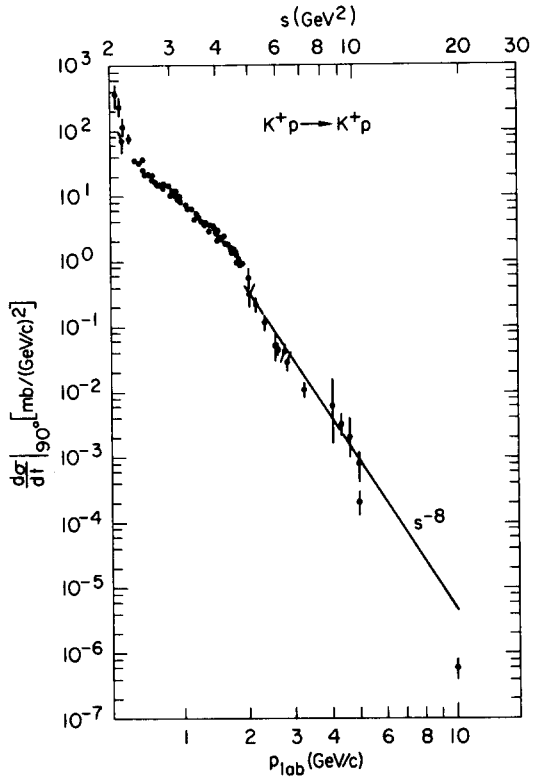

Fig. 2.1.6. K^+p scattering at 90° in the c.m.

This factorization is indicated more clearly in fig. 2.1.8 where the pp cross section data at different energies normalized to the 90° cross section are plotted as a function of $\cos\theta$. It is interesting to investigate possible corrections to eq. (2.1.2) but we will defer this until we can discuss the implications of various possible models for the cross section.

The systematics of differential cross section measurements are important but if we are to deduce amplitude structure for the various processes it is necessary to have more information. Polarization measurements are obviously important but, because of the small counting rates, there have been very few polarization experiments extending to large angles. The data of Abshire et al. [2] include polarization measurements for pp elastic scattering out to $t = -6$ GeV^2. This data is shown combined with some small-t polarization measurements in fig. 2.1.9. Two features are notable. The polarization does not vanish at large t at this energy and there is evidence for some structure, perhaps double zeros at $t \cong -1, -2.5, -4$ GeV^2. We can conclude that a single spin amplitude does not dominate in this range of momentum transfer and that the different amplitudes have potentially complicated behavior at large momentum transfer.

Another type of structure which may be important at large t consists of rapid fluctuations of amplitudes with energy or with angle. This behavior, known as Ericson Fluctuations [113], is familiar in nuclear physics. Experiments designed to look for Ericson fluctuations in pp elastic scattering have not reported any evidence for the phenomenon. Allaby et al. [5] examined pp → pp at 16.9 GeV/c over a range of angles and Akerlof et al. [3] looked at $\theta_{CM} = 90°$ over a range of

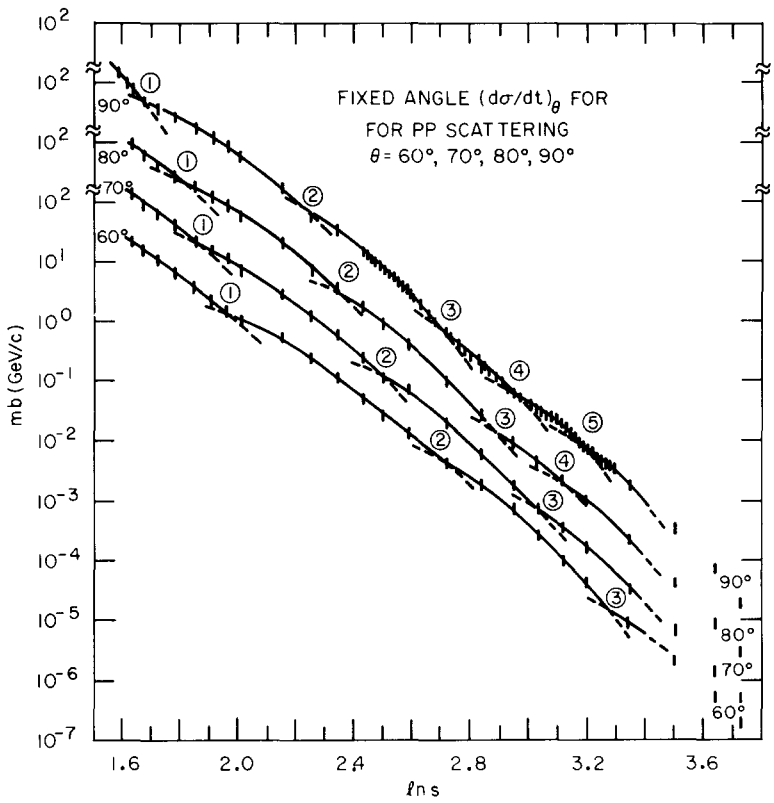

Fig. 2.1.7. pp elastic scattering at fixed c.m. angles as a function of ln (s/s_0) with $s_0 = 1$ GeV^2. Figure taken from Hendry [146]. Data are from LBL summary.

energies without seeing any sharp structure. F. Schmidt et al. [210], motivated in part by a prediction of Frautschi [123], have looked at $\pi^{\pm}p \to \pi^{\pm}p$ at 5 GeV/c. The incident beam possessed at a momentum spread $\Delta p = 120$ MeV/c but the final state scattering angles were measured with sufficient accuracy to calculate the incident momentum of a given event to $\Delta p = 14-20$ MeV/c. This allowed the data to be divided into two bins with momentum greater than or less than average. At each t, an asymmetry parameter was defined by

$$A = \frac{N(+) - N(-)}{N(+) + N(-)}. \tag{2.1.3}$$

Data on A are shown in fig. 2.1.10. The large asymmetry, particularly indicates that, in some t bins, the cross section may change by a factor of 3 when the incident energy varies by 36 MeV. It would be interesting to verify this result in other experiments and look for these fluctuations in different reactions and at different energies.

In summary, the main features which can be extracted from the data on large angle exclusive scattering are quite simple. The falloff with energy of differential cross sections is roughly like $s^{-8} - s^{-10}$ in contrast with the $s^0 - s^{-2}$ observed in high energy peripheral peaks. There is the possibility that this rapid falloff is connected to the energy dependence of cross sections close to

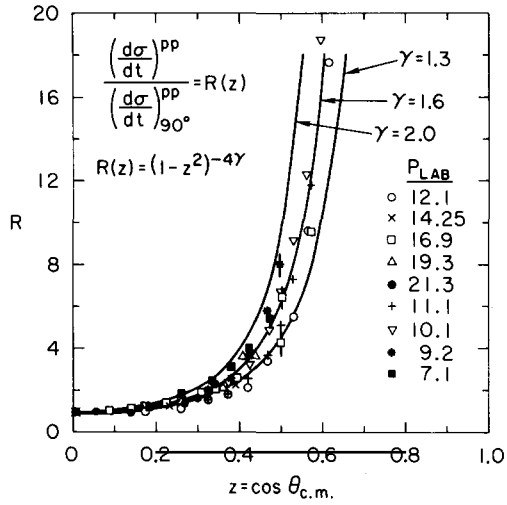

Fig. 2.1.8. Figure from Brodsky [58] showing the angular distribution of pp scattering normalized to the 90° value at various values of the incident momentum. The curves show possible fits to the angular distribution.

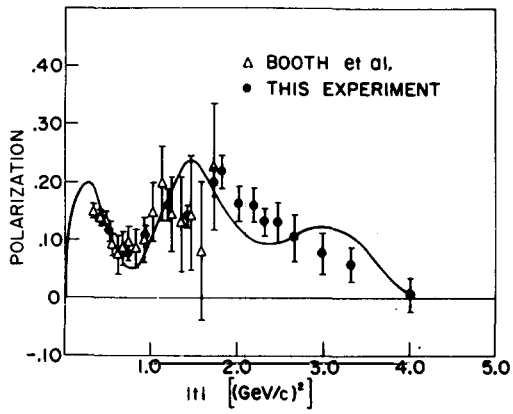

Fig. 2.1.9. Polarization in elastic pp scattering. Data from Abshire et al. [2], Borghini et al. [52, 53].

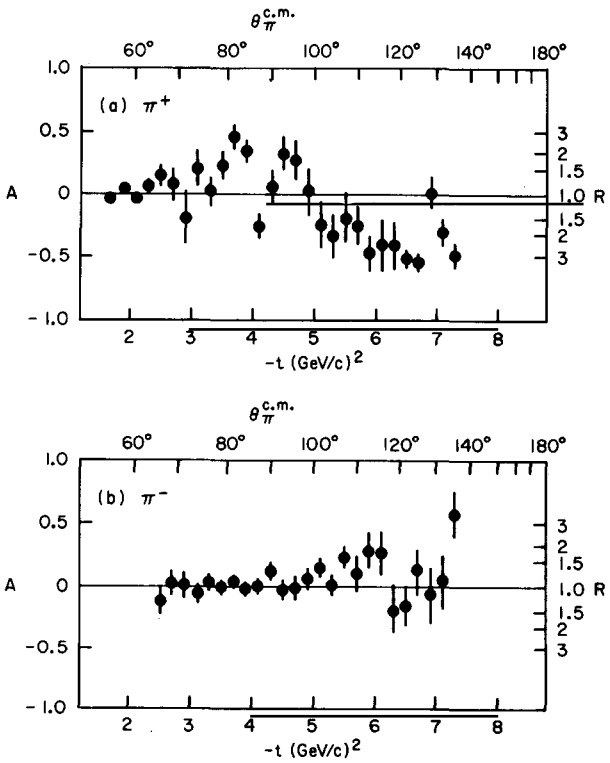

Fig. 2.1.10. The asymmetry parameter (2.1.3), in $\pi^{\pm}$p elastic scattering.

threshold so at large angles we have a smooth continuation from high energies to low energies. The pp elastic cross section is much higher than $\pi^{\pm}$p, $K^{\pm}$p and $\bar{p}$p elastic but may be falling more rapidly. There are some indications from new data on polarization and Ericson fluctuations that large angle amplitudes are not completely smooth and featureless. The question of whether all these features of the data can be accommodated within the framework of existing theoretical ideas is very interesting and we will address this problem in some detail below.

2.2. Single particle inclusive experiments

In this section we discuss experimental data on the single-particle inclusive process

$$AB \to C + \text{anything}\,, \tag{2.2.1}$$

where the detected particle is observed to have large transverse momentum. The important features of the data include the shape and energy dependence of the inclusive spectra, particle ratios, and the connection of the high-p_T spectra to those measured at low p_T.

The first high-p_T single-particle inclusive measurements at the CERN–ISR reported a yield much larger than had previously been expected. As shown in fig. 2.2.1, the invariant cross section for producing hadrons with $p_T = 5$ GeV/c is approximately 10^5 times larger than the value given by a simple extrapolation of the exp $(-6p_T)$ dependence found to be valid in the region $0.15 \lesssim p_T \lesssim 1.0$ GeV/c. The current high energy experiments with substantial data for the production of particles with $p_T > 2.0$ GeV/c are listed in table 2.1 along with some of the important experimental characteristics. This table is an updated version of a similar listing given by Ellis and Thun [111].

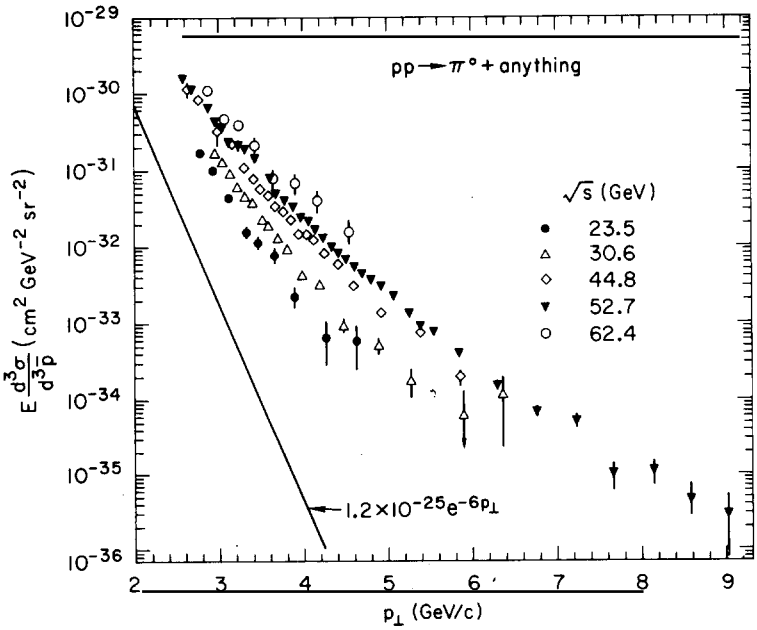

Fig. 2.2.1. Data from the CCR collaboration at the CERN–ISR on the inclusive process pp → π^0 near 90° in the CM demonstrating the excess yield over an extrapolation of the form exp $(-6p_T)$ fitted to the low p_T data.

Table 2.1
Measurements of inclusive single-particle cross sections at large p_T

Experiment	Reaction	Detector	c.m. energy (GeV)	p_T range (GeV/c)	c.m. angle (Degrees)
CERN–Columbia–Rockefeller (ISR) Busser et al. [66]	$pp \to \pi^0$ + anything	Lead-glass	23.5 30.6 44.8 52.7 62.4	2.8–4.6 3.0–6.4 2.6–5.9 2.6–9.0 2.9–4.6	90 30
Saclay–Strasbourg (ISR) Banner et al. [23]	$pp \to X^{\pm}$ + anything (X not identified) $pp \to \pi^{\pm}$ + anything $pp \to \gamma$ + anything	Magnetic spectrometer and shower counter	23.2, 30.4 44.4, 52.7 44.4, 52.7 44.4, 52.7	1.0–3.0 3.0–5.0 1.0–3.0	90
British–Scandinavian (ISR) Alper et al. [7–9]	$\pi^{\pm}$ $pp \to K^{\pm}$ + anything $p\bar{p}$	Single-arm spectrometer with two magnets Čerenkov counters added?	44 53 23–62 44 53	1.3–3.2 1.3–5.0 1.5–4.7 1.5–4.6	59 39 59 90 90
Chicago–Princeton Fermilab Cronin et al. [93]	$\pi^{\pm}$ $pW \to K^{\pm}$ + anything $pBe \to p, \bar{p}$ dd	Magnetic spectrometer	19.4 23.8 27.3	0.8–7.3 0.8–7.6 0.8–7.2	77 89 96
Fermilab Carey et al. [71,72]	$pp \to \gamma$ + anything	Lead-glass	9.8–27.4	0.2–3.0	Fixed angle in lab = 100 mrad
Columbia–Fermilab Appel et al. [12]	$pp \to \pi^0$ + anything $pp \to h^-$ + anything	Lead-glass			
CERN–Paris–Heidelberg Karlsruhe Cottrell et al. [90]	$pp \to h^+$ + anything	ISR split field magnet facility	52.5	2–4	9–21

The fact that the number of completed experiments is still small enough so that they can be included in this table is important as a reminder of how new this subject really is.

A notable fact of table 2.1 is that all the experiments we will discuss here measure proton–nucleon collisions. Experiments with pion or other types of secondary beams are still only in the preliminary stage. As we go through the following outline of results it is important to keep in mind that the various experiments are in substantial overall agreement. There are some problems concerning the relative normalization of the data from different experiments but these are minor in view of the fact that, with the steeply falling cross sections, a 10% error in measuring the absolute value of the transverse momentum can lead to more than a factor of two in the absolute value of the cross section.

The CERN–Columbia–Rockefeller collaboration (CCR), have measured π^0 production at the CERN–ISR. Gamma rays from the decay of a π^0 are detected in an array of lead-glass counters. The two photons from the decay of a π^0 are not spatially resolved and the total photon energy is

measured. The contamination in the signal at large p_T from η production is suppressed since the decay of an η would lead to photons in different counters and would be counted as two π^0's with lower transverse momentum. A more recent experiment shows that η^0/π^0 ratio = 0.55 ± 0.11 for p_T in the interval 3 to 5.6 GeV/c (Busser et al. [67]). Due to the large kinematic region spanned by this experiment, the global dependence of the data is extremely important. The claim is that all the data can be fit to the empirical form (GeV units)

$$\frac{E\mathrm{d}^3\sigma}{\mathrm{d}^3p} = \frac{A}{p_T^n} \exp(-bx_T) \tag{2.2.2}$$

(see eq. (1.2.3) in the Introduction) where $x_T = 2p_T/\sqrt{s}$, A = 15.4 mb, n = 8.24 ± 0.05 and b = 13.05 ± 0.25. Because of the systematic errors the data are consistent with n = 8 which was the power predicted by the constituent interchange model (Blankenbecler, Brodsky and Gunion [41, 42]) for this process.

Three other experiments have measured γ-ray yields. The Saclay–Strasbourg collaboration (SS) have data on pp → γ for values of $p_T \lesssim 3.0$ GeV/c. These measurements can be converted to π^0 spectra assuming there is no other major source of high energy photons so that the interpretation of the data requires suppression of η production. The SS results generally support the p_T and energy-dependence of the CCR data in the region of overlap except that an overall normalization factor of approximately 0.7 is needed which brings (2.2.2) into agreement with the SS rate (see Busser et al. [67]).

The FNI collaboration (Carey et al. [71,72]) measured pp → γ + anything at Fermilab for fixed lab angles of 80, 100 and 120 mrad. For incident proton energies from 50 to 400 GeV/c. This translates to a range of θ_{CM} from 40° to 110°. Converting to a π^0 invariant cross section they fit their data at all angles to the form (GeV units)

$$\frac{E\mathrm{d}^3\sigma}{\mathrm{d}^3p}(\mathrm{pp} \to \pi^0\mathrm{X}) \propto (1-x_R)^4 (p_T^2 + 0.86)^{-4.5}, \tag{2.2.3}$$

where $x_R = p^*/p_{max}$ is the radial scaling variable. Since the bulk of the data is at a lower energy than either CCR or SS, it is difficult to make a direct comparison. There appears to be no direct conflict but the form (2.2.3) when extrapolated does not agree with other data.

The final γ experiment we will be discussing here, a Columbia–Fermilab collaboration (CF) (Appel et al. [12]), used a beryllium target. When converted to produce the cross section per nucleon the experimental results indicate a good agreement with a modification of the CCR fit designed to fit smoothly onto the low-p_T data. The quoted parametrization, given in eq. (1.2.3), gives some support to the results of CCR but there are some normalization problems associated with the nuclear target which we will discuss below.

The inclusive production of charged particles in proton–nucleon collisions has been measured by three groups, the Saclay–Strasbourg collaboration (SS) and the British Scandinavian collaboration (BS) at the CERN–ISR and the Chicago–Princeton (CP) group at Fermilab.

The Saclay–Strasbourg group (Banner et al. [23]) measured both charged particles and π^0's. One of the first high p_T experiments, their original results are consistent with the more detailed results reported since.

The CP experiment (Cronin et al. [93, 94]) has measured the production of charged hadrons at p_{LAB} = 200, 300, 400 GeV/c at Fermilab. The measurements were taken at fixed laboratory angles but these were chosen to be near 90° CM in the energy range scanned (77°, 89°, 96°, respectively).

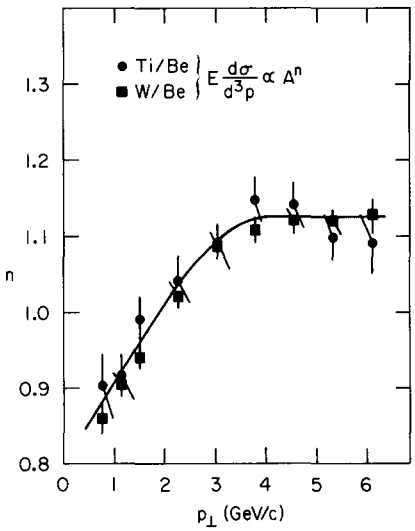

Fig. 2.2.2. Dependence on the atomic number A of the nuclear target for the reaction p + A $\rightarrow \pi$ + anything as a function of p_T. Data from CP collaboration.

The experiment was run with nuclear tungsten target. At 300 GeV/c the measurements were repeated with other targets in an attempt to understand the nuclear effects. The first result, indicated in fig. 2.2.2, is that the variation of the invariant cross section for π production with the atomic number A is approximately linear for large p_T. This suggests the approximate validity of the impulse or single-scattering approximation inherent in the parton model. At small p_T the cross section is supposed to scale more like $A_{eff} = \sigma_{abs}/\sigma_p$. The fact that the large p_T cross section is closer to being proportional to $A^{1.1}$ than $A^{1.0}$ and that particle ratios depend on A in a nontrivial way at large p_T, indicates there may be some additional rescattering effects but these will not be considered further here.

One important aspect of this experiment is the large values of $x_T = 2p_T/\sqrt{s}$ at which cross sections are measured. For $\pi^\pm$ production they measure out to an x_T of 0.72 while the CCR measurements for π^0 are all taken below $x_T = 0.35$. This means that CP are sensitive to the x_T dependence of the data in spite of their comparatively small range of $\sqrt{s}$. For $x_T \geqslant 0.4$, the pion data can be parametrized by a form

$$\frac{E\,d^3\sigma}{d^3p} \propto s^{-5.5\pm0.2} \exp\{-(36.0 \pm 0.4)x_T\}\,. \tag{2.2.4}$$

For $x_T < 0.35$ the data agree with the CCR experiment. The effective power of s in the CP data (see Cronin [92]) is shown in fig. 2.2.3 plotted against x_T. For low x_T, the power of s in this type of parametrization is sensitive to finite mass effects and, for $x_T = 0$, must equal zero in order to agree with Feynman scaling.

Particle ratios in the CP experiment are shown as a function of p_T in figs. 2.2.4 and 2.2.5. In view of the evidence that there might be some nuclear effects which are important in the particle ratios, it is important to look at the particle composition from pp collisions. The British Scandinavian data on particle composition at $\sqrt{s} = 52.8$ GeV is shown as a function of p_T in fig. 2.2.6. The

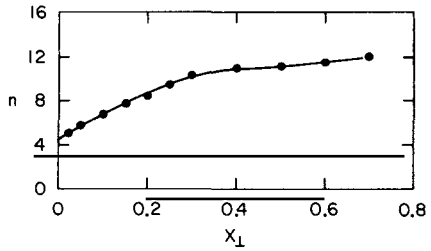

Fig. 2.2.3. The effective power of s in a fit to the CP data on $pp \to \pi$ of the form $E\,d^3\sigma/d^3p \propto s^{-n} f(x_T)$. Figure from Cronin [92].

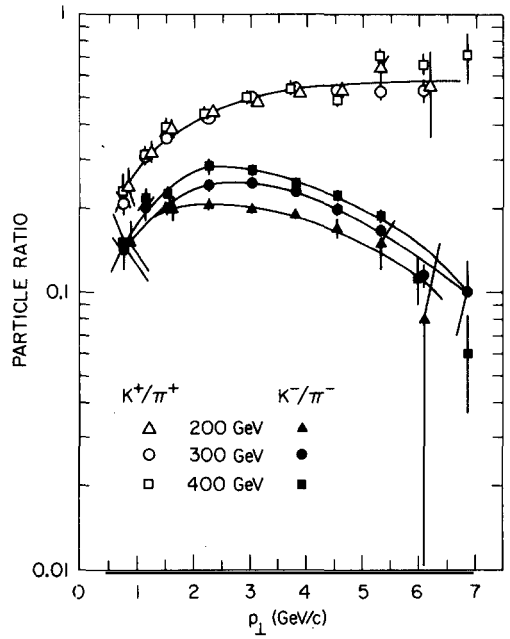

Fig. 2.2.4. K/π ratios at FNAL. Data from CP collaboration.

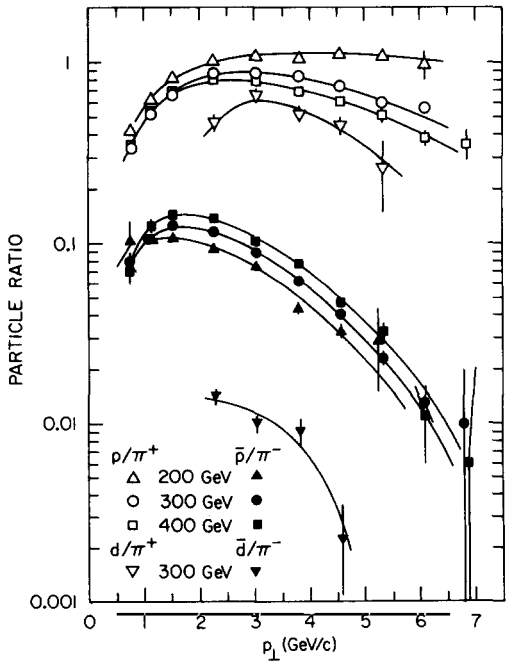

Fig. 2.2.5. Particle ratios at FNAL. The d/π and $\bar{d}/\pi$ ratios are multiplied by 10^2. Data from CP collaboration.

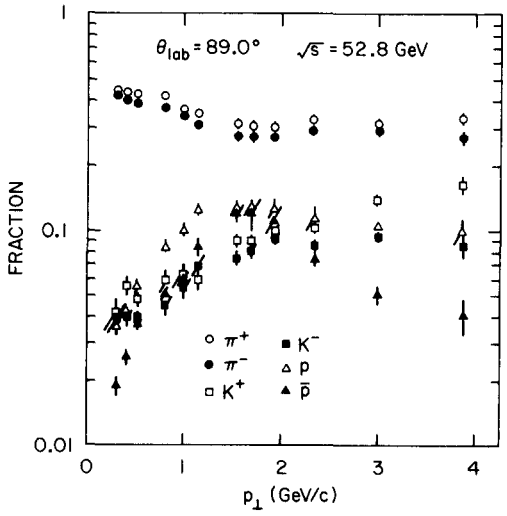

Fig. 2.2.6. Charged particle composition as a function of p_T at $\sqrt{s} = 52.8$ GeV. Data from CP collaboration.

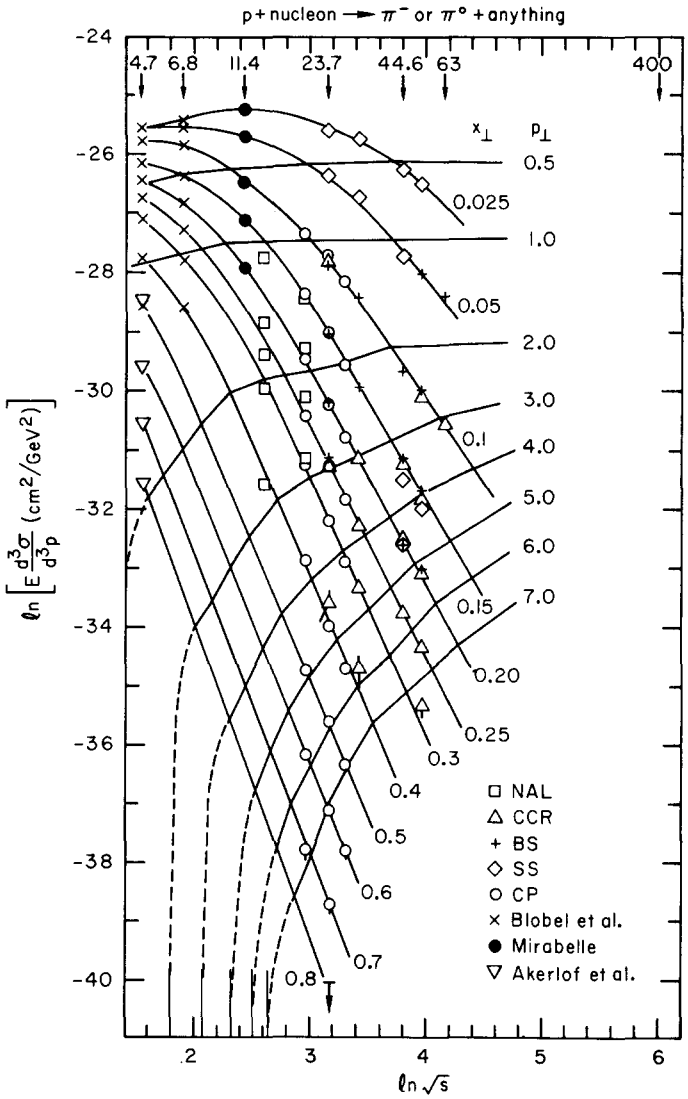

Fig. 2.2.7. Figure from Cronin [92]. Global dependence of data on pN → πX is demonstrated by the behavior of cross section at fixed p_T and fixed x_T.

overall agreement is quite good. It is notable that the ratio K^+/π^+ appears to approach an asymptotic constant while K^-/π^- and $\bar{p}/\pi^-$ are falling. It is interesting that $\bar{p}/p \cong 1$ near $p_T = 1\frac{1}{2}$ GeV/c.

Another important measurement from these two groups is the detection of heavy particles. The CP data on deuteron and antideuteron production are shown in fig. 2.2.5. In the momentum interval $2 < p_T < 5$ GeV/c the BS collaboration report a ratio

$$\bar{p}/\bar{D} = 1.2 \times 10^3 \qquad (2.2.5)$$

and a ratio

$$d/\bar{d} = 3.5 \pm 1.5\,. \qquad (2.2.6)$$

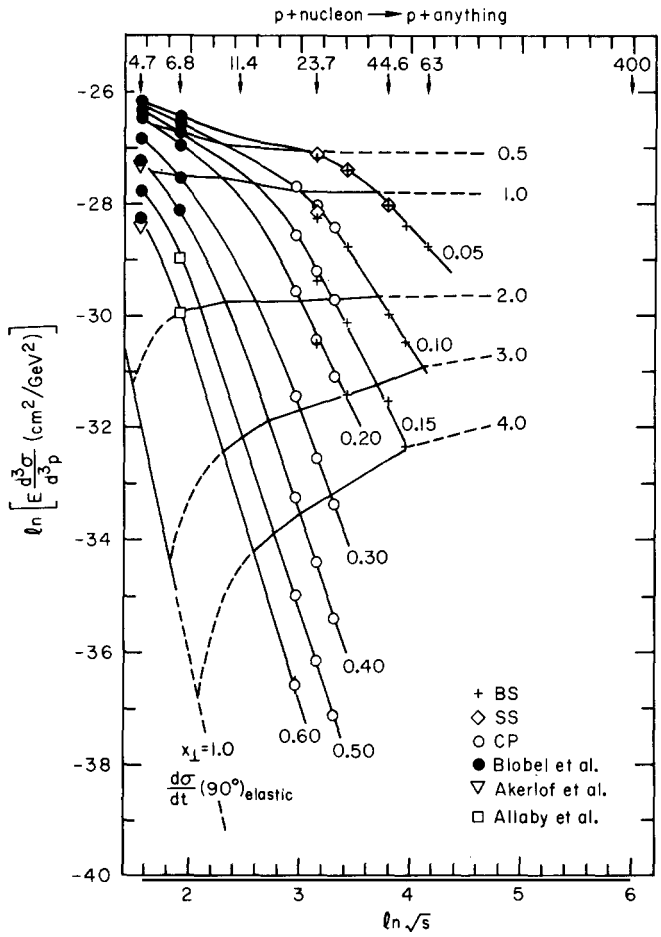

Fig. 2.2.8. Figure from Cronin [92]. Data on pN → pX at 90°.

Comparison with the deuteron–antideuteron ratio of CP shows that the ratio (2.2.6) is strongly s-dependent and consistent with approaching 1 at small p_T.

To study the global dependence of single particle inclusive data the plots in figs. 2.2.7 and 2.2.8 due to Cronin [92] are valuable. These graphs show the cross section on a logarithmic scale plotte against ln s. The lines drawn in are contours of constant p_T and constant x_T. These figures clearly show the absence of and importance of data extending to large values of x_T in the CERN–AGS-Serpukhov energy regimes. In view of the smoothness with which exclusive cross sections at large angle continue down to low energy it would be extremely interesting to see the "low-energy" behavior of the large p_T cross sections observed at Fermilab and the CERN–ISR. What low-energy data does exist joins smoothly onto the large p_T–large s data and, on this plot, there does not appear to be a sharp distinction between the large p_T and the low p_T regimes. An interesting fact (Walker [225]) is that the energy dependence of the large p_T π-production data is similar to the energy dependence of $\bar{p}$ production at low p_T. This is illustrated in fig. 1.4, reinforcing the feeling of continuity between the large p_T and small p_T regimes. Perhaps the initial conclusions empha-

sizing the difference of the two regimes based on an extrapolation of the exp $(-6p_T)$ form were not well founded.

The single particle inclusive spectra presented here will soon be supplemented by new data in other kinematic regions and with other beams. We will return to expectations for this data based on fits with current models to the existing data in section 5.

2.3. Data on correlations and associated multiplicities

The most decisive tests of models based on specific dynamical mechanisms involve the complete phase space structure of individual events containing a large p_T particle. Until such data are available we can construct partial tests using available data on two-body correlations and associated multiplicities. Since the experiments which measure these quantities are much more difficult than single-particle inclusive measurements, we can only make a beginning at answering those questions which enable us to discriminate between different models.

In order to understand the issues involved, recall that hard scattering models assume the existence of a quasi-two-body subprocess which leads to large transverse momentum in a single step. This substructure can be used to define the jet hypothesis. Event-by-event, the population of secondary hadrons is confined to the usual low p_T region and to two approximately coplanar regions along the direction of the high p_T particles. These jet axes approximately coincide with the direction of the underlying constituents after scattering. The jet hypothesis is illustrated in fig. 1.6 taken from Savit [208].

When we detect a large transverse momentum hadron, say with a finite value of $x_T = 2p_T/\sqrt{s}$, we know that its momentum must be balanced by the other particles in the event. It is a dynamical question *how* this balancing takes place. If it is balanced *only* by particles with small transverse momentum, one obviously needs a large number of these associated particles, at least

$$\langle n_A \rangle \simeq \tfrac{1}{2} x_T \sqrt{s}/\langle p_T \rangle \cong p_T/\langle p_T \rangle . \tag{2.3.1}$$

If, on the other hand, there is an underlying hard interaction the momentum can be balanced by one particle with equal and opposite transverse momentum. Most models choose intermediate behaviors for associated multiplicity, often logarithmic. A more detailed discussion of the model predictions can be found in the review of Bjorken [34].

One type of experiment which is extremely valuable is that done by a Brookhaven–Purdue–Virginia Polytechnic collaboration (Anderson et al. [11]). Using a multiparticle spectrometer system (ARGO) they measured the mean charged multiplicity associated with a high transverse-momentum proton or pion. The data on $\langle n_c(p_T, \mathcal{M}) \rangle$ for the reaction

$$pp \to p + X$$

at $p_{LAB} = 28.5$ GeV/c are shown in fig. 2.3.1b as a function of the transverse momentum of the proton for different values of missing mass. A striking feature of the data is a rise of $\Delta\langle n_c \rangle$ charged particles over an interval of approximately 0.3 GeV/c in p_T. The location of the structure moves to smaller p_T as the missing mass increases. The position of the structure is found to be approximately fixed in angle at around $\theta_{CM} = 33°$ ($\tan\theta_{CM} = 0.66$). The structure is seen in all pronged cross sections. Outside the region of the rise $\langle n_c(p_T, \mathcal{M}) \rangle$ is approximately independent of transverse momentum except for possible kinematic effects. This type of sudden structure was not predicted by any model. Possible explanations such as a change over from one fireball to two

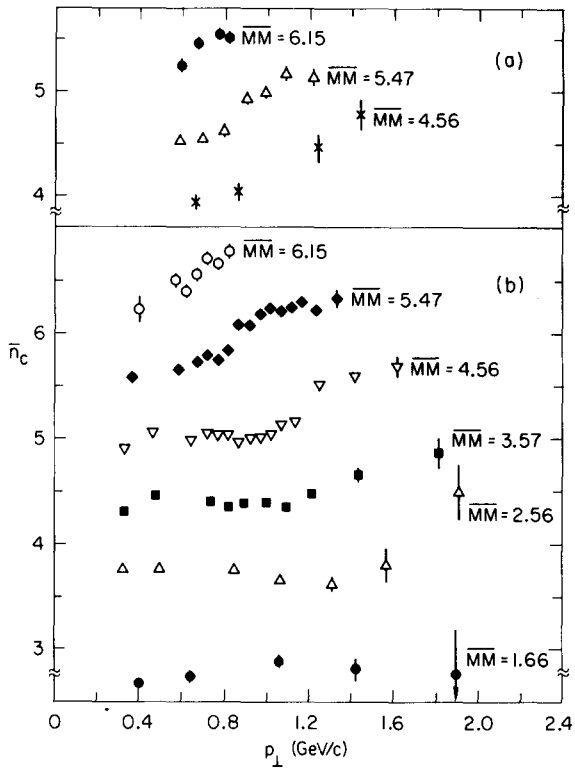

Fig. 2.3.1. Figure from Anderson et al. [11]. (a) shows data on associated multiplicities for the reaction pp → π^+MM and (b) gives associated multiplicities for pp → p + MM. In both reactions the multiplicities plotted include the trigger particle.

fireballs or a damping of bremsstrahlung in a hard scattering model do not seem to work in detail. However, Alonso and Wright [6], find the sharp transition in multiplicity can be accommodated in a two component model consisting of a hard scattering term plus a normal hadronic background. There is a definite need for more theoretical work in this area as well as more experiments of this type at both higher and lower energies.

The same group has also presented data on $\langle n_c^\pi(p_T, \mathcal{M}) \rangle$ in the reaction

$$pp \to \pi^+ + \text{anything}$$

which is plotted in fig. 2.3.1a. These data also show a jump structure. An interesting fact is that the difference $\Delta = \langle n_c^p(p_T, \mathcal{M}) \rangle - \langle n_c^\pi(p_T, \mathcal{M}) \rangle$ is almost independent of both p_T and $\mathcal{M}$ over the entire kinematic region. A plot of this quantity is shown in fig. 2.3.2.

As interesting as the Brookhaven–Purdue–Virginia Polytechnic data are, we cannot be sure that we are at high enough energy to be sensitive to the same dynamics that dominate FNAL and ISR. Its real importance for our present purposes is that it provides a basis of comparison for higher energy data to come. We therefore turn to data from three ISR experiments which have reported results on multiplicities associated with a large transverse momentum particle. None of these experiments measure the momentum of the associated particles and none have acceptance over the full solid angle.

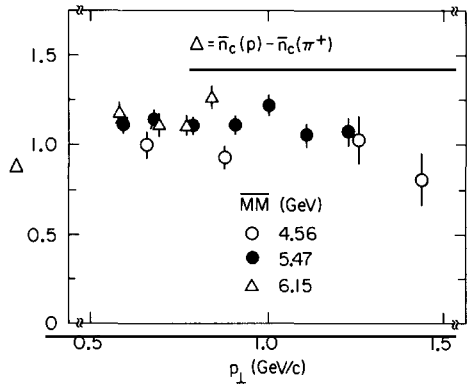

Fig. 2.3.2. Data from Anderson et al. [11] on the difference in associated multiplicities for pp → p + MM and pp → π^+MM. Various bins in missing mass are plotted as a function of p_T.

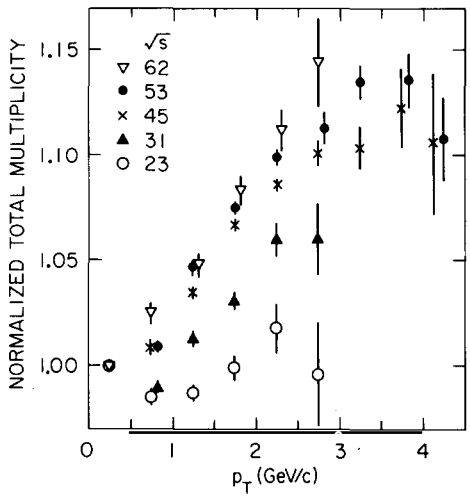

Fig. 2.3.3. Pisa–Stony Brook data on average normalized multiplicity of charged particles at $\sqrt{s}$ = 23, 31, 45, 53 and 62 GeV as a function of p_T of a trigger photon detected at $\theta_{CM} = 90°$.

The Pisa–Stony Brook experiment (see Del Prete [98]; Finocchiaro et al. [120] on charged multiplicities associated with a large transverse momentum γ has a detection system covering around 80% of the full solid angle. Data in fig. 2.3.3 demonstrate the rise in multiplicity as a function of p_T of a γ emitted near $\theta_{CM} = 90°$. The data are normalized to the multiplicities at each energy with a low p_T trigger.

In the absence of any measurements of the momentum of the associated particles, the experimenters made a parametrization

$$\langle n_A(\sqrt{s}, p_T)\rangle = \langle n^{low}(\sqrt{s} - 2p_T)\rangle + \langle n^{jet}(\sqrt{s}, p_T)\rangle \,, \tag{2.3.2}$$

where $\langle n^{low}(\sqrt{s} - 2p_T)\rangle$ is the value of the average multiplicity of low transverse momentum events evaluated at the "reduced" energy $\sqrt{s} - 2p_T$. With this crude correction for phase-space effects the value of $\langle n_{jet}(\sqrt{s}, p_T)\rangle$ is found to be roughly independent of energy

$$\langle n^{jet}(\sqrt{s}, p_T)\rangle \simeq 0.5\, p_T \,, \tag{2.3.3}$$

see fig. 2.3.4. Comparison with eq. (2.3.1) shows a contradiction unless $\langle p_T\rangle \cong 2$ for the balancing particles.

When we ask where the extra particles associated with a large p_T γ appear in phase space, we see from fig. 2.3.5 that they are concentrated in the opposite hemisphere from the trigger in a large neighborhood around zero rapidity. Momenta are not measured so the data are plotted as a function of $\eta = \log \tan(\theta_{CM}/2)$. Since the data are normalized to low p_T triggers the usual two particle correlation effect is divided out or, depending on your point of view, folded in. The basic behavior of associated multiplicities with energy and p_T is confirmed by the other experiments.

The azimuthal dependence of the multiplicity in a region around $\eta = 0$ is shown in fig. 2.3.6. Again the data is renormalized to a small p_T trigger. The multiplicity does peak in the direction

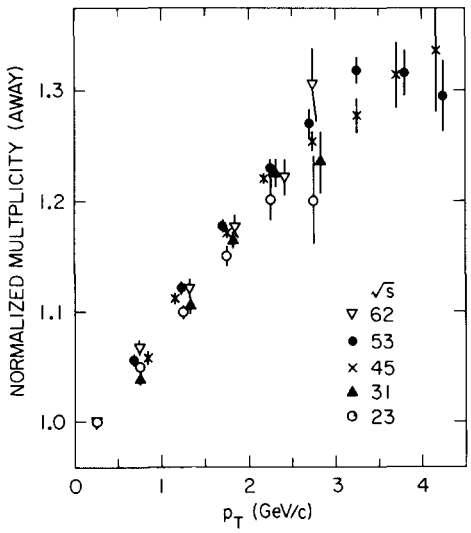

Fig. 2.3.4. Normalized multiplicities detected in a region opposite the trigger photon.

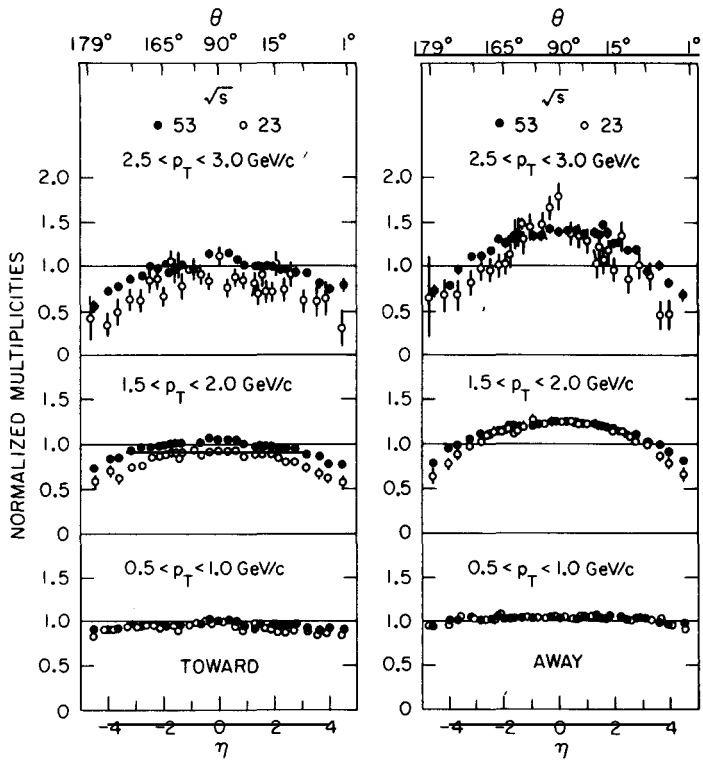

Fig. 2.3.5. Normalized partial multiplicities as a function of $\eta = \log(\tan \theta_{CM}/2)$ in the two hemispheres for $\sqrt{s}$ = 23 and 53 GeV.

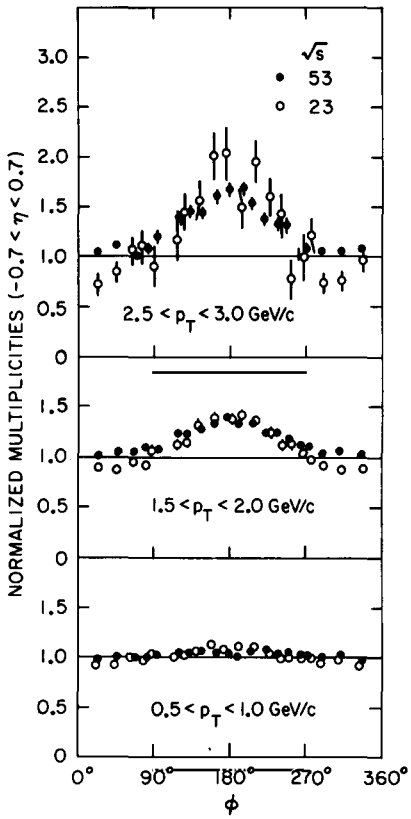

Fig. 2.3.6. Data from the Pisa–Stony Brook collaboration on normalized partial multiplicities in the interval $-0.7 < \eta < 0.7$ as a function of the azimuthal angle between the charged particle and the trigger photon.

opposite the detected γ as suggested by simple ideas concerning the conservation of momentum. The width of the distribution in the azimuthal angle ϕ is quite broad, corresponding to $\Delta\phi \approx 100°$ FWHM. The data may also be consistent with a simple form of the jet hypothesis if, in addition to a large transverse momentum jet in the opposite hemisphere there are also many low transverse momentum particles. Momentum measurements of the associated particles would prove very interesting. Data from the CCR group on azimuthal correlations between π^0's has been parametrized

$$C(\phi) = \exp\left[-B \sin \Delta\phi\right] , \tag{2.3.5}$$

where $\Delta\phi$ is the deviation in azimuthal angle from 180°. When both π_0's are restricted to be larger than 2 GeV/c they find $B = 1.5 \pm 0.2$. This translates into an average component of momentum normal to the hypothetical scattering plane of

$$\langle p_N \rangle \cong 1.3 \text{ GeV}/c .$$

This is considerably broader than is expected from simple ideas concerning jets where the spread around the hypothetical jet axis is expected to be about the same as the average momentum spread around the beam direction in "soft" scattering events. One way of quantifying this lack of

coplanarity (due to J.D. Bjorken) is to make the strong assumption of a random walk around the jet axis so that the normal component of momentum is expected to be

$$\langle p_N \rangle \cong \frac{\langle p_T \rangle}{\sqrt{2}} \sqrt{n} , \tag{2.3.6}$$

where $\langle p_T \rangle$ is the average transverse momentum in a typical hadronic process. In the parton model this equation might be expected to be approximately true with $n = 4$ reflecting the $2 \to 2$ nature of the hard scattering process while $\langle p_T \rangle \cong 0.3 - 0.4$ GeV/c. If we do not introduce a new large mass scale into the large p_T processes we are left with the alternative of considering a large number of degrees of freedom,

$$n \cong 20\text{–}35 \tag{2.3.7}$$

in (2.3.6). Since this number is not small compared to the average number of particles produced in a collision at the ISR, it suggests that most particles participate in the "balancing" of the transverse momentum.

The Pisa–Stony Brook collaboration have also triggered their apparatus at $E_{CM} = 53$ GeV on a large transverse momentum photon coming out at $\theta_{CM} = 17.5° \pm 4°$ ($\eta = 1.9 \pm 0.2$) instead of $\theta_{CM} = 90°$. In the new setting a photon has nearly 3 times the CM energy of a photon with the same transverse momentum at $\theta_{CM} = 90°$. The normalized total multiplicity, shown in fig. 2.3.7, still displays a rise with p_T but it is less rapid and begins at a larger value of p_T than in the 90° data. The angular distributions of the normalized multiplicity are compared with the 90° data in fig. 2.3.8. There is a substantial depletion in the number of particles at angles equal to or smaller than that of the photon. This effect may be due to energy and longitudinal momentum conservation. Remember that the data are normalized to low transverse momentum events where there is a positive correlation when two particles both have $\eta \cong 2$.

The direct comparison of the data at 90° and 17.5° suggest that, roughly independent of the longitudinal momentum of the trigger particle, its transverse momentum is balanced by the emis-

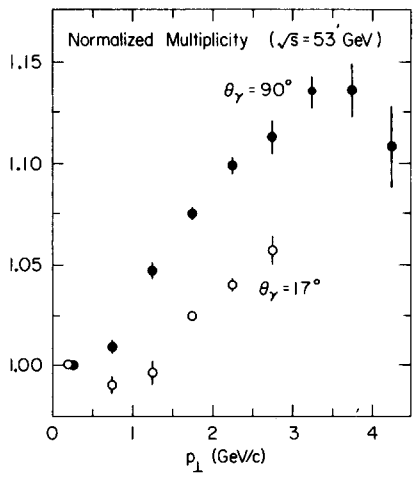

Fig. 2.3.7. Average total multiplicities of charged particles as a function of the p_T of the detected photon at $\theta_{CM} = 90°$ and $\theta_{CM} = 17.5°$.

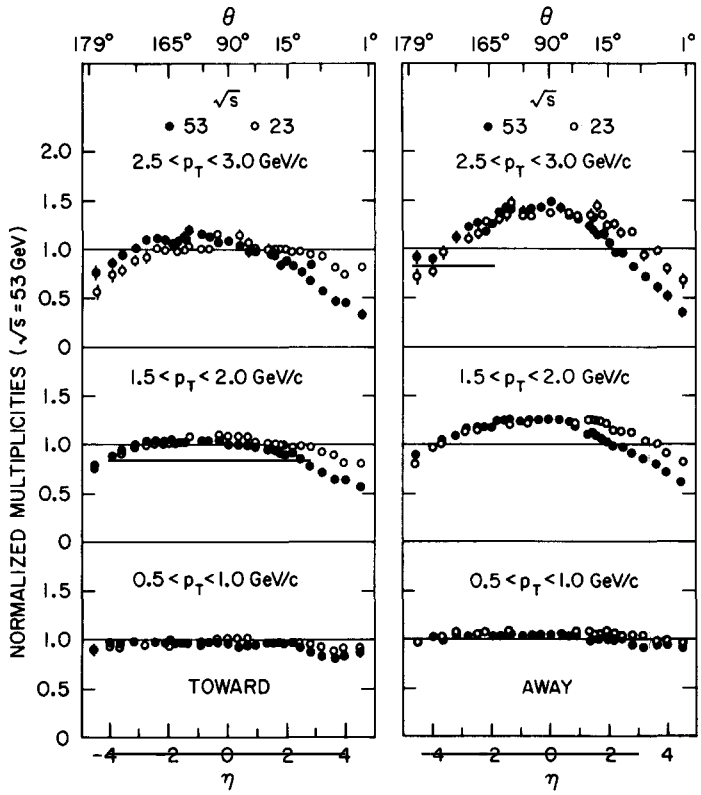

Fig. 2.3.8. Normalized partial multiplicities of charged particles as a function of $\eta = \log(\tan \theta_{CM}/2)$ in the two hemispheres towards and away from the detected photon. Detected photon at $\theta_{CM} = 90°$; detected photon at $\theta_{CM} = 17.5°$.

sion of particles at approximately $\theta_{CM} = 90°$ and spread over a wide range of azimuthal angle. The behavior is roughly consistent with a jet hypothesis but might conflict with the most naive forms of the parton model with narrow coplanarity.

In the studies of events associated with high p_T photons the Aachen–CERN–Heidelberg–Munich collaboration (Betev et al. [31]), triggered on a photon and then examined the correlation between two other particles. This important correlation function was positive over a range of $\eta \simeq 2$ and seemed to have no strong dependence on the transverse momentum of the trigger γ. This tends to say that the short-range-order hypothesis (i.e., that the correlation distribution has a fixed range in rapidity) does not break down for those events containing large p_T particles.

The CERN–Columbia–Rockefeller collaboration (Busser et al. [67]) have measured the correlation function

$$R(p_1, p_2) = \frac{E_1 E_2 \, d\sigma/d^3p_1 \, d^3p_2}{(E_1 \, d\sigma/d^3p_1)(E_2 \, d\sigma/d^3p_2)}, \tag{2.3.8}$$

for two large p_T π^o's. The data for π_0's on opposite sides are shown in fig. 2.3.9 and compared with curves calculated from the "uncorrelated jet model". The "uncorrelated jet model" consists of a factorizable matrix element and no dynamic correlations. To the extend the data agree with

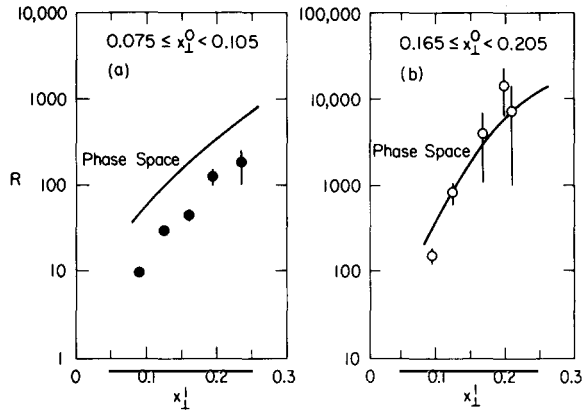

Fig. 2.3.9. Data from the CERN–Columbia–Rockefeller collaboration on the correlation function, e.g., (2.3.8), for $pp \to \pi^0\pi^0 X$, the curves represent calculations in the uncorrelated jet model (phase space).

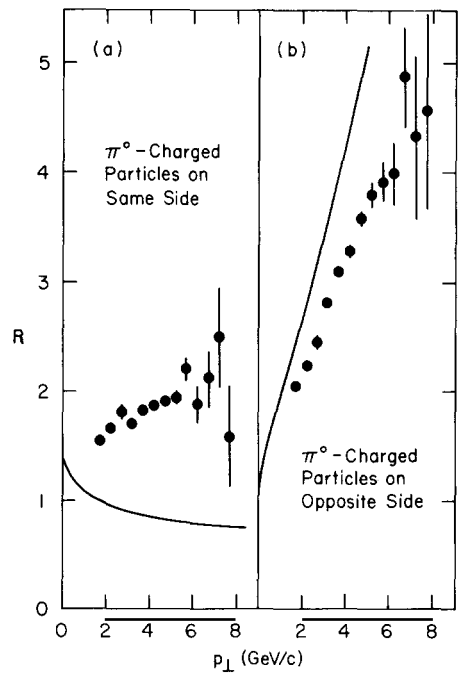

Fig. 2.3.10. Correlation function for two large p_T π^0's on the same side.

these curves we can conclude that the observed correlation is just a reflection of conservation of momentum. The correlation on the same side, fig. 2.3.10, indicates a substantial probability for producing π_0's in clusters. Whether this is just the same clustering effect observed at small p_T is not known. The plot of the distribution in the invariant mass of the $2\pi^0$ system is displayed in fig. 2.3.11.

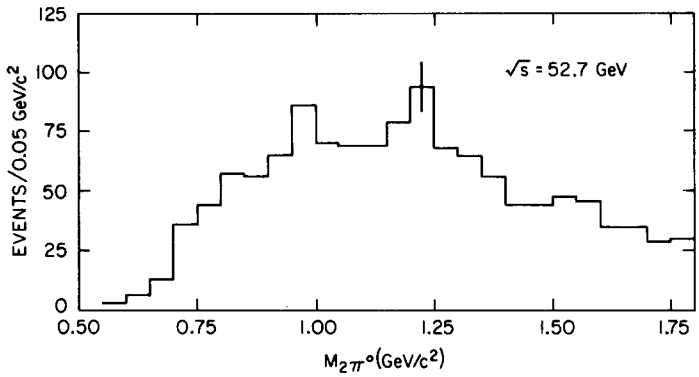

Fig. 2.3.11. Plot of the invariant mass of two π^0's on the same side of the CCR experiment. The acceptance of the apparatus suppresses low mass pairs.

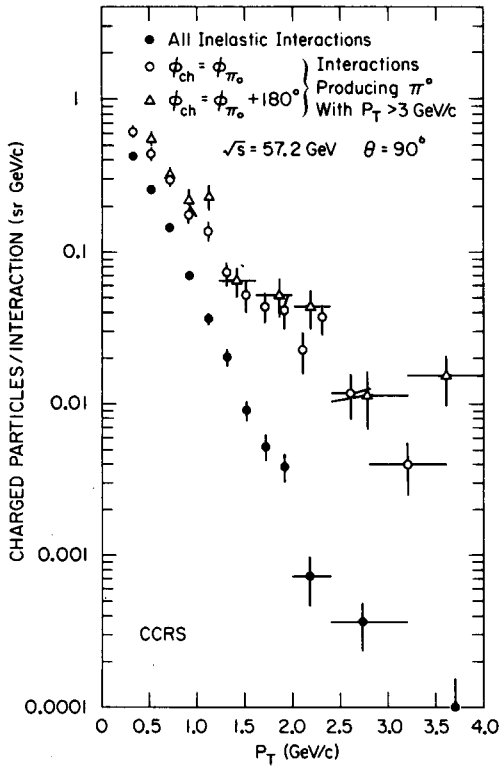

Fig. 2.3.12. Data from the CERN–Columbia–Rockefeller–Saclay experiment on the probability for detecting a charged particle with and without a trigger on a π^0 with $p_T > 3$ GeV/c. • All inelastic interactions; ○ Trigger on π_0, charged particles in same azimuthal direction of π_0. △ Trigger on π_0, charged particles in opposite hemisphere from π_0.

The CERN–Columbia–Rockefeller–Saclay group have arranged lead glass behind a magnetic spectrometer on one side of the ISR storage rings and a magnetic spectrometer on the other side

in order to study π^o-charged particle correlations. They trigger on a π^o with $p_T > 3$ GeV/c and measure the associated probability of having a large p_T charged particle. The data at $\sqrt{s} = 52.7$ GeV is shown in fig. 2.3.12. When the charged particle is opposite the π^o we see an enhancement such as that which might be expected on the basis of momentum conservation. When the charged particle is on the same side as the π^o we not only see some correlation such as might be expected from clustering but the probability of having a large p_T charged particle is approximately equal to what it is on the other side. This feature does not seem to be natural in any simple model and it is important to find out whether it persists at other energies and other choices for the particles involved. The center-of-mass motion of the hard subprocess can effect the normalization of the opposite side correlation.

We will return to the theoretical interpretation of these data in section 5.

2.4. The direct production of leptons

Another process which has attracted considerable theoretical and experimental attention involves the production of a single lepton pair. In most of the hard scattering models we discuss here, this process is related dynamically to the production of large transverse momentum hadrons and we therefore feel justified in including in this section a brief digression from our main topic. In addition, the recent observation of a heavy, narrow enhancement with mass 3.105 GeV in the reaction $pp \to \ell^+\ell^-$ + anything (Aubert et al. [17]) has intensified interest in understanding the process away from the resonant peak. In this section we review the data on the hadronic production of lepton pairs and the inclusive cross sections for single leptons and discuss briefly their implications for models.

Fig. 2.4.1 shows the data of Christenson et al. [81, 82] on the cross section for the inclusive production of lepton muon pairs. The shoulder in these data is now associated with the production of the sharp enhancement observed by Aubert et al. [17] smeared by the resolution of the spectrometer. The smooth curve is the experimentalists estimate of the "background" process $pp \to \gamma$ + anything $\to \ell^+\ell^-$ + anything. The continuum is parametrized at 29.5 GeV/c by

$$\frac{d\sigma}{d\mathcal{M}} = 2 \times 10^{-32}(\text{cm}^2)(1-\tau^4)/\mathcal{M}^{5.8}\,, \tag{2.4.1}$$

where $\tau = \mathcal{M}/(s^{1/2} - 2m_p)$.

The most popular theoretical model for the production of a massive time-like photon is the Drell–Yan mechanism (Drell and Yan [102]) in which the virtual photon is creased as a result of a quark from one initial hadron annihilating with an antiquark from the other. This contribution can be written in the form

$$\frac{d\sigma}{d\mathcal{M}} = \left(\frac{4\pi\alpha^2}{3}\right)\frac{2}{\mathcal{M}^3}\left\{\tau^2\int_0^1 dx\,dy\left[\sum e_i^2(F_i(x)\,\bar{F}_i(y) + \bar{F}_i(x)\,F_i(y))\right]\delta(xy-\tau^2)\right\}, \tag{2.4.2}$$

where the $F_i(x)$ are the quark distribution functions. Perhaps the closest analogy with large p_T hadronic processes involves the subprocess quark–antiquark annihilation into two high p_T mesons as described by Landshoff and Polkinghorne [174–176].

Since the quark distribution functions are in principle separately determined from data on electroproduction and neutrino interactions, the formula (2.4.2) involves no undetermined coeffi-

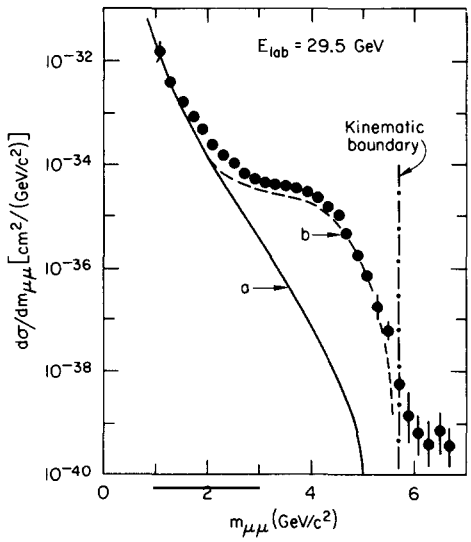

Fig. 2.4.1. Figure taken from Lederman [179] displays the data on pN → $\mu^+\mu^-$ + anything at BNL. The solid curve represents a fit after the effects of the $\psi(3100)$ and $\psi(3700)$ are removed.

cients. There is an uncertainty of a factor of 3 depending on whether or not quarks carry SU(3) color. This contribution alone does not seem able to describe the data. Note particularly that the $\mathcal{M}$-behavior at fixed τ does not agree with (2.4.1).

A different model has been suggested by Berman, Levy and Neff [30] in where there is the production of a virtual charged particle which bremsstrahlungs a massive photon. This model is not absolutely normalized since we need to make some assumptions about the production of off-mass-shell particles. Using something like inverse vector dominance logic we can argue that any of the mechanisms we have discussed, CIM, fireball models, etc., which can create vector mesons can be used to make massive photons. These extra mechanisms may perhaps make up the difference between the data and the contribution from quark–antiquark annihilation.

Recently a number of experiments have reported data on the inclusive reaction (Jain et al. [157]; Boymond et al. [56]; Appel et al. [13])

$$\text{p + nucleon} \to (\text{lepton})^{\pm} + \text{anything}\,, \tag{2.4.3}$$

(where the "direct" leptons are those not attributable to π or K decays) for $\sqrt{s}$ between 11 and 53 GeV. As demonstrated in figs. 2.4.2 and 2.4.3 experiments are in agreement with the observation that the ratio

$$\mu/\pi \cong 10^{-4} \tag{2.4.4}$$

is approximately independent of p_T. The Drell–Yan mechanism and the other methods of producing massive lepton pairs can contribute but are to be small. Since the ratio is roughly constant, this employs a power p_T^{-8} at fixed $\mathcal{M}^2/s$ approximately the same as hadronic production, which is quite difficult from the p_T^{-4} prediction of the Drell–Yan mechanism. Of course, we expected contributions from the decays of ρ^0, ω^0 and ϕ^0. Since these are expected to have the correct p_T dependence,

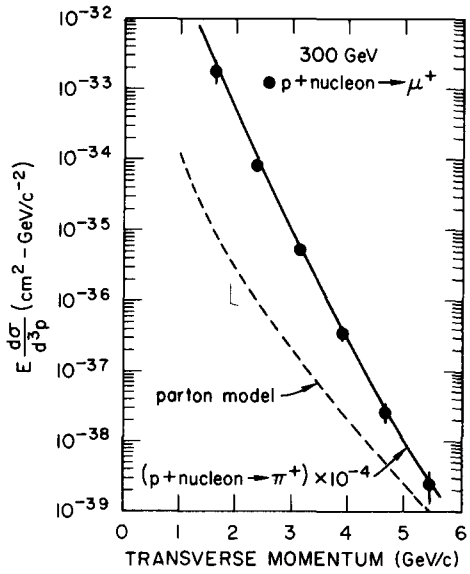

Fig. 2.4.2. Data on pN → μ^+ + anything at 300 GeV/c from the Chicago Princeton collaboration. As do many other experiments, they find muon/pion ratio of approximately 10^{-4} independent of p_T.

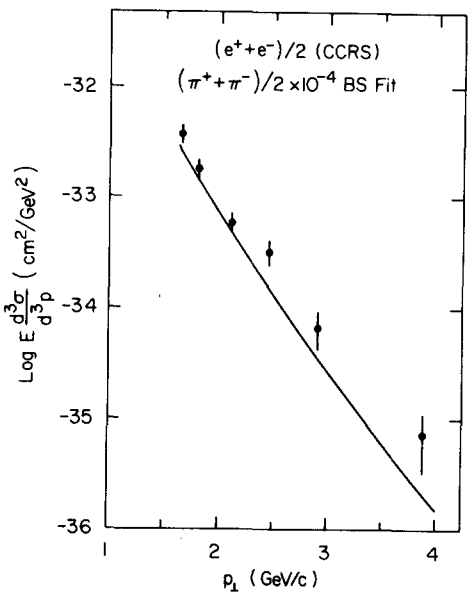

Fig. 2.4.3. A comparison of direct electron production as measured by the CCRS group with charged pion production as measured by the BS group.

let us see whether the ratio (2.4.4) can be attained. In the spirit of cluster models (see the review of Ranft [203]), let us consider the most extreme case and assume that a significant fraction of all π's observed come from the decay of the known vector mesons. With equal production of

$$\rho^+, \rho^-, \rho^0, \omega^0 \to 3\pi^+ + 3\pi^- + 3\pi^0 + (0.67 + 0.76) \times 10^{-4} \mu^+\mu^-$$

we could expect a ratio

$$\mu^+/\pi^+ = \tfrac{1}{3} \times 1.43 \times 10^{-4} = 0.48 \times 10^{-4}\,.$$

Now if there are substantial ϕ's produced a reasonable contribution from their leptonic decays can be expected. If we assume $\sigma(\rho^0) = \sigma(\rho^\pm) = \sigma(\omega)$ and put in the fact that the production of ϕ's from proton–proton collisions should be suppressed dynamically $\sigma(\phi_0) = \epsilon\sigma(\rho^0)$ we get a ratio

$$\frac{\mu^+}{\pi^+} = \frac{1.43 + 2.5\epsilon}{3 + 0.15\epsilon} \times 10^{-4}\,,$$

which can be made roughly consistent with the experimental ratio if ϵ is fairly large. The experimental data on ϕ production (Busser et al. [67]) yields

$$\sigma(\phi_0)/\sigma(\pi^-) \leqslant \sigma(\phi_0)/3\sigma(\rho_0) = \tfrac{1}{3}\epsilon \leqslant 0.2$$

but from other sources (for example, $\{d\sigma/dt\,(\pi^- p \to \phi n)\}/\{d\sigma/dt(\pi^- p \to \omega n)\} \lesssim 1/280$), we might expect ϵ to be much smaller.

If we neglect ϕ production as a source of μ's we are left with a large cross section to explain, for example, the production of charmed particles or of ψ, ψ'.

Now because of the large branching fraction of the $\psi(3105)$ into lepton pairs (Augustin et al. [18]) we can use the single lepton cross section to put an upper bound on the production of ψ's in high energy pp collisions. Using the above assumption we get

$$\sigma(\psi)/\sigma(\rho_0) < 2.8 \times 10^{-3}, \qquad \sigma(\psi)/\sigma(\pi^{\pm}) < 9.3 \times 10^{-4}.$$

This is considerably larger than the observed ratio of cross sections at BNL or FNAL so that unless the amount of ψ production grows significantly with energy the new particles do not give a major contribution to the single lepton rate.

3. Models without pointlike constituents

It is an interesting exercise to see how we would go about describing the large-transverse momentum behavior of hadronic models without pointlike constituents. Since the quarks within hadrons are well hidden, it is possible that, at some level, we do not need to invoke quarks as essential degrees of freedom to describe the dynamics of hadronic collisions. It seems evident, for example, that the diffractive scattering of high energy hadrons has very little to do with the interactions of individual quarks. On the other hand, deep inelastic lepton scattering data display strong evidence for quark-like constituents in the proton. Without careful discrimination, it is not immediately clear whether large-transverse-momentum hadronic processes will be sensitive to quark structure.

We shall see here that nonparton approaches to large-angle scattering processes have been relatively successful. For present data, their predictions are at least as successful as those of constituent models. To describe inclusive data, however, models without partons must apparently find a new framework or new dynamical mechanisms in order to be competitive.

3.1. Nonparton models for fixed-angle scattering

Models for the scattering of two hadrons through a large angle at high energy are divided naturally into two classes according to whether the underlying interactions is governed by a distance scale or whether it is pointlike. Dual models (Krzywicki [166, 167]), geometrical models (Chu and Hendry [83, 84], Schrempp and Schrempp [212, 213]), statistical models (Frautschi [123], Eilam et al. [105]) belong to the former class while the second group relies on ideas based on pointlike constituents tested in electroproduction. The parton model (Abarbanel, Drell and Gilman [1], Horn and Moshe [148]), constituent interchange model (Blankenbecler et al. [41,42]), the massive quark model (Preparata [200]), and the constituent counting rules of Brodsky and Farrar [62] and Matveev et al. [183] based on study of Feynman diagrams are examples of models without a distance scale. More details can be found in the article by Sivers [216].

Historically, one of the first formal discussions of high energy fixed angle amplitudes was in the form of a lower bound developed by Cerulus and Martin [75]. This work was very important in that it first showed how an amplitude at fixed angle is constrained by analyticity postulates.

The bound of Cerulus and Martin occurs if we assume:

1. The amplitude, $A(s,z)$, has the usual Mandelstam analyticity. That is, it is analytic in the z plane cut from $-\infty$ to $-(1+c/s)$ and from $(1+c/s)$ to $+\infty$ where c is some constant;

2. There is a finite domain in the z-plane in which the amplitude is bounded by s^N.

Through the use of a clever conformal mapping and the application of Hadamard's three circle

theorem, Cerulus and Martin showed that these assumptions imply the fixed angle lower bound,

$$|A(s,z)| \geqslant d \exp\left[-c(z)\, s^{1/2} \ln s\right] , \tag{3.1.1}$$

where $c(z)$ is some positive function of $z = \cos\theta$.

Aside from being a triumph in the application of complex variable techniques to high energy physics, the bound (3.1.1) has turned out to have phenomenological impact. Motivated, in part, by an empirical fit to the differential cross section of pp scattering by Orear [192],

$$(\mathrm{d}\sigma/\mathrm{d}\Omega) \cong A \exp(-q_T/q_0) = A \exp(-q \sin\theta/q_0) , \tag{3.1.2}$$

where $A = 34$ mb/sr and $q_0 = 0.151$ GeV/c, Kinoshita [159] proposed that the bound (3.1.1) may be saturated by physical amplitudes for angles outside of the peripheral peaks. He formulated the principle of a "minimal interaction" which implies that fixed angle scattering amplitudes should assume the smallest value consistent with the general requirement of analyticity and unitarity. This hypothesis implies the absence of any really "hard" component in hadronic scattering so that instead of observing frequent collisions in which hadrons scatter through large angles we find instead the production of new hadrons at high energy.

Using the uncertainty relation, Kinoshita's conjecture can be given a simple geometrical interpretation. Let us, for example, assume that there is an absence of fine structure so that the uncertainty relation can be interpreted as an approximate equality for some $\Delta L(s)$, the range in angular momentum in which the scattering amplitude is significant,

$$A(s,\theta)/A(s,0) \cong \exp\{-\Delta L(s)\, \theta\} , \qquad \theta \leqslant \pi/2 . \tag{3.1.3}$$

For pp scattering we can ask whether (3.1.3) can be valid with $\Delta L(s)$ determined by the diffractive channel alone,

$$\Delta L(s) \cong \tfrac{1}{2} b_0\, s^{1/2} , \tag{3.1.4}$$

with $b_0 \cong 1$ fm $(5.1.\ \mathrm{GeV}^{-1})$. For the 90° ($\theta = \pi/2$) differential cross section this predicts

$$s^2 \frac{\mathrm{d}\sigma}{\mathrm{d}t}(s, \theta = \pi/2) \propto \exp\left\{-5.1 \frac{\pi}{2}\sqrt{s}\right\} \propto \exp\{-8.0\, s^{1/2}\} , \tag{3.1.5}$$

which is much more rapid than the experimental falloff. We conclude that diffraction is negligible at 90° and that a geometrical model for pp scattering must contain a peripheral component as well as a diffractive one.

In fig. 3.1.1 we compare data on 90° pp scattering with a form

$$s^2 \frac{\mathrm{d}\sigma}{\mathrm{d}t}(s, \theta = \pi/2) \sim \text{const} \exp\{-(\Delta b)^2 \pi\, s^{1/2}\} , \tag{3.1.6}$$

where Δb can be interpreted as the width of a peripheral band of partial waves. The value

$$\Delta b \cong 0.48 \text{ fm} \tag{3.1.7}$$

is suggested by a study of the impact parameter in K p scattering (Schmid [209a]). On the same graph the constituent counting prediction

$$\frac{\mathrm{d}\sigma}{\mathrm{d}t}(s, \theta = \pi/2) \sim \text{const}\, s^{-10} \tag{3.1.8}$$

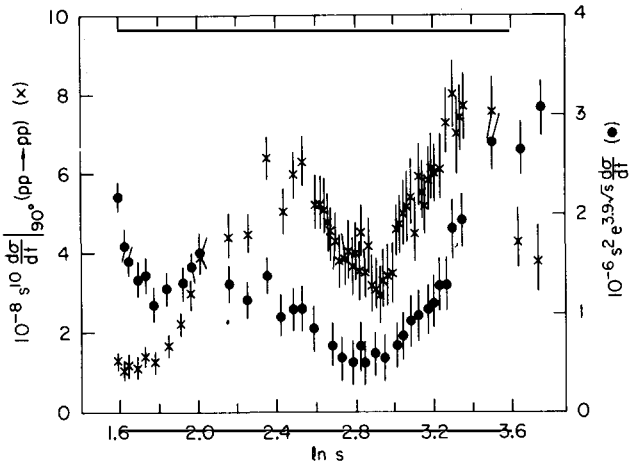

Fig. 3.1.1. Comparison of the form (3.1.6) and (3.1.8) with elastic scattering data. The data are divided by the asymptotic form of the constituent counting prediction (X) and the minimal geometric prediction (•). If we were in a region where the asymptotic predictions of the model were valid the plot should be approximately constant. Both approaches do reasonably well.

is compared with the data. In view of the fact that the corrections to the asymptotic form expected from each model are not known, the agreement of the data with the two alternatives is comparable.

As emphasized by Hendry [146] one advantage of the geometrical approach is the possibility of a simple and direct understanding of the structure in the cross section in terms of fixed-t dips associated with Bessel function (or Legendre function) zeros. The approximate double-zero structure of the large-angle pp polarization data, fig. 2.1.9, is fairly direct evidence for a central plus peripheral decomposition of the pp scattering amplitudes (Hendry and Abshire [147]).

Another reason for studying geometrical models is to test the region of validity of field theory approach. The asymptotic constituent counting rules should be strictly valid in a regime where all spin amplitudes are proportional so there is no polarization and where the amplitudes are smooth and featureless. The present data may be in a transition region where both approaches are approximately valid due to some sort of duality which makes the application of simple asymptotic estimates valid right down to small energies. Kane [158] has shown how the introduction of absorption effects into hard scattering models leads to an oscillating factor of t modifying fixed angle powerlaw behavior predictions.

An alternate approach to fixed angle scattering assumes the existence of a large number of direct channel resonances such as in dual models. While dual models in their simplest form violate the Cerulus–Martin bound they can be interpreted in the spirit of statistical bootstrap models (Frautschi [123]). If we consider the process ab → cd, neglecting spin and assume that in the region of interest $|A|^2$ can be approximated by the incoherent sum of resonances

$$|A(s,z)|^2_{\theta\cong 90^\circ} \cong \sum_{i,l} \frac{(2l+1)^2 P_l^2(\cos\theta)(\gamma^{il}_{ab})^2(\gamma^{il}_{cd})^2}{(\sqrt{s}-m_{i,l})^2+\frac{1}{4}\Gamma^2_{i,l}}. \tag{3.1.9}$$

The sum in l extends over the range $l \in (0, qR)$, where R is a typical hadronic radius. If we neglect the dependence of the residues over this range we can factor out the θ dependence

$$\xi(s,\theta) = \sum_{0}^{qR} (2l+1)^2 P_l^2(\cos\theta) / \sum_{0}^{qR} (2l+1) , \tag{3.1.10}$$

and deal with the appropriate average quantities in the form

$$|A(s,z)|^2 \cong \frac{(2\pi)(\gamma_{ab}(\sqrt{s}))^2 (\gamma_{cd}(\sqrt{s}))^2 \rho(\sqrt{s})\, \xi(s,\theta)}{\Gamma(\sqrt{s})} . \tag{3.1.11}$$

Now the further statistical assumption of equal partition of probability among channels

$$(\gamma_{ab}(\sqrt{s}))^2/\Gamma(\sqrt{s}) \cong (\gamma_{cd}(\sqrt{s}))^2/\Gamma(\sqrt{s}) \cong 1/\rho(\sqrt{s}) \tag{3.1.12}$$

allows us to simplify further

$$\left.\frac{d\sigma}{d\Omega}\right|_{\theta\cong 90^\circ} \cong \frac{1}{64\pi^2 s} \frac{\Gamma(\sqrt{s})}{\rho(\sqrt{s})}\, \xi(s,\theta) . \tag{3.1.13}$$

By simple space-time arguments we know that a resonance cannot decay before a signal can pass across a typical hadronic radius and that

$$\Gamma(\sqrt{s}) = O(\sqrt{s}) . \tag{3.1.14}$$

The statistical bootstrap model gives, of course, a specific prediction for both $\Gamma(\sqrt{s})$, and $\rho(\sqrt{s})$ and has been compared to data by Eilam et al. [105]. The only parameters are an overall normalization factor in the expression for the density of states and a small ambiguity concerning the value of kT_0. Fits to πp and $\bar{p}$p elastic scattering at 90° are shown in fig. 3.1.2 and compared to the power behavior of constituent models. The agreement with the data is good.

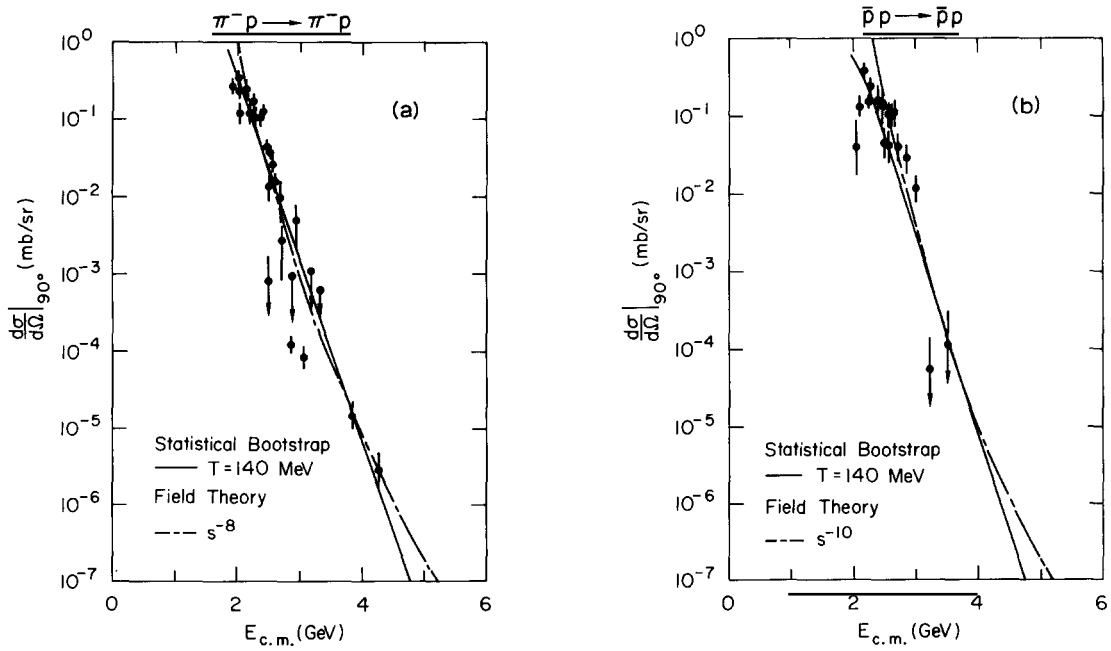

Fig. 3.1.2. Comparison of statistical bootstrap and constituent models for (a) π^-p and (b) $\bar{p}$p elastic scattering at 90°.

A major flaw in the statistical approach is that no predictions are made for the behavior of fixed angle cross sections in exotic channels. One possible way around this is to extend the observed spectrum to exotic channels and just state that the density of states in exotic channels is small. This would then imply, for example

$$\left.\frac{d\sigma/d\Omega\,(pp \to pp)}{d\sigma/d\Omega\,(\bar{p}p \to pp)}\right|_{\theta \cong 90^\circ} \gg 1 \tag{3.1.15}$$

$$\left.\frac{d\sigma/d\Omega\,(K^+p \to K^+p)}{d\sigma/d\Omega\,(K^-p \to K^-p)}\right|_{\theta \cong 90^\circ} \gg 1\,, \tag{3.1.16}$$

which is in agreement with present observations. It would also seem that the naive approach would imply large fluctuations about the mean in such exotic channels. This is not observed. Presumably, the correct answer for exotic channels involves getting the spectrum in nonexotic channels right and then implementing crossing.

There exists one solid piece of support for the existence of high mass resonance states of the type necessary for the statistical approach discussed here. This consists of the rapid fluctuations with energy of the large t differential cross section for $\pi^{\pm}p$ elastic scattering observed by F. Schmidt et al. [210] and illustrated in fig. 2.1.10. The existence of these rapid fluctuations was predicted on the basis of a statistical treatment of overlapping resonances by Ericson [113]. Their importance in terms of the statistical bootstrap program has been emphasized by Frautschi [123]. Basically we expect a large number of overlapping resonances which, on the average, have random phases to be partially coherent in local regions of energy. The period of the fluctuations produced should give a measure of the average resonance width and the relative size of the fluctuations should vary inversely with the density.

It is impossible to learn on the basis of the single observation of fluctuations reported by Schmidt et al. whether they correspond in period or size with those predicted by the statistical model. Many more measurements of this type are needed but it does seem most natural to attribute these data to some sort of high-mass resonance phenomena.

One of the most crucial distinctions between finitely-composite hadrons and infinitely-composite hadrons involves the asymptotic form of Regge trajectories. There has been a considerable effort to extend the constituent interchange model from the fixed-angle region into the fixed-t region. This effort has resulted in predictions for the large-t behavior of Regge trajectories. Let us consider here the status of the predictions

$$\lim_{t\to\infty} \alpha_{\pi p}(t) = -1\,, \qquad \lim_{t\to\infty} \alpha_{pp}(t) = -2\,. \tag{3.1.19}$$

This predictions can be tested by measuring the effective trajectory in $\pi^-p \to \pi^0 n$ and pp elastic scattering. In contrast, dual or geometrical ideas would require infinitely falling trajectories.

Barger, Halzen and Luthe [25] have calculated an effective trajectory in pp scattering using

$$\ln \frac{d\sigma}{dt}\,(pp \to pp) = (2\alpha_{\mathrm{eff}}(t) - 2)\ln s + \ln \beta(t)\,. \tag{3.1.20}$$

This is shown in fig. 3.1.3. Blankenbecler et al. [47] have calculated the effective trajectory in fig. 3.1.4a using

$$\ln \frac{d\sigma}{dt}(pp \to pp) = (2\alpha_{eff}(t) - 2) \ln(-u) + \ln \beta(t) , \tag{3.1.21}$$

which they claim is more consistent with the duality properties of the pp elastic amplitude. The difference in the t-dependences of these two trajectory functions is primarily due to

$$\ln(-u) = \ln(s + t - 4m^2) = \ln(s) + \ln\left(1 + \frac{t - 4m^2}{s}\right), \tag{3.1.22}$$

and so the fact that the trajectory of Barger et al. falls below -2 should therefore not necessarily rule out (3.1.19).

The ρ-trajectory extracted from charge exchange data of Brockett et al. [57] seems to fall below the expected value of -1. However, elastic $\pi^- p$ analyzed by Blankenbecler et al. [47] as shown in fig. 3.1.4b supports (3.1.19).

Possibly more significant evidence concerning the large-t behavior of Regge trajectories is the study using finite energy sum rules of the amplitude structure of $\pi^- p \to \pi^0 n$. Elvekjaer et al. [112] report that the large-t region the amplitudes are very similar to what is expected from a simple ρ-Regge pole with a linear trajectory. In particular they point out the right-signature zero at $t = -1.6$ and a second wrong-signature zero at $t \cong -2.4, -2.5$ consistent with the places where a linear trajectory would pass through -1 and -2 respectively. Their results are shown in fig. 3.1.5. There is some feedback through the "optimized convergence" finite energy sum rule of the form assumed for the trajectory function and the structure in the amplitude. However, if this structure

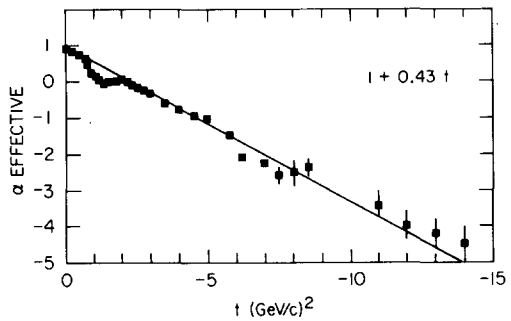

Fig. 3.1.3. Effective trajectory in pp scattering of Barger, Halzen and Luthe [25].

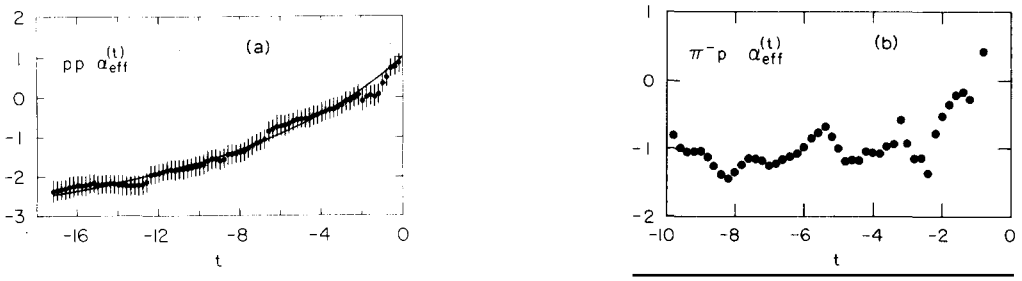

Fig. 3.1.4. (a) Effective trajectory in pp scattering of Blankenbecler, Tran Than Van, Gunion and Coon [47]. (b) Effective trajectory in $\pi^- p$ scattering.

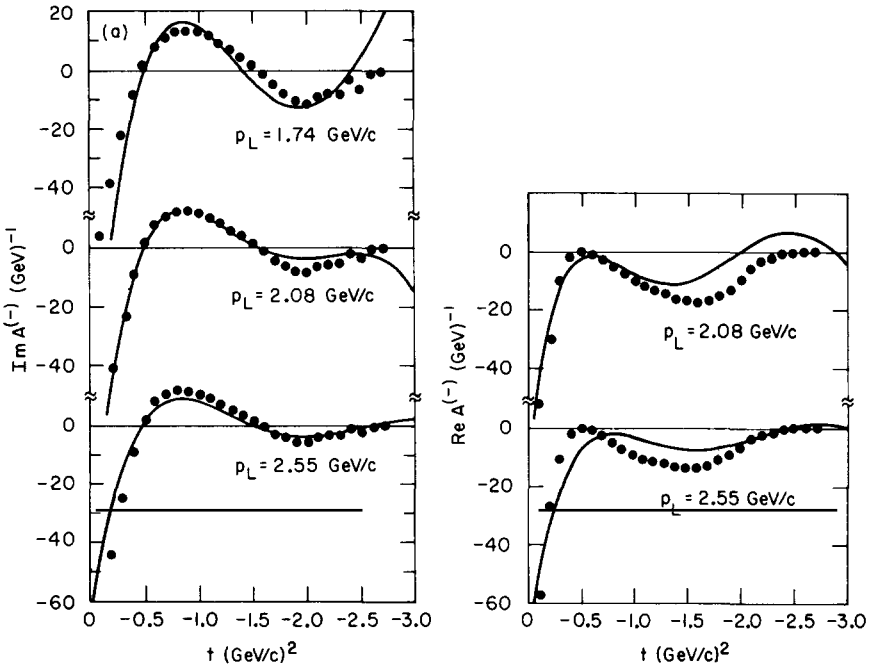

Fig. 3.1.5. Evidence for second wrong signature zero in $A(\pi^- p \to \pi^0 n)$ discussed by Elvekjaer et al. [112].

is confirmed independently, for example, by amplitude analysis at large t then it would argue quite strongly for the existence of indefinitely falling trajectories.

3.2. Hadronic fireball approaches to large p_T inclusives

In this section we turn our attention to models which attempt to explain high p_T phenomena without invoking quark-like structureless constituents. These hadronic models instead relate the production of large transverse momentum particles to ideas which have proved useful in understanding low p_T data.

The first, and one of the most important, thing to keep in mind is that based on purely hadronic ideas there is no reason to expect large p_T inclusive cross sections anywhere near as large as they have been observed to be. We can be more explicit about this. Two reasonably complete and self-consistent models have made predictions for the p_T distributions of inclusive hadronic processes. The dual resonance model (DeTar et al. [99]) predicts

$$E\,\mathrm{d}^3\sigma/\mathrm{d}^3p\big|_{p_L\cong 0} \propto \exp(-4\alpha' p_T^2) \tag{3.2.1}$$

(which conflicts with a simple extension of the Cerulus–Martin bound to inclusive process). The statistical bootstrap model (Hagedorn and Ranft [138], Hagedorn [137]) gets

$$E\,\mathrm{d}^3\sigma/\mathrm{d}^3p\big|_{p_L\cong 0} \propto \exp(-p_T/m_\pi)\,. \tag{3.2.2}$$

Within the context of these models there is no apparent need for large p_T events from some sort of violent subprocess. The observation of large cross sections characterized by eq. (1.2.3) or

fig. 1.1 then indicates that these models are wrong or, at best, incomplete and that they need to be modified. The hadronic models we discuss here make modifications of a somewhat *ad hoc* nature, invoking new mechanisms or new, unsuspected mass scales but we will temporarily overlook the lack of internal theoretical motivation. The unexpected, large cross sections are motivation enough. As is evident in the rest of this review the hard scattering models in which large cross sections are expected are not without their own shortcomings. One main purpose in considering non-parton models is to gain further insight into the problem of just how important it is that we consider quarks to be an essential dynamical degree of freedom in large p_T hadronic interactions.

Before we go on to consider the *ad hoc* models which attempt to describe the current data, let us try to get the flavor of the two models which predict exponentially falling cross sections at large p_T. The dual resonance model prediction is based on a Mueller–Regge analysis of the dual 6-point function. Consider, for example, the term with the ordering of particles shown in fig. 3.2.1.

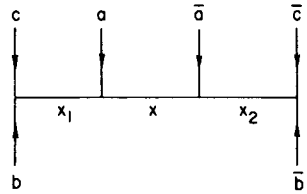

Fig. 3.2.1. Labelling of the particles for the dual amplitude, eq. (3.2.3).

The dual model amplitude with this ordering has the discontinuity

$$\mathrm{disc}_{\mathcal{M}^2} B_6 \sim \frac{a\pi \mathrm{i}}{\Gamma(\alpha_{a\bar{a}}+1)}(\alpha)^{\alpha_{a\bar{a}}}\left(\frac{-\alpha_{ac}}{\alpha}\right)^{\alpha_{bc}}\left(\frac{-\alpha_{\bar{a}\bar{c}}}{\alpha}\right)^{\alpha_{\bar{b}\bar{c}}}\int_0^\infty\int_0^\infty \mathrm{d}y_1\,\mathrm{d}y_2\,\theta(1-y_1-y_2)\,y_1^{-\alpha_{b\bar{c}}-1}\,y_2^{-\alpha_{\bar{b}\bar{c}}-1}$$

$$\times\left(1-\frac{\alpha}{\alpha_{ac}}\,y_1\right)^{\alpha_{bc}+\alpha_{b\bar{b}}-\alpha_{a\bar{a}\bar{c}}}\left(1-\frac{\alpha}{\alpha_{\bar{a}\bar{c}}}\,y_2\right)^{\alpha_{\bar{b}c}+\alpha_{b\bar{b}}-\alpha_{\bar{a}ac}}\left(1-\frac{\alpha}{\alpha_{ac}}\,y_1-\frac{\alpha}{\alpha_{\bar{a}\bar{c}}}\,y_2\right)^{-\alpha_{a\bar{a}}-\alpha_{b\bar{b}}+\alpha_{a\bar{a}c}+\alpha_{\bar{a}ac}}$$

$$\times(1-y_1-y_2)^{\alpha_{a\bar{a}}}, \tag{3.2.3}$$

where $\alpha_{a\bar{a}} = \alpha((p_a+p_{\bar{a}})^2)$, $\alpha = \alpha((p_a+p_b+p_c)^2) = \alpha(\mathcal{M}^2)$, etc., are the linear trajectory functions. At fixed x_L and large p_T we have

$$\alpha_{bc} \cong \alpha_{\bar{b}\bar{c}} \cong -\alpha' p_T^2/x_L\,, \tag{3.2.4}$$

and we get a contribution from the integrand near $y_1 = y_2 = \frac{1}{2}$ proportional to (Virasoro [224a])

$$\exp\left[-2\alpha' p_T^2\left(\frac{1}{x_L}\ln\left(\frac{1+x_L}{1-x_L}\right)\right)\right]. \tag{3.2.5}$$

In the central region, $x_L = 0$, this continues into the form (3.2.1).

The exponential falloff in p_T^2 in the inclusive distribution of the dual model is related quite closely to the fixed-angle behavior of the dual 4-point function. The absence of Regge cuts or multiplicative fixed poles in the J-plane allows the exchange of a linear Regge trajectory to dominate at large momentum transfers. It is important to keep in mind the fact that the dual model

does not implement unitarity and that the simple predictions (3.2.1) and (3.2.5) are probably not stable under the unitarization of the model. There have been some attempts to generalize such results (Ellis and Freund [109], Sivers [216, 217]) but these remain very speculative. The predictions (3.2.1) and (3.2.5) are, of course, in drastic conflict with the data. This fact along with the inability of dual models to define reasonable current amplitudes and form factors must now be considered a major challenge to the continued application of the dual approach.

Hagedorn's statistical bootstrap (Hagedorn [137]) constitutes another fundamental model which does not invoke structureless quarks in order to make a definite prediction for the transverse momentum distribution. The basic postulate of the statistical bootstrap (Frautschi [122]) is that there exists a spectrum of high mass hadrons and that the energy of interaction in hadron–hadron collisions goes predominantly into the production of these massive fireballs. Consistency arguments based on the unitarity equation then require that the density of hadronic levels is given by

$$\rho(\mathcal{M}) = C\mathcal{M}^a \exp(\mathcal{M}/T_0), \tag{3.2.6}$$

where T_0 is a temperature and $a \leqslant \frac{5}{2}$. This hadronic density seems to be approximately realized in nature by the observed low mass states as demonstrated by fig. 3.2.2. From this we deduce $T_0 \cong 160$ MeV.

The distribution in transverse momentum of the secondary decay products in the statistical bootstrap model then follows from the fact that the dominant decay mode of the high-mass fireballs is the so-called cascade decay $M^* \to M^{*\prime} + m_c$. To the extent that we can neglect recoil momentum we expect this distribution in the fireball rest frame to be given by a Boltzmann factor

$$\exp[-(p_L^2 + p_T^2 + m_c^2)^{1/2}/T], \tag{3.2.7}$$

where the temperature, T, is closely related to the temperature in the density of states, (3.2.6),

$$T \lesssim T_0 . \tag{3.2.8}$$

In high energy collisions, the superposition of fireballs with different longitudinal velocities smears out the Boltzmann factor in the longitudinal direction but, since most fireballs are produced with small transverse momentum, the dependence in the transverse direction remains almost unchanged.

The fact that for a reasonable range of intermediate momenta the experimentally observed transverse momentum behavior

$$E\mathrm{d}^3\sigma/\mathrm{d}^3p \simeq c(p_L)\exp(-6p_T) \qquad (0.1 \leqslant p_T \leqslant 1.0\ \mathrm{GeV}/c) \tag{3.2.9}$$

agrees quite well with (3.2.7) where the value of T is given by T_0 in the density of states, (3.2.6), was originally considered an outstanding success of the model. Now that we have to deal with new observations indicating that the data at high transverse momentum be several orders of magnitude above (3.2.9) we are faced with a problem. Do we believe that the agreement of low p_T data with (3.2.9) fortuitous or do we recognize the model as having limited range of validity? If we take the latter viewpoint we can imagine that relaxing some of the assumptions of the model will enable us to extend our understanding out to larger p_T.

Most of the models we discuss here, whether or not they follow precisely the spirit of the statistical bootstrap model, retain the concept of the fireball and therefore share many conceptual features. The idea of a fireball or cluster of hadrons has, of course, been a valuable aid in under-

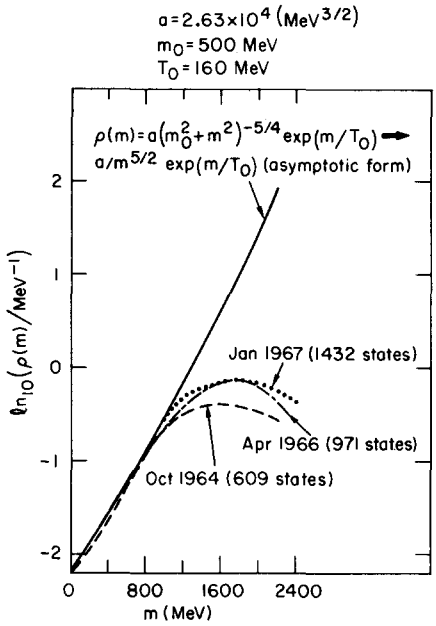

Fig. 3.2.2. The density of states in the statistical bootstrap of Hagedorn compared with observed hadronic resonances.

standing the correlations in low p_T data. The review of Ranft [203] is particularly instructive in outlining the importance of this concept.

One simple approach to large transverse momentum discussed by Jabs [151] is to introduce a new *class* of fireballs. A high energy collision is assumed to proceed via two distinct mechanisms, fragmentation and pionization. The pionization component coincides roughly with the usual statistical bootstrap ideas but fragmentation is handled separately. Specifically, Jabs assumes that the fireballs carrying the quantum numbers of the leading particles have quite different properties than those produced in the pionization region.

The contributions of the fragmentation fireballs to the inclusive cross section in this model is

$$\left.\frac{E\mathrm{d}^3\sigma}{\mathrm{d}^3p}\right|_{\mathrm{FRAG}} \propto M_{\mathrm{F}}^{*} p_{\mathrm{T}} \int_{1}^{\gamma_{\mathrm{F}}^{\max}} \gamma_{\mathrm{F}}\, w(\gamma_{\mathrm{F}})\, \mathrm{d}\gamma_{\mathrm{F}} \exp\left[-\frac{p_{\mathrm{T}}}{kT_{\mathrm{F}}}\gamma_{\mathrm{F}}\right], \tag{3.2.10}$$

where γ_{F} is the Lorentz factor given approximately by

$$\gamma_{\mathrm{F}} = \left(\frac{\sqrt{s} - E_{\pi}}{2M_{\mathrm{F\,min}}^{*}(p_{\mathrm{T}})}\right), \tag{3.2.11}$$

where E_{π} is the amount of C.M. energy going into pionization and $w(\gamma_{\mathrm{F}})$ is a normalized distribution of fireballs. By taking these fireballs to occasionally be very massive and hence slow in the C.M. system and assuming they decay statistically with a temperature $T_{\mathrm{F}} \cong 2T_0$, the single particle inclusive data can be roughly understood.

While there can be no fundamental objection to the *ad hoc* introduction of a new temperature or mass scale it is not inherently satisfying. A simplifying assumption used by Jabs is that the fireballs are produced strictly along the collision axis; without further clarification of how reasonable

this assumption is, the understanding of the production is incomplete.

Pokorski and van Hove [195] have a similar view of the origin of high p_T particles. They point out that if the leading fireball is assumed to be produced diffractively in the spirit of the diffractive dissociation model (Hwa and Lam [149]) or the nova model (Jacob and Slansky [155]), then the low masses of diffractive fireballs and the competition of different channels combine to keep transverse momenta of decay products low. At NAL or ISR, however, the production of *heavy* fireballs can lead to large transverse momenta.

In a separate paper Pokorski and van Hove [196] also make an interesting connection between fireball models and quark parton models. They note that the average fraction of C.M. energy carried off by protons in proton–proton inelastic collisions is near one-half. Also, the average fraction of the proton's momentum carried by quarks as deduced from analysis of lepton–proton inelastic scattering is close to a half. This suggests that the fragmentation fireball can be considered to carry the quantum numbers and approximately the same C.M. energy as the initial quarks. The assignment of a large mass to this fireball can then be considered roughly equivalent to giving the valence quarks a large relative momentum and the "decay" of a large mass fireball to produce high transverse momentum hadrons can have the same underlying dynamics as the quark–parton model. In the synthesis of Pokorski and van Hove it is unspecified at what level the underlying fundamental constituents become the important dynamical entities instead of the fireball. More explicit calculations are needed. One thing which is clear is that it is over-simplifying things to consider only fireballs which themselves have no transverse momentum.

An interesting calculation in the context of statistical models has been performed by Bouquet, Letessier and Tounsi [54]. The heavy clusters which are formed are assumed to decay in a sequential cascade mechanism. This would lead to the Boltzmann distribution eq. (3.2.7) for the transverse momentum of the decay products if the recoil momentum of the heavy cluster is neglected. They then observe that the buildup of successive recoils to produce a large momentum is statistically unlikely but not so unlikely as to be unable to produce the observed yield of high transverse momentum hadrons. Detailed numerical calculations described in their paper yield the curve shown in fig. 3.2.3. The calculations are complicated enough that it is difficult to abstract any features of the data which will conclusively support their contention. It remains an interesting piece of work which shows that it can be dangerous to use statistical arguments when the number of particles in the decay mode is still relative small.

One modification of the statistical model which has not received much attention is the possibility that high mass fireballs have a small "fission" decay mode where they decay into two approximately equal mass objects as well as the usual cascade decay mode. A reasonable branching fraction into a fission mode can result in substantial large p_T inclusive cross sections. Of course, this decay mode could also give jet-like structure to the population of hadrons in the final state. Detailed calculations on this approach have not been made although the formalism is available (Barnett and Silverman [26]).

A distinct version of the fireball model is advocated by Berger and Branson [27]. In their approach low mass fireballs are produced at large θ through a hard scattering mediated by the current–current interaction of Berman and Jacob [29]. The invariant cross section for the production of these baryonic clusters in fig. 3.2.4 is given by

$$\frac{E_c\,d\sigma_c}{d\mathcal{M}_c^2\,d^3p_c} = \frac{c}{\pi s} F_2(\omega_1) F_2(\omega_2) \left(\frac{s^2}{t^2\omega_1\omega_2} + \frac{s}{t} + \frac{\omega_1\omega_2}{2}\right) + [\cos\theta \leftrightarrow -\cos\theta]\,, \tag{3.2.12}$$

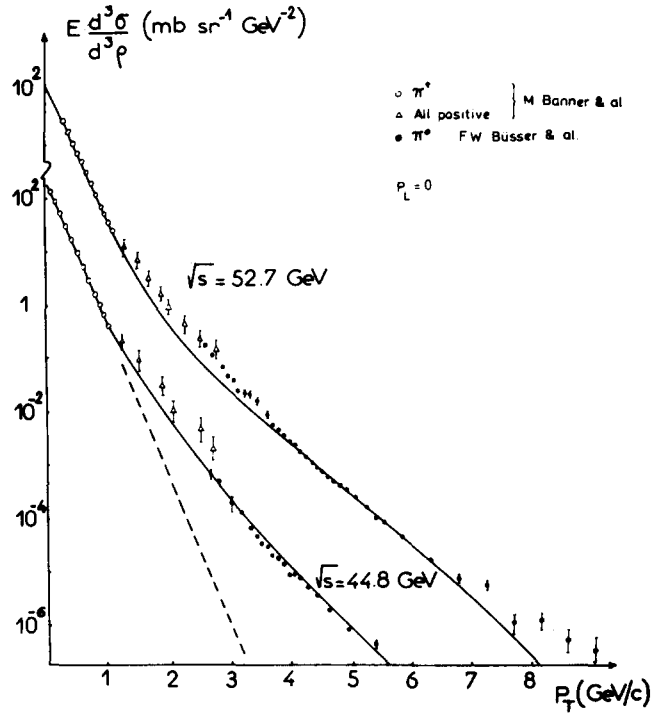

Fig. 3.2.3. Transverse momentum distribution in the fireball model of Bouquet, Letessier and Tounsi [54].

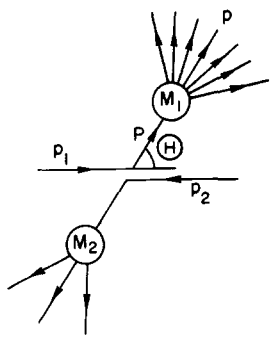

Fig. 3.2.4. The low mass fireball model of Berger and Branson [27].

where F_2 is the usual dimensionless scaling function νW_2 and

$$\omega_1 = \frac{1}{t}[s^{1/2}(m_1^2+p^2)^{1/2} - 2m_p^2 - (s-4m_p^2)^{1/2} p\cos\theta] ,$$
$$\omega_2 = \frac{-1}{t}[s - s^{1/2}(m_2^2+p^2)^{1/2} - 2m_p^2 - (s-4m_p^2)^{1/2} p\cos\theta] . \qquad (3.2.13)$$

The cross section (3.2.12) when integrated over all finite region of phase gives a contribution to the total inelastic cross section which rises linearly with s. Because of the magnitude of the large p_T cross section this rise is not a problem at current energies but there must be some sort of

mechanism, possibly a natural cutoff, which removes this linear divergence.

Because the fireballs in Berger and Branson's calculation have baryon number one and a small mass, they predict the proton/pion ratio to be quite large. A value of 5 for this ratio is cited in their paper but the actual value is sensitive to the input mass spectrum for the fireballs. However, the observed value $p/\pi \simeq 1$ at $p_T = 3$ GeV/c (see figs. 2.2.5 and 2.2.6) is uncomfortably small for a model with light baryonic fireballs.

An approach related to fireball models which attempts to incorporate an idea of the space-time structure of a collision is the "hydrodynamical" model originally proposed by Landau [168]. The picture is that some portion of the hadronic matter goes to form a massive fireball localized in some volume characteristic of the incident energy. One idea of the time evolution of this fireball is that it expands adiabatically for some period during which the behavior of the hadronic matter is governed by the classical dynamics of a perfect fluid. The expansion continues as the system "cools" until a temperature of order m_π is achieved and the system condenses into pions and other hadrons.

In a detailed study of the hydrodynamic equations done by Carruthers and Duong-Van [74], approximate solutions for the particle distribution due to condensation suggests a gaussian dependence on rapidity. In the longitudinal rapidity $y_L = \frac{1}{2}\ln\{(E+p_L)/(E-p_L)\}$

$$\frac{E\,d^3\sigma}{d^3p} \propto \exp(-y_L^2/R_L^2)\,, \tag{3.2.14}$$

the width, R_L, is approximately related to the Lorentz contraction

$$R_L \cong \tfrac{1}{2}\ln(s/s_0)\,. \tag{3.2.15}$$

From symmetry arguments, Carruthers and Duong-Van suggest that the 90° inclusive cross section should also be given by a gaussian in transverse rapidity, $y_T = \frac{1}{2}\ln\{(E+p_T)/(E-p_T)\}$

$$\left.\frac{E\,d^3\sigma}{d^3p}\right|_{y_L\cong 0} \propto \exp(-y_T^2/R_T^2)\,, \tag{3.2.16}$$

where the width is now approximately independent of incident energy. The data is roughly consistent with this gaussian form over many orders of magnitude although it is hard to understand the s-dependence of the high p_T cross section unless correction terms derived from beam fragmentation are important. One interesting suggestion is to take the hydrodynamical model for the dependence of the hadron irreducible interaction in a hard scattering picture for the interaction like that described by the graph shown on fig. 1.5.

A suggestion due to Dumont and Heiko [103] and Heiko [145] is that although the bulk of particles can appear only at the condensation stage, some particles may escape from the hadronic matter at any time and will have a momentum reflecting the "temperature" at that time. They divide, rather arbitrarily, the progression of the fireball into the formulation or initial stage, the expansion stage, and the condensation stage. For particles escaping from the initial fireball they expect a distribution in p_T approximately given by

$$\left.\frac{E\,d^3\sigma}{d^3p}\right|_{\text{init}} = A\,x_T \exp(-Bp_T/s^{1/4})\,, \tag{3.2.17}$$

which can be understood in terms of the original Fermi statistical model [118a] where the highest

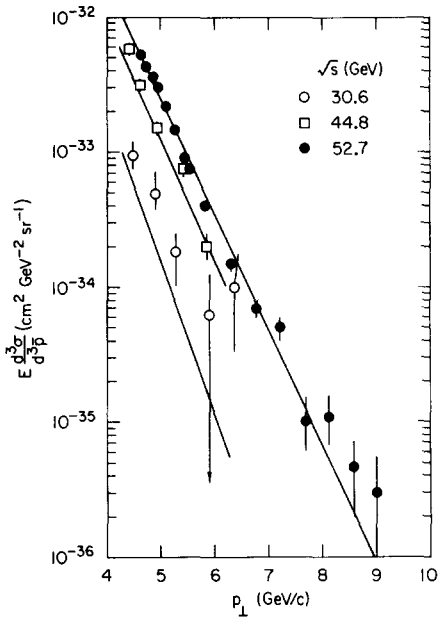

Fig. 3.2.5. The prediction of the model of Dumont and Heiko [103] for the inclusive p_T distribution.

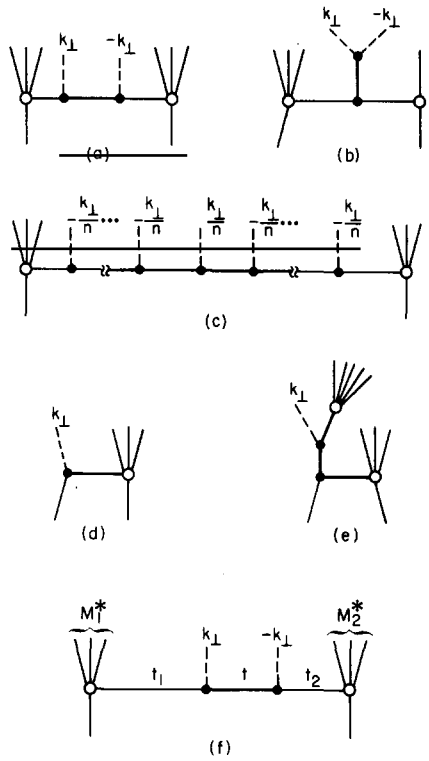

Fig. 3.2.6. The graphs which contribute to large p_T hadrons in the bootstrap model of Harte.

temperature achieved is proportional to $s^{1/4}$. For particles escaping during the expansion stage they propose an empirical form

$$\left.\frac{E\mathrm{d}^3\sigma}{\mathrm{d}^3p}\right|_{\mathrm{exp}} = Cp_T \exp\{-p_T/(D+Es^{1/4})\}\,, \tag{3.2.18}$$

so that the effective temperature interpolates the initial temperature and the breakup temperature $T \cong m_\pi$. The small p_T data is then fit by the usual Hagedorn spectrum (3.2.7).

With the fair number of parameters displayed in the model they can achieve a reasonable fit to the inclusive cross section. A typical fit and the values of the parameters are shown in fig. 3.2.5. The global display of the data given by Cronin, fig. 2.2.7, does not favor such an arbitrary division but the essence of the idea is that there is a continuum of temperatures between $T = Bs^{1/4}$ and $T = m_\pi$ which are important, and this would not argue for the existence of breaks. Meng Ta-Chung [185] has proposed an alternate form where the temperature is proportional to $s^{1/8}$.

An alternate hadronic model which should stand separately from fireball models is the so-called asymptotic bootstrap model of Harte [142, 143]. This model assumes that hadrons are infinitely composite in the sense that there are no poles in the irreducible kernel of a Bethe–Salpeter-type integral equation which represents unitarity. Self-consistency arguments are then used to derive the asymptotic behavior of vertex functions when one or more momentum transfers is large.

The model has predictions for electroproduction not too dissimilar from present data. In con-

trast, it predicts that the cross section $\sigma_{e^+e^-\to h}$ falls *faster* than $1/Q^2$. The predictions we want to mention here start with the predicted behavior of electromagnetic form factors

$$F(t) \sim \exp\{-af(m^2, m^2)(-t)^{1/4}\}, \tag{3.2.19}$$

(see also Stack [218]). This is in good agreement with the data. The fixed angle behavior of exclusive amplitudes in this model is also expected to fall exponentially with $(-t)^{1/4}$. The inclusive production of hadrons at large p_T in this model come from graphs such as that shown in fig. 3.2.6 where the heavy line is a $p^2 = 0$ propagator. In diagram a of this figure the maximum contribution comes from t near t_{min} and leads to an inclusive cross section behaving asymptotically as

$$\left.\frac{E\,d^3\sigma}{d^3p}\right|_{90°} \sim f(s, x_T)\exp(-cp_T^{1/2}), \tag{3.2.20}$$

where c is a universal constant and f is slowly varying. A comparison of this single contribution with data on $pp \to \pi^0$ from the CCR group is shown in fig. 3.2.7. The other diagrams have not been computed.

None of the models discussed here can be considered completely successful in the sense that the large inclusive cross sections for high p_T hadrons are a natural expectation. Several models cannot be ruled out with existing data but these cannot be considered attractive because they contain *ad hoc* features. One important constraint is that the models make interesting nontrivial predictions for two-body inclusives, multiplicity correlations, etc. which can be compared to new data. An important consequence of the work of Pokorski and van Hove is that it may be possible to make a synthesis of fireball and quark–parton models which allows all kinematic ranges to be dealt with on a uniform basis. This exciting possibility deserves careful exploration.

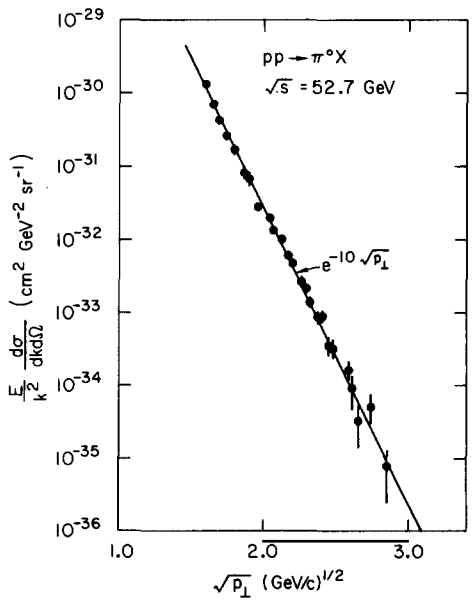

Fig. 3.2.7. The CCR data compared with Harte's prediction.

4. Hard scattering models

4.1. Introduction

Hadronic reactions involving the production of particles at large transverse momentum possess the exciting possibility of directly reflecting the underlying structure of hadrons and the interaction of their possible constituents at very short distances. Although the underlying dynamics are certainly more complex than the simple parton model description of deep-inelastic lepton–hadron scattering, an important first question is whether one can adequately describe the behavior of large p_T reactions in terms of a few simple but general constituent scattering mechanisms, and whether the quark model does in fact determine the essential degrees of freedom of hadronic matter at short distances.

In the following, we shall attempt to describe the simplest approaches to this objective in the class of hard scattering models. The rules of dimensional counting will be discussed and then applied to a more definite constituent model of the hadrons to discuss exclusive and inclusive reactions. A similar type of theory using the eikonalization properties of softened vector meson theories will be discussed also, and the possible connection with constituent theories will be elaborated upon.

4.2. Counting laws for large p_T reactions

As we have emphasized, the inclusive cross section for $A + B \to C + X$ in any hard scattering model is given simply by the sum of cross sections for each contributing subprocess $a + b \to c + d$ at large p_T weighted by the fractional momentum fragmentation probabilities $G_{a/A}$, $G_{b/B}$ and $\tilde{G}_{C/c}$. Since the fragmentation probabilities are scale-invariant, the large p_T scaling behavior of $E\,d\sigma/d^3p\ (A + B \to C + X)$ reflects the scaling behavior of the subprocess cross section $d\sigma/dt'(a + b \to c + d)$. Depending on the model, the interacting particles a, b, c, d can each be hadrons, quarks, or diquarks. In order to compute the contribution of each type of subprocess we can use the dimensional counting rules which are based on an underlying scale-invariant theory. The counting rules for elastic scattering and form factors were derived independently by Brodsky and Farrar [62] using renormalizable field theory methods and by Matveev, Muradyan and Tavkhelidze [183] using the ansatz of scale-invariance or "automodality" of the quark scattering amplitudes. Some applications to the p_T power of inclusive reactions were also discussed by Brodsky and Farrar [62]. A complete discussion of the generalized structure functions and the threshold behavior of inclusive reactions was given by Blankenbecler and Brodsky [40]. Some of these results were obtained by different methods by Gunion [134]. The rules are as follows: First, one counts the minimum number of "active" elementary fields participating in the large p_T process

$$n_{\text{active}} = n_a + n_b + n_c + n_d\,, \tag{4.2.1}$$

and the minimum number of spectators (noninteracting fragments) or "passive" fields in A, B, and C:

$$n_{\text{passive}} = n(\bar{a}A) + n(\bar{b}B) + n(\bar{C}c)\,. \tag{4.2.2}$$

Then following the quide of simple Born graphs in renormalizable field theories one can derive the following result for each contributing subprocess:

$$\frac{E\mathrm{d}\sigma}{\mathrm{d}^3p}(\mathrm{AB}\to\mathrm{CX})\Big|_{\substack{s,u,t\\ \text{large}}} \propto \frac{1}{(p_\mathrm{T}^2)^N} f(\theta_\mathrm{CM},\epsilon) \underset{\epsilon\to 0}{\sim} \frac{1}{(p_\mathrm{T}^2)^N} f(\theta_\mathrm{CM})\epsilon^F , \tag{4.2.3}$$

for $\epsilon = \mathcal{M}^2/s$ fixed, where

$$N = n_{\text{active}} - 2 , \tag{4.2.4}$$

and

$$F = 2n_{\text{passive}} - 1 . \tag{4.2.5}$$

It is physically clear that N should increase as the number of fields forced to change direction increases, and that F (the degree of "forbiddenness") should increase as increasing numbers of spectators take away the available phase space. The reader can readily check that the usual scale-invariant parton predictions for deep inelastic lepton scattering or Compton scattering are included as special cases of the above rules. For ep → eX, $n_{\text{active}} = 4$ (for eq → eq) and $n_{\text{passive}}^{\text{hadronic}} = 2$ giving $\nu W_2(x) \sim (1-x)^3$ for $x \to 1$. For scattering on antiquarks (or strange or charmed quarks) in the proton, $n_{\text{passive}} = 4$ and $\nu W_{2(\bar{\mathrm{q}})} \sim (1-x)^7$. This last result has been used by Gunion [134] and Farrar [117] as a simple parametrization of the nucleon's antiquark distribution. Notice for pp → μX, the Drell-Yan mechanism ($\mathrm{q\bar{q}} \to \mu^+\mu^-$) predicts $N = 2$, and $F = 11$ (for 6 spectators).

More generally, the spectator rule gives for $x \to 1$

$$G_{\mathrm{a/A}}(x) \sim (1-x)^{2n-1}, \qquad n = n(\bar{\mathrm{a}}\mathrm{A}) \tag{4.2.6}$$

for the fractional longitudinal momentum distribution of (off-shell) hadron A in hadron B. Some examples are $G_{\bar{\mathrm{q}}/\pi} \sim (1-x)$, $G_{\pi/\mathrm{p}} \sim (1-x)^5$, $G_{\bar{\mathrm{p}}/\mathrm{p}} \sim (1-x)^{11}$, etc. One can also use this result to predict decay distributions (see section 5.5) and the diffractive dissociation contributions to inclusive reactions A + B → C + X in the triple Regge region. Writing

$$\frac{E\mathrm{d}\sigma}{\mathrm{d}^3p} \sim (1-x)^{1-2\alpha_{\mathrm{eff}}(0)} , \tag{4.2.7}$$

one obtains $\alpha_{\mathrm{eff}} = 1 - n(\bar{\mathrm{a}}\mathrm{A})$ if a = C. Generally, there are also contributions from two step processes which give

$$\alpha_{\mathrm{eff}}(0) = \tilde{\alpha}(0) - n(\bar{\mathrm{a}}\mathrm{A}) ,$$

where $\tilde{\alpha}(0)$ is the trajectory for the process a + B → C + anything. For the case of electromagnetic couplings, e.g., leptons or quarks to a photon, there are corresponding equivalent photon or equivalent lepton distributions as discussed by Chen and Zerwas [77]. For these processes the spectator rule (4.2.5) is generalized to (Blankenbecler et al. [44])

$$F = 2n_{\text{passive}}^{\text{hadronic}} + n_{\text{passive}}^{\text{e.m.}} - 1 , \tag{4.2.8}$$

where $n_{\text{passive}}^{\text{e.m.}}$ is the number of spectator quarks or leptons coupling to a photon. Note that photons are *not* counted in the spectator rule, although extra factors of $\log s$ arise.

4.2.1. Exclusive processes

The general result (4.2.3) can also be applied to exclusive two body processes, $n_{\text{passive}} = 0$, to yield

$$\frac{\mathrm{d}\sigma}{\mathrm{d}t}(\mathrm{AB}\to\mathrm{CD}) \sim \frac{1}{s^{n_\mathrm{a}+n_\mathrm{b}+n_\mathrm{c}+n_\mathrm{d}-2}} f(\theta_\mathrm{CM}) , \tag{4.2.9}$$

which, for eh → eh gives the result

$$F_h(t) \sim t^{1-n_h}, \tag{4.2.10}$$

for the asymptotic behavior of spin-averaged form factors. For multiparticle exclusive processes the prediction is

$$\Delta\sigma \sim s^{-1-N_M-2N_B}, \tag{4.2.11}$$

where $\Delta\sigma$ is the cross section integrated over some fixed region of many body invariant phase space such that all two-particle invariants are large. In (4.2.11) N_M is the number of meson ($q\bar{q}$) states and N_B the number of baryons (qqq). For example, this result makes predictions for specific exclusive channels in $\bar{p}p$ or e^+e^- annihilation. The region of phase space considered must be chosen to be outside of possible prominent resonance contributions.

The prediction (4.2.9) is compared with pp elastic scattering data in fig. 4.2.1 and with πp and Kp in fig. 4.2.2. The predictions for form factors are discussed in section 4.3. Other comparisons, including photoproduction, are discussed by Brodsky and Farrar [62, 63].

The dimensional counting rules are derived assuming that the composite systems have zero internal orbital angular momentum. Brodsky and Farrar [63] present arguments which indicate higher orbital states can be dealt with by assuming that they contain extra elementary vector fields. It is also possible that there exist suppressions of various contributions from a more careful treatment of quantum numbers than is possible from just counting constituents. For example, the p–Δ electromagnetic transition may be suppressed due to the isotopic spin structure of the wave functions. This possibility is discussed in more detail by Scott [214] and Gunion [134–136]. Although not conclusive, the predictions using quark counting are sufficiently consistent with experiment that it becomes an important question to understand the theoretical conditions for their validity. This is done in some detail for the form factors in the following section, where it is found that up to finite powers of log t the result (4.2.9) is the canonical expectation for general classes of scale-invariant theories, and can be proved rigorously in certain field theories. The validity

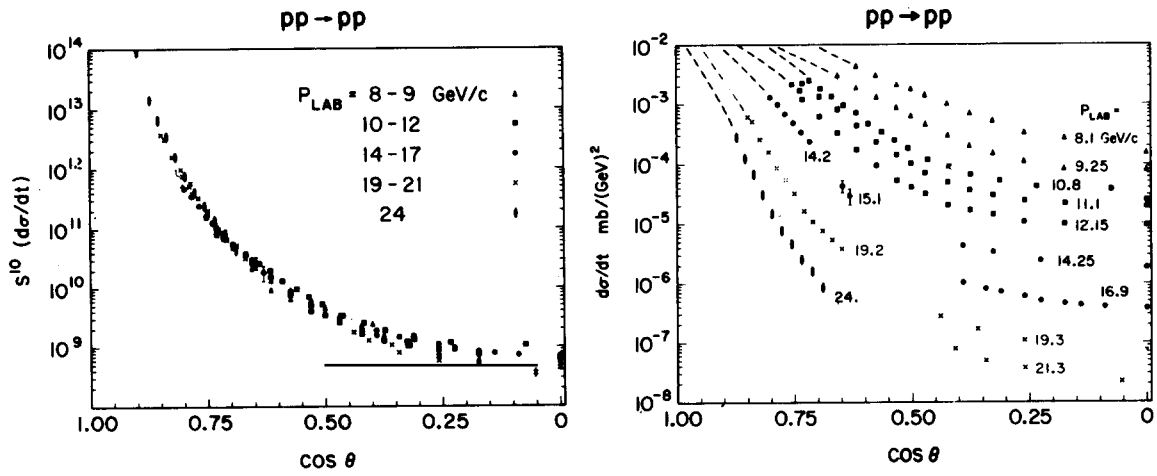

Fig. 4.2.1. s^{10} dσ/dt (pp → pp) and dσ/dt (pp → pp) plotted against cos θ.

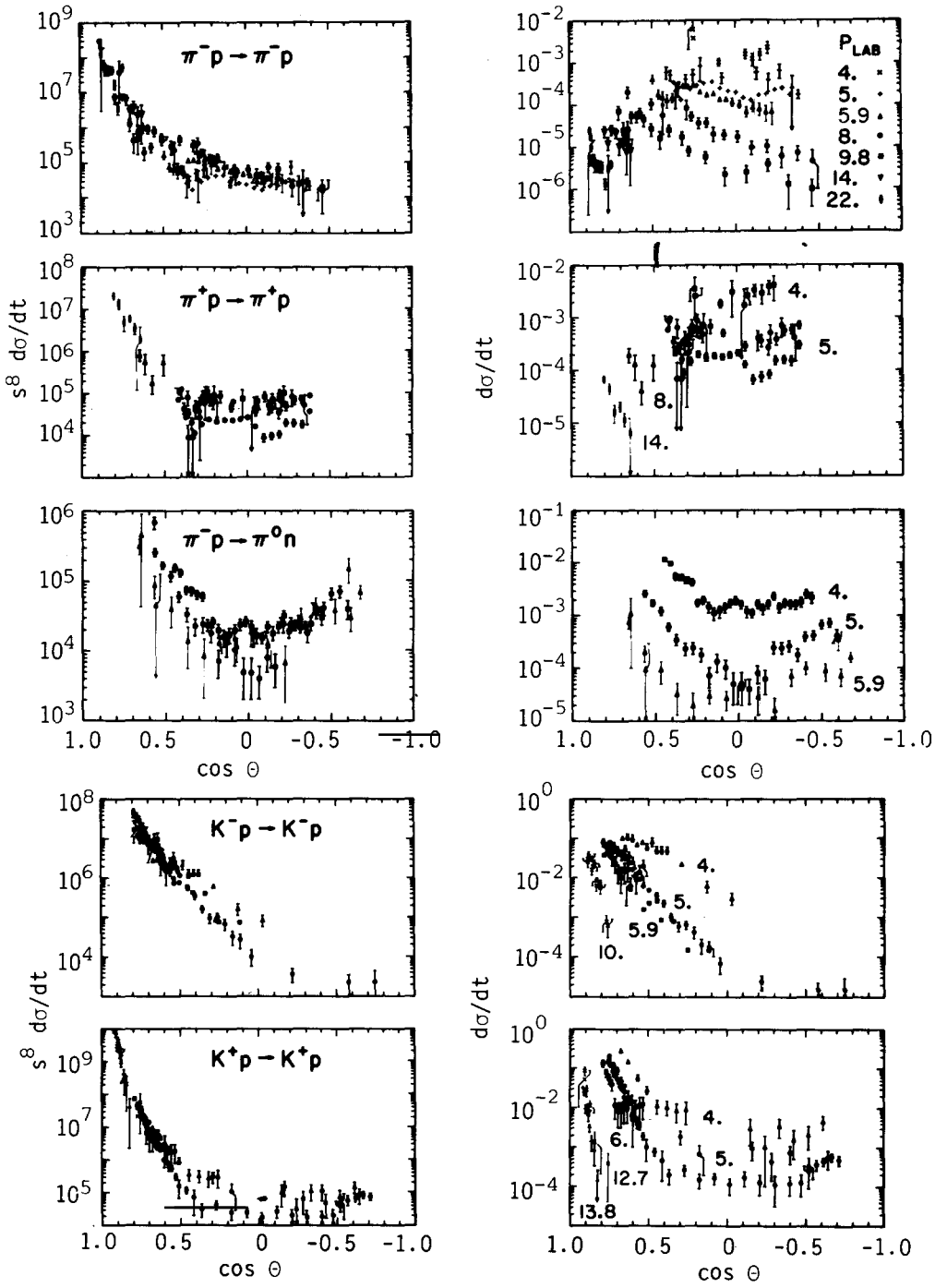

Fig. 4.2.2. $s^8\, d\sigma/dt$ and $d\sigma/dt$ for $\pi^- p \to \pi^- p$, $\pi^+ p \to \pi^+ p$, $\pi^- p \to \pi^0 n$, $K^- p \to K^- p$, $K^+ p \to K^+ p$. The counting rules (4.2.9) suggest that $s^8\, d\sigma/dt$ should be independent of energy for all these reactions.

of the rules for hard processes in field theories of composite hadrons is also discussed there.

4.2.2. Application to inclusive processes

If we apply the dimensional counting rules for inclusive hadronic interactions, then the quark model predicts a sum of terms in eq. (4.2.3) with $n_{\text{active}} = 4, 6, 8 \ldots$ as more and more constituents participate in the large p_T subprocess. The fact that a scale invariant term, p_T^{-4}, is not observed could be due to any number of possible reason:

(a) The gluon coupling strength could be very weak – at least at short distances. Of course, at order α^2, electromagnetic and/or weak contributions to quark–quark scattering are expected, but such contributions should not be important until $p_T > 25$ GeV (Berman, Bjorken and Kogut [28]).

(b) The p_T^{-4} term could be suppressed via the quasi-exclusive nature of $pp \to \pi X$, but still be present in the measurement of "jet" production $pp \to J + X$, where the jet is defined as a group of hadrons with $p_T^{\text{jet}} = \Sigma_i p_T^i$ the total transverse momentum measured on one side (Ellis [107]). Accordingly, calorimeter-type measurements will be very interesting. The idea that the cross section is suppressed if a large fraction of the momentum of a scattered parton needs to be transferred to a single hadron is in apparent conflict with the simple Drell–Yan scaling predictions for semi-inclusive deep inelastic scattering processes $ep \to ehX$. However, in the case of asymptotic freedom theories at very large momentum transfers, the predicted deviation from scaling and suppression of the three structure functions $G_{q/A}$, $G_{q/B}$, $\tilde{G}_{C/q}$ (each required with $x \gtrsim \frac{1}{2}$) could be sufficient to diminish the importance of the $qq \to qq$ term (Cahalan et al. [68]). Measurements of $ep \to \pi X$ and $\mu p \to \pi X$ might help to clarify the situation. The conventional parton prediction has a scale-invariant contribution from $\ell q \to \ell q$ (if the lepton balances the pion momentum) and a contribution $p_T^{-6}(\log(s/m_e^2))$, from $\gamma q \to \pi q$ (if a hadron balances the pion momentum). If $G_{q/\pi} \sim (1-x)$, then the p_T^{-4} coefficient should have ϵ^5 behavior for small ϵ.

(c) The process $q + q \to q + q$ may be suppressed when the quarks are effectively near their mass shells due to exponentiation of infrared factors; in the Fried and Gaisser [125] model p_T^{-4} behavior is expected only for very small x_T (see section 2). As pointed out by Polkinghorne [198], and by Appelquist and Poggio [15], one could still retain scale-invariance of the $qq \to qq$ interaction in the "light cone" region where all quark legs are off-shell, and thus preserve the dimensional counting rules for exclusive processes.

(d) In the massive quark model of Preparata [199, 200], scale-invariance only occurs in the case of double-fireball production $\bar{q}q \to F\bar{F}$. This is suppressed by the $\bar{q}$ distribution in the nucleon, $G_{\bar{q}/p} \sim (1-x)^7$, as well as by a possible large mass scale. Similarly $qq \to qq$ may be suppressed relative to $q\bar{q} \to q\bar{q}$ if one uses duality as a guide. The latter gives a contribution of order $p_T^{-4}\epsilon^{13}$ for $pp \to \pi X$, since $n_{\text{passive}} = 7$. Such a term could well be hidden by the CIM contributions at NAL and ISR energies. Furthermore, the Landshoff [170] contributions to exclusive scattering are absent, except for $p\bar{p}$ scattering.

(e) Another possibility, suggested by Gunion [134–136], is that the coherent sum of *all* gluon exchange contributions generates the Pomeron contribution to $qq \to qq$. Single gluon exchange would thus be suppressed at high p_T.

In the constituent interchange model, an explicit quark–quark interaction is never introduced. This idea was originally motivated by the fact that the observed angular dependence $f_{A+B\cdots C+D}(\theta_{CM})$ for exclusive processes can be rather simply explained in terms of quark-exchange diagrams. Quark-interchange is analogous to rearrangement collisions in atomic and molecular physics. This also seems to be a natural way for hadrons to scatter in the "bag" models. In any

event, the quark–hadron amplitude must exist just by the existence of the hadronic wave function. A review of the applications of the CIM to effective trajectories and θ_{CM} dependence in the interchange model may be found in section 5.

The leading processes for $pp \to \pi X^-$ in the CIM derive from quark–hadron interactions. The minimum ($n_{active} = 6$) terms correspond to $q + M \to q + M$ and $q + q \to B + \bar{q}$ or their crossing variants. An excellent fit to the CCR–ISR data for $pp \to \pi^0 X^-$ (but not the NAL data) can be obtained from eq. (4.2.6) with $G_{q/\pi} \sim (1-x)^5$, $G_{q/p} \sim (1-x)^3$ giving $E\,d\sigma/d^3p \sim (p_T^2 + M^2)^{-4}\epsilon^9$ since $n_{passive} = 5$. Similar fits have been given by Ellis [107, 108] and by Barnett and Silverman [26]. The relative importance of the two $n_{active} = 6$ contributions can be settled by measurements of quantum-number correlations.

However, for the Chicago–Princeton–NAL data, which involves $x_T > 0.4$, $a \sim p_T^{-11}$ scaling law is observed. This data, which is closer to the exclusive limit, indicates that other terms involving a larger number of active particles must be involved as ϵ becomes smaller. This is perhaps not unnatural: in general, as one approaches the exclusive limit, $\epsilon \to 0$, we can expect that more active quarks are required in order to produce a hadron with a sizable share of the available center-of-mass energy. In the CIM, the terms which contribute to $pp \to \pi X$ with $n_{active} = 8$ and minimal $n_{passive}$ (= 3) derive from the subprocesses $q + (qq) \to B^* + \pi$ or $p + q \to B^* + q\ (\to q + \pi)$ and give $p_T^{-12}\epsilon^5$. This suggests fits to the data of the form

$$\frac{E\,d\sigma}{d^3p} = \frac{A}{(p_T^2 + m_8^2)^4}\epsilon^9 + \frac{A}{(p_T^2 + m_{12}^2)^6}\epsilon^5 . \tag{4.2.12}$$

The fits are quite good and even are consistent with data at BNL energies. For the ISR data the p_T^{-12} term is negligible; the p_T^{-8} and p_T^{-12} are of comparable importance in the NAL-range, with the p_T^{-12} term dominant at large p_T due to its slower falloff in ϵ. Further details on these predictions and fits are discussed in section 5. It is interesting to note that p_T^{-12} contribution derives from subprocesses in which a baryonic system balances the large transverse momentum of the detected pion. For any subprocess, however, one expects resonance contributions (i.e., clusters) and a single particle in the recoil system is not likely. The effect of two contributions in $E\,d\sigma/d^3p$ implies that the effective power p_T^{-n} will vary from 8 to 12 as p_T increases across the NAL range, but remains close to 8 for the ISR data. However, at small $p_T < 2$ GeV the effective value of n will drop due to the mass terms and also the nonasymptotic behavior of the effective trajectory $\alpha(t)$. This last effect corresponds to the Reggeization due to the emission and absorption of hadronic bremsstrahlung softens the falloff of the subprocess in t.

Clearly there are a myriad number of contributions from subprocesses in which more and more constituents participate in the large p_T subprocesses. In order to make a simple classification, we can utilize the correspondence principle of Bjorken and Kogut [36] which assures a smooth connection between the form of the inclusive cross section for $\epsilon = \mathcal{M}^2/s \to 0$ and a corresponding exclusive cross section. This is a generalization of Bloom–Gilman [48] duality which has been proposed for deep inelastic lepton scattering. Thus if a contribution to the inclusive cross section for $A + B \to C + X$ at fixed θ_{CM} is to join smoothly for $\epsilon \to 0$ to an exclusive cross section for $A + B \to C + B$, we have

$$\int^{\bar{M}^2} d\mathcal{M}^2 \frac{d\sigma}{dt\,d\mathcal{M}^2}(A + B \to C + X) = \int^{\bar{M}^2} d\mathcal{M}^2 \frac{\pi}{s}\frac{1}{(p_T^2)^N}\epsilon^F f^{incl}(\theta_{CM}) = \frac{1}{s^{p_{excl}}} f_{A+B\to C+D}(\theta_{CM}) . \tag{4.2.13}$$

We thus have [62,114]

$$N + F + 1 = N + 2n_{\text{passive}} = p_{\text{excl}} = n_A + n_B + n_C + n_D - 2 , \tag{4.2.14}$$

and the identification

$$f^{\text{incl}}(\theta_{CM}) = f_{A+B\to C+D}(\theta_{CM}) \sin^2(\theta_{CM})^N . \tag{4.2.15}$$

Thus, generally speaking, for large p_T and small ϵ, one would expect contributions from those allowed subprocesses (a + b → c + d) which correspond to the minimum number of hadrons in the related exclusive channel to dominate. Note further that all of the contributions which yield the same p_{excl}, i.e., are dual to the same exclusive channel, may be summed in the form

$$\frac{d\sigma}{d^3p/E} \sim \frac{1}{(p_T^2)^N} \epsilon^F \left[1 + O\left(\frac{M^2}{p_T^2\epsilon}\right)^2 + \ldots + O\left(\frac{M^2}{p_T^2\epsilon}\right)^{F+1}\right] f^{\text{incl}}(\theta_{CM}) , \tag{4.2.16}$$

where the first term dominates for $p_T^2\epsilon \gg M^2$, and where the subsequent terms correspond to allowing additional passive spectator quarks to become active participants in the large momentum transfer reaction. The last term gives the exclusive channel contribution. Note that the corrections to the leading term are of the same form as that obtained by expanding $(p_T^2)^N \epsilon^{-1}(\epsilon')^{F+1}$ where $\epsilon'^2 = \epsilon^2 + O(M^4/p_T^4)$. This is analogous to the corrections to scaling introduced by the Bloom–Gilman variable $\omega = -(p\cdot q + M^2)/q^2$ in the analysis of deep inelastic scattering. Note that the ω' correction terms for ep → eX automatically includes the nonscaling contribution from the subprocess e(qq) → e(qq).

Thus the leading contributions in the CIM can be classified according to their dual exclusive channel (which determines $N + F$) and the distribution of active and passive quarks. To obtain the CIM candidates we only need to exclude the basic subprocesses qq → qq and q(qq) → q(qq). A list of various contribution subprocesses for the inclusive processes involving meson and baryons, using meson and baryon or electromagnetic beams is discussed by Blankenbecler and Brodsky [40] and Gunion [134–136].

The scaling laws (4.2.3) naturally take into account the underlying scale invariance at the constituent level, and correlate dynamical measurements with the degrees of freedom of the hadron in the simplest possible way. The rules also lead to simple asymptotic predictions for Regge trajectories and residue functions. These are reviewed in section 5. We also emphasize the importance of crossing behavior in models of large p_T reactions. The CIM combined with the rules (4.2.3) give the simplest possible realization of a theory with correct crossing behavior; the exclusive-inclusive connection, and a natural continuity with the Regge region for exclusive and inclusive reactions. These results are developed and reviewed in section 5.4.

4.3. Theories of the elastic form factor

The asymptotic dependence of the elastic form factors of hadrons plays a critical role in theories of large-angle scattering. Physically, the elastic form factor is the probability amplitude for a hadron to remain a single hadron after the transfer of momentum. Thus, in the model of Wu and Yang [227] (large t gluon exchange) or the CIM (large t quark interchange), the falloff of the exclusive scattering amplitude at large momentum transfer is controlled by the same physics that controls the falloff of the form factors. Many models, in fact, satisfy a relation conjectured by Theis [222] for the spin-averaged amplitude

$$\mathcal{M}_{AB\to CD}(s,t) \sim s^{-1/2(p_A+p_B+p_C+p_D)} f(t/s)\,, \tag{4.3.1}$$

for $s \to \infty$, fixed t/s, where $F_A(t) \sim t^{-p_A}$, etc. for the spin-averaged form factor. This result has been recently proven by Creutz and Wang [91] in elementary pseudoscalar field theory, and also holds in the CIM with dimensional counting (neglecting logarithmic modifications), the automodality model, and the eikonal model of Fried et al. [127–130].

It is well known that the proton form factors are quite adequately described by the dipole form $G_M(t) = \mu(1 - t/0.71\ \mathrm{GeV}^2)^{-2}$ and the scaling law $G_M(t) = \mu G_E(t)$. A graph of $t^2\, G_M^{exp p}(t)$ (fig. 4.3.1) shows that the asymptotic dependence of t^{-2} is consistent with the data. The pion form factor is less well known experimentally, but both spacelike (from $ep \to e\pi p$) and timelike data (from $e^+e^- \to \pi^+\pi^-$) are consistent with a falloff $F_\pi(t) \sim t^{-1}$ or slightly faster. A plot of $F_\pi(t)$ is shown in fig. 4.3.2. A very important result, obtained by Bonneau et al. [50] using a rigorous analysis of the data, shows that if the asymptotic falloff of $F_\pi(t) \sim t^{-n}$ on the average for $|t| > 2\ \mathrm{GeV}^2$, then $n < 1.2 \pm 0.3$. Thus the pion form factor cannot fall faster asymptotically on the average than $t^{-3/2}$. On the other hand if asymptotia begins at much larger $|t|$, say $|t| > 9\ \mathrm{GeV}^2$, then the bound is much less restrictive (Pham and Wright [194]).

The central theoretical question is thus the origin of the asymptotic behavior of the form factors. It is clear that one cannot give an a priori answer to this question without exact knowledge of the short distance structure of the hadrons. In the following we shall outline some of the main theoretical approaches to this question. An extensive *Physics Report* review has recently been given by Gourdin [132]. (For other reviews, see also Appelquist and Primack [16] and Brodsky and Farrar [62].)

There are three basic views of the short-distance structure of the hadrons which can be distinguished. (1) The constituent models – based typically on internal quark degrees of freedom; (2) models based on elementary field theories; and (3) infinitely composite systems – the hadronic bootstrap. In the following we will discuss in some detail the composite models and the connection to large transverse momentum phenomena.

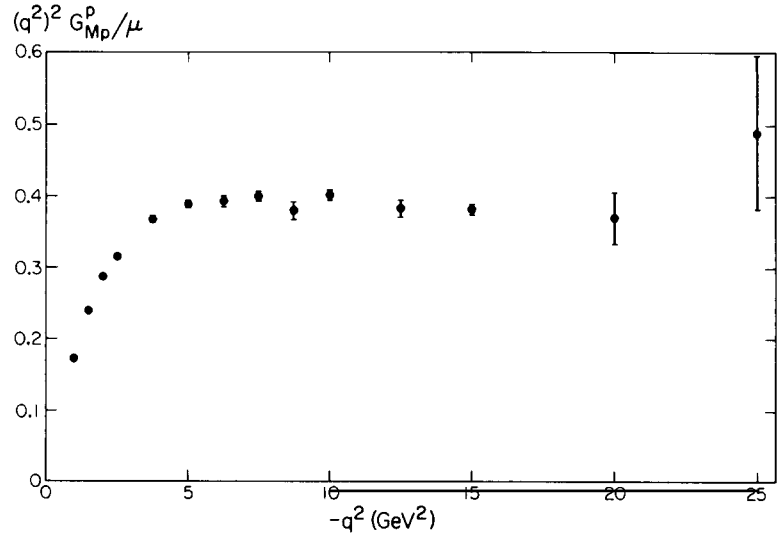

Fig. 4.3.1. Plot of $t^2 G_M(t)$ versus t where $G_M(t)$ is the experimental magnetic nuclear form factor.

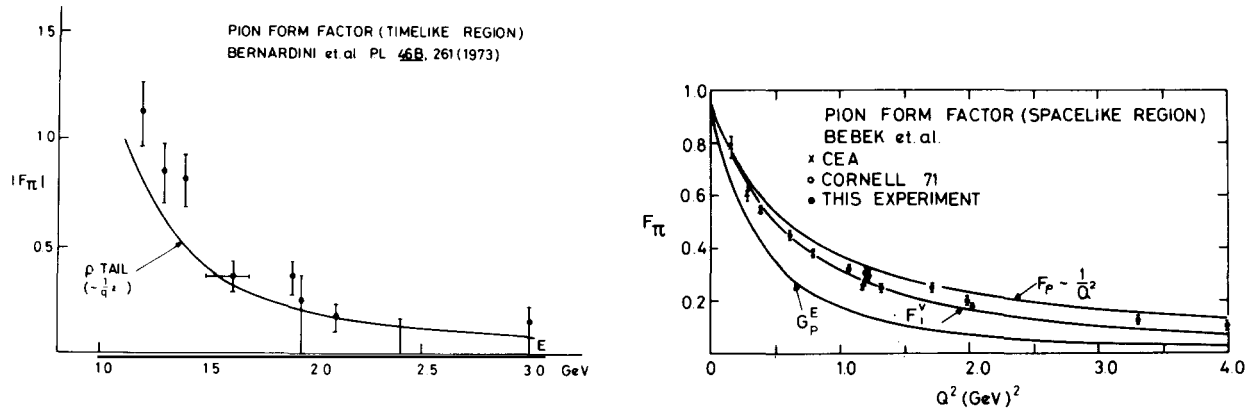

Fig. 4.3.2. The pion form factor in the timelike and spacelike regions.

4.3.1. Constituent models and dimensional counting

The quark-constituent approach has the important virtue of connecting naturally with SU(3) or SU(6) spectroscopy, current algebra, and the quark–parton phenomenology of deep inelastic lepton scattering processes. We can make the following assumptions:

(a) The prominent mesons and baryons are $\ell = 0$ Bethe–Salpeter bound states of two and three quark fields respectively. Thus in the limit of zero binding, the hadrons would become free quark states:

$$|B\rangle \to |qqq\rangle\,, \qquad |M\rangle \to |q\bar{q}\rangle\,.$$

The higher particle number components can be shown to produce nonleading terms to the scaling law at large momentum transfer. Also, as we discuss below, we assume a simple physical limit on the high energy momentum components in the wave function which ensures the finiteness of the wave function in coordinate space.

(b) The interaction of the hadron constituents are asymptotically scale invariant, as implied by Bjorken scaling.

With these assumptions we can derive the dimensional counting and automodality prediction (modulo powers of $\log t$)

$$F_H(t) \sim t^{1-n_H}\,, \qquad t \to \pm\infty\,, \tag{4.3.2}$$

for the asymptotic dependence of the spin-averaged form factor of a hadron H containing n_H elementary fields. This constituent-counting rule thus predicts $F_{1p}(t) \sim t^{-2}$ and $F_\pi \sim -t^{-1}$ consisting with the data, and naturally accounts for the faster falloff of the baryon wavefunction relative to that of the mesons. Physically, the rule allows a factor of t^{-1} for each additional quark line which changes direction from along p to along $p + q$. The scale invariant assumption (b) requires the quark form factor itself to be pointlike – consistent with Bjorken scaling, and leads to dominance of spin nonflip amplitudes, i.e.: the dominance of the Dirac form factor $F_{2p}/F_{1p} \to 0$, and $G_E(t) \sim G_M(t)$.

A simple illustration of how the dimensional counting rule arises in the Bethe–Salpeter computation of the meson form factor is illustrated in fig. 4.3.3. If we assume a falloff of the Bethe–Salpeter wavefunction at large relative momentum, corresponding to a wavefunction which is finite at the origin in coordinate space, then the leading contribution to the asymptotic form factor comes from iterating the Bethe–Salpeter kernel wherever large relative momentum is

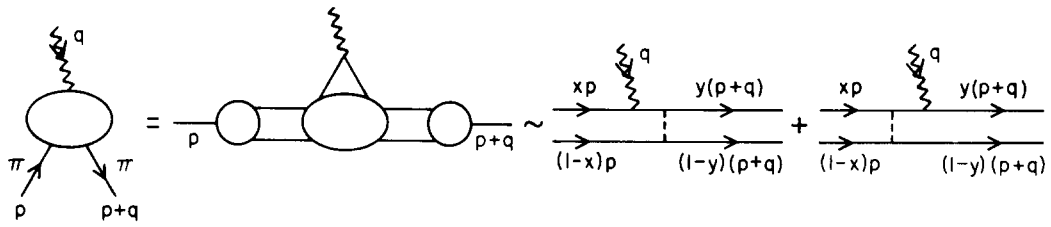

Fig. 4.3.3. Bethe–Salpeter computation of the meson form factor.

required, as indicated in the diagram. Thus one obtains for large q^2

$$(2p+q)^\mu F_M(q^2) \sim \int \frac{id^4k}{(2\pi)^4} \int \frac{id^4l}{(2\pi)^4} \psi^\dagger_{p+q}(l) \mathcal{M}^\mu \psi_p(k) , \tag{4.3.3}$$

where $\mathcal{M}^\mu$ is the connected amplitude for the photon coupling to the quark and antiquark with momenta k^μ and $(p-k)^\mu$ to l^μ and $(p+q-l)^\mu$. The integrations are limited to the dominant region of each wavefunction: $k = xp + \kappa$, $l = y(p+q) + \kappa'$, with $\kappa \cdot p = \kappa' \cdot (p+q) = 0$, and $\kappa'^2 \sim \kappa^2 \sim O(m^2)$. Thus $\mathcal{M}^\mu$ represents the scattering of photon on the quark constituents, each of which has a finite fraction of the hadron momenta: $p_i \sim x_i p$, $\Sigma x_i = 1$. It is exactly the connected amplitude which occurs when hadronic binding is turned off adiabatically, in which case $x_i \to m_i/M_H$. In the case of spin, $\mathcal{M}^\mu$ is defined to include the on-shell spinor factors.

A simple computation then gives $F_M(t) \sim t^{-1} \log t$ (where the logarithm arises from the $x \sim 1$ integration) since we have assumed a scale invariant kernel. The inverse factor of t^{-1} comes from the off-shell quark propagation. For an n-body state, $n-1$ quark lines are off-shell, giving the result (4.3.2). Notice that the minimum field description gives the leading asymptotic behavior.

We can also see how these results follow from simple dimensional analysis. After iteration of the interaction kernel, we are dealing with the scattering of a lepton on n_H near-mass-shell quarks each sharing a finite fraction of the momentum of the initial and final hadron. This amplitude which has $n = 2n_H + 2$ external legs and dimensions [length]$^{n-4}$, then must scale as $[\sqrt{t}]^{4-n}$ at fixed angle (t/s fixed, $|t| \to \infty$) if the internal interactions are scale-free and the coupling constants are dimensionless. This then gives the scaling (4.3.2) for form factor.

The finiteness of the Bethe–Salpeter wavefunction is crucial for the above derivation. The coefficient of the asymptotic power dependence and mass scale of the meson form factor is set by the value of

$$\psi_p(x_\mu = 0) = \int \frac{d^4k}{(2\pi)^4} \psi_p(k) , \tag{4.3.4}$$

which we require to be finite. This requires, at minimum, that $\psi_p(k)$ converges in the ultraviolet faster than $k^{-4} \log^{-1-\epsilon} k^2$, with $\epsilon > 0$.

There are a number of arguments which imply that $\psi_p(x)$ is in fact regular at $x_\mu \sim 0$. A quite general proof by Ezawa and Nishijima [115] shows that the existence of a composite field operator for a meson and the assumption that it lies on a Regge trajectory requires $\psi_p(0) < \infty$. Similarly, computations of weak and electromagnetic decays in current algebra are based on the finiteness of the wavefunction at the origin. These arguments, however, do not give an insight into how this result can arise dynamically.

Important progress has been made on the dynamical requirements of the wavefunction condi-

tion by Appelquist and Poggio [15]. They show that for the case of asymptotic freedom theories without infrared complications, the asymptotic ultraviolet behavior of the full Bethe–Salpeter kernel (including the self energy insertions on the incoming legs) is exactly one logarithm more convergent at large relative momentum than indicated by ladder approximation (scale invariance). They can then show that the Bethe–Salpeter wavefunction is finite at the origin up to a calculable logarithm, $[\log(x)]^d$, where d depends on the coupling constant. Assuming that the wavefunction has no anomalous behavior when one quark leg goes on the mass shell (we discuss this further, below), then one can show that $F_M \sim t^{-1}$ (modulo calculable logarithms).

We should emphasize here that the use of ladder approximation instead of the full Bethe–Salpeter kernel is misleading for the determination of asymptotic behavior in renormalizable theories, although this has been the historical approach. In ladder approximation the wavefunction has a power-law singularity which depends on the coupling constant, which in turn must be restricted *ad hoc* by hermiticity and normalization requirements. However, such behavior is unstable upon the addition of any additional contribution from the full kernel, e.g., a crossed-ladder graph, and cannot be obtained as the smooth limit of a regulated theory (e.g., dimensional regulation or the use of a Pauli–Villars spectrum). Furthermore, the ladder approach is inconsistent because some operators like the electromagnetic current and energy-momentum tensor do not have the correct (canonical) dimensions. The ladder equation difficulties are analogous to the mathematically-singular behavior of the Dirac wavefunction for the Coulomb potential for $r \to 0$. The physical wavefunction is in fact regular at the origin if the finite mass or size of the source or radiative corrections are taken into account.

In the case of quantum electrodynamics, the full Bethe–Salpeter kernel including radiative corrections undoubtedly falls faster than the simple ladder approximation, again arguing for a finite wavefunction at the origin. The true asymptotic dependence of the QED kernel to all orders in perturbation theory is not rigorously known, but neglecting higher order binding corrections, the form factor of positronium is known to obey the dimensional counting rule – modulo powers of $\log(t)$.

4.3.2. Composite systems and renormalizable theories

An important approach to the study of the asymptotic properties of composite systems is the investigation of those renormalizable field theories (such as asymptotic freedom theories) which insure conformal or scale invariance at short distances. A straightforward calculational technique is to assume that the full Bethe–Salpeter kernel has the effective scaling $(q^2)^{-\epsilon}$. The scale-invariant limit $\epsilon \to 0^+$, corresponding to a renormalizable theory, is taken at the end of the calculations. The results given by Ezawa [114], Brodsky and Farrar [62] (using the iteration method), and Alabiso and Schierholz [4] (which include an analysis of the three particle wavefunction) are consistent (modulo finite powers of $\log t$) with dimensional counting.

A very interesting ansatz for the quark–quark interaction has been recently proposed by Ezawa and Polkinghorne [116]. They assume that the effective Bethe–Salpeter kernel for $k_1 + k_2 \to k_3 + k_4$ is of the form $\gamma_\mu K \gamma^\mu$ where

$$K = \frac{1}{q^2} \prod_{i=1}^{4} \left[\frac{k_i^2}{k_i^2 + q^2} \right]^n , \qquad n > 0 . \tag{4.3.5}$$

This form is "asymptotically scale free", i.e.: is only scale-invariant when q^2 and all the external

masses k_i^2 are large together. This form has the following advantages:

(a) The Bethe–Salpeter wavefunction and form factors rigorously satisfy the dimensional counting conditions without cumulative logarithmic effects for any $n > 0$.

(b) The Landshoff "pinch" contribution (see below) is suppressed below the interchange and single gluon exchange contributions if $n > 1/16$. The fixed angle dimensional counting scaling law then (4.2.9) holds rigorously.

(c) The p_T^{-4} scale-invariant contributions to inclusive large p_T hadron reactions become suppressed below p_T^{-8} for $n > \frac{1}{4}$.

(d) Bjorken scaling is obtained for electroproduction with large multiplicities in the photon fragmentation region.

(e) The form (4.3.5), which suppresses the role of on-shell quarks may be relevant to the question of quark confinement. The ultimate origin of this effective interaction remains unknown.

Recently there has been considerable progress employing the more formal tools of the operator product expansion, the renormalization group, and dimensional regularization to analyze the asymptotic properties of composite systems. It has been shown by Shei [215], Borenstein [51], and Tiktopolos [223] that for various renormalizable theories, *excluding* vector gluon and gauge theories, the asymptotic behavior of the on-mass-shell form factors is rigorously related to the short-distance behavior of the theories. In particular, if the Gell-Mann–Low eigenvalue conditions are satisfied (ultraviolet-stable fixed points) then the asymptotic behavior of the form factor has power behavior $(-q^2)^{-\eta}$ where η can be related to the anomalous dimensions of the particle's field. A phenomenology of form factors can thus be based on these anomalous dimensions.

The intriguing question is then whether the anomalous dimension of an interpolating field for a hadron can be related to its degree of compositeness. Let us restrict ourselves to the conformal invariant or asymptotically free theories where the product of elementary fields at short distances has the canonical scaling of free fields. In particular, this guarantees Bjorken scaling in deep inelastic scattering. The asymptotic freedom theories automatically yield Bjorken scaling modulo logarithmic corrections since the interactions become weaker at short distances. Thus the short distance behavior of the Bethe–Salpeter wavefunction

$$\Psi_P(x) = \langle 0 | T(\psi(\tfrac{1}{2}x)\, \psi(-\tfrac{1}{2}x)) | P \rangle , \tag{4.3.6}$$

is controlled at $x^2 \to 0$ by the canonical dimensions of the quark fields. This in turn determines the scaling of the momentum space wavefunction $\Psi_P(k_1^2, k_2^2)$ in the "light-cone" limit $k_1^2 \to \infty$, $k_2^2 \to \infty$, where the mass of both logs become asymptotic.

However, the dominant contribution to the asymptotic behavior of the form factor involves contributions where one constituent leg is close to the mass shell. Thus we instead require the *form factor* limit of $\Psi_P(k_1^2, k_2^2)$ which is $k_1^2 \to \infty$, with k_2^2 *fixed*. In the case of renormalizable scalar-constituent field theories, such as ϕ^3 in six dimensions, and ϕ^4 in four dimensions, Menotti [187] has, in fact, shown that the only asymptotic scaling behavior of the complete wavefunction which gives consistent results for both fig. 4.3.4a and the convolution of the wavefunction shown in fig. 4.3.4b is that of uniform scaling behavior in both the light-cone and form-factor limits. Thus, in these scalar field theories the asymptotic momentum space Bethe–Salpeter wavefunction in both limits and the form factor of the composite system are controlled by the short-distance scaling behavior of the product of free field. In the absence of anomalous dimensions of the constituent fields one thus obtains the dimensional counting prediction (4.3.2), modulo the usual finite power of a logarithm; this is consistent with the Appelquist–Poggio result.

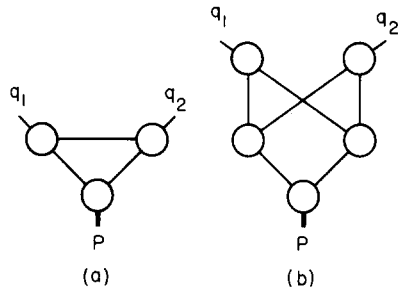

Fig. 4.3.4. Graph from Menotti showing diagrams which contribute in light cone and form factor limits.

The formal analysis of the composite particle form factor in spinor field theories is considerably more involved, and thus far theories with vector interactions are not completely understood because of possible infrared complications. Recent analyses have been given by Ciafaloni and Ferrara [85] and by Callan and Gross [69]. It should be emphasized that in the case of the spinor theories, the light-cone limit and form-factor limits of the Bethe–Salpeter wavefunction *do not* give the same scaling results, see Menotti [186–188]. The light-cone limit $\Psi_P(k_1^2, k_2^2)$, $k_1^2 \to \infty$, with k_2^2/k_1^2 finite will reflect the dimension of the constituent spinor field (and thus will fall one power faster in k_1^2 relative to the spinless case because the dimension of a spin $\frac{1}{2}$ field is [length]$^{-3/2}$ while the dimension of a spin 0 field is [length]$^{-1}$). However, as shown explicitly by Ciafaloni and Ferrara, in a spinor theory with scalar interactions, the form factor limit is controlled by the large $x \cdot p$ behavior of the coordinate wavefunction. This is the same asymptotic behavior as in a renormalizable theory with spinless constituents and again the dimensional counting result (4.3.2) is recovered for the meson form factor, independent of the constituent spin. The results are, thus, as expected. The analysis of Ciafaloni and Ferrara [85] is based on explicit solutions to the Dyson-type bootstrap equation for the propagator of the fundamental quark fields, which is however, obtained by replacing the full Bethe–Salpeter kernel with an effective local potential with an equivalent scaling behavior. Their solution requires the coupling constant and anomalous dimensions to vanish as a dimensional regulator goes to zero. The composite particles in this theory are effectively weakly-bound, with scale-invariant constituent interactions and thus conform to the dimensional counting analysis.

In the recent work of Callan and Gross [69], which applies renormalization group techniques to the analysis of the Bethe–Salpeter wavefunction, the difference between the light-cone and form-factor limits of $\Psi(k_1^2, k_2^2)$ can be traced to the presence of a zero-mass singularity which arises when one fermion leg goes on-shell. These authors also show that the leading contribution to the form factor for a meson with spin $\frac{1}{2}$ constituents derives from the disconnected contribution to the vertex function rather than the connected contribution shown in fig. 4.3.5 which arises from insertions into the cross graph kernel, etc. *

The derivation of dimensional counting which utilizes the iteration of the kernel in eq. (4.3.3) and the wavefunction condition (4.3.4) makes it clear that the spin of the constituents is irrelevant

* *Note added in proof*: However as shown by Menotti [188], the fermion anomaly utilized in [69] and [85] actually cancels, and the above arguments are not reliable. The situation has now been clarified by Polyakov [198a]. He argues that the asymptotic behavior of the form factor is controlled by the short-distance behavior of an optimum interpolating field, rather than ψ itself. Polyakov's results (for zero anomalous dimension) agree with the dimensional counting scaling laws and are independent of the spin of the constituents.

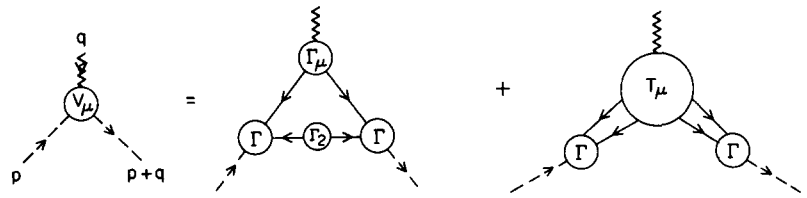

Fig. 4.3.5. Leading contributions to the form factor of a meson with spin-$\frac{1}{2}$ constituents.

if the kernel is scale-invariant, since the connected amplitude $\mathcal{M}^\mu$ always has the same dimensional scaling. The condition (4.3.4) in the spin case actually refers to the coefficient of on-shell spinors, $\psi^{+-}(x)$ as defined in the Salpeter formalism. The wavefunction $\psi^{+-}(x)$ has similar short distance properties and scaling as the scalar Bethe–Salpeter wavefunction (see Brodsky and Farrar [65]).

Thus we see that despite the diversity of the above methods, the physics is identical: the scaling of the amplitudes in these theories is equivalent to that obtained in the weak binding approximation. The scattering effectively occurs on nearly free constituent particles which share a finite fraction of the hadronic momenta.

4.3.3. Infrared effects

As we have seen a natural realization of the dimensional counting rules for the form factors of composite systems may be the asymptotic freedom theories. However, because of the yet unknown and perhaps critical effects of infrared behavior, a rigorous application of the asymptotic freedom gauge theories with vector gluon or gauge interactions has yet to be given. The simplest application of the renormalization group method to on-shell amplitudes fails due to the potential mass-zero singularities of such theories. The most familiar example of such phenomena is the fermion form factor in massive QED; summing leading logarithms from the infrared region in each order of perturbation theory, one obtains (Appelquist and Primack [16], Sudakov [219], Jackiw [152,153])

$$F(q^2) \sim \exp\left[-\frac{\alpha}{2\pi^2}\log^2(-q^2/\mu^2)\right], \tag{4.3.7}$$

where μ^2 depends on the photon mass and external leg masses. One can use this form to successfully parametrize the hadron form factors. However, in such a model there is then no connection with short distance behavior or evident reason for Bjorken scaling. Note that it is incorrect to use (4.3.7) which is derived from on-shell quarks as the constituent quark form factor, which is to be interpolated with a composite hadron "body" form factor, since the quark legs can be effectively far-off shell inside the hadron. Thus, there is considerable uncertainty on the effects of the infrared region on the form factors. However, there is an optimistic point of view. As discussed by Brodsky and Farrar [63] and by Appelquist and Poggio [15] (see also Tiktopolos [223]), the fact that a hadron may be taken to be *neutral* with respect to the charges of the gauge group leads to an explicit *cancellation* of the infrared divergences in perturbation theory. Further as we have noted, the quark legs are off-the-mass shell and thus regulate the theory in the infrared so that wavelengths larger than the size of the system are not effective. Additionally, if we take the gluons as color octets and hadrons as color singlets, then gluon emission changes quantum numbers and is not soft; there is thus no reason why an eikonal-like exponentiation or serious modification of the hadronic scaling laws should occur in such models.

4.3.4. Quark confinement, large transverse momentum and form factors

An implicit assumption in the use of the quark–parton model is that the interactions at short distances are unaffected by quark confinement. The usual view is that the confinement of quarks is basically a large distance phenomenon which operates over distance scales of order 1 fm. This assumption can be partially justified by the success of the quark–parton model in electroproduction, but since it plays such a central role in most treatments of large-transverse momentum processes, it is important to achieve more theoretical understanding.

There have been many theoretical approaches. For example, Bjorken [33] and Coon [88] have shown in the context of simple potential models that closely spaced bound state levels can mimic a continuum of free states in deep inelastic scattering. The currently popular "bag" models (Chodos et al. [79,80], Bardeen et al. [24]) represent dynamical attempts to build in the intuitive notion that quarks can essentially be treated as free particles in their short-distance behavior while being confined within hadronic matter. Jaffe [156] has argued that Bjorken scaling can be obtained in a simplified version of the MIT bag model.

In a theory with quark confinement, the momentum space quark propagator has no physical particle pole as is evident from the fact that in configuration space the propagator has only finite support. Simple quark–parton diagrams are therefore strictly defined only in terms of the propagation within the space-time envelope of the hadron and the usual Feynman rules only apply for quark lines which are far off mass shell. The massive quark model (MQM) proposed and developed by Preparata [199, 200] heroically attempts to take into account the complicated consequences of this fact. For deep inelastic lepton scattering, the usual "handbag" diagram is replaced in this model by allowing for a $J=1$ final-state-confining interaction of the quarks. The effective quark propagator has no pole but is peaked at small masses and falls off exponentially along the p^2 real axis. Despite many complexities, the model can be shown to give parton-like behavior.

For large-angle hadron hadron scattering in the MQM the actual systems that are interchanged always have hadronic quantum numbers. In spite of the fact that the diagrams contain an extra internal loop the amplitudes calculated in this model have the same power law scaling behavior as in the CIM discussed previously, and the cross sections agree with dimensional counting.

For inclusive reactions, the predictions of the MQM are again not too dissimilar from those of the CIM. A fit to the reaction $pp \to \pi +$ anything in the kinematic regimes of the CCR and CP collaboration (Preparata [199, 200]) argues for the presence of at least two terms. In the MQM, one of these falls as p_T^{-8} and the other as p_T^{-10}. At small x_T and very high energies where $\bar{q}q \to$ two fireballs can be important ($s > 10^4$ GeV^2) the model also predicts a scale-invariant p_T^{-4} contribution. More details of the phenomenology of the MQM should be sought in the review of Preparata [199, 200].

The consequences of quark confinement are not fully understood, to say nothing of the mechanism. The intuitive feeling that large transverse momentum phenomena should be insensitive to quark confinement has not been fully confirmed, especially in gauge theories with infrared singularities. The fact that the MQM has many features in common with simple quark parton models and the CIM in spite of vastly different mathematical formalism remains large mysterious.

Throughout the discussion we have assumed that the quark confinement mechanism does not affect the short distance properties of the Bethe–Salpeter wavefunction nor the asymptotic form factor.

In the MIT "Bag" model (Chodos et al. [79]) one can expect that the form factor is controlled asymptotically by a mechanism similar to that of the momentum partition model. After one quark

receives the momentum transfer q, a single vector gluon exchange (possibly with a rather weak coupling constant) is required to restore the motion of both quarks along the final direction $p+q$. Thus the dimensional counting result would be obtained. Intuitively, it is expected that the bag boundary itself would not be effective to cause the momentum transfer between quarks. On the other hand, Shiff [209] has considered a model for a meson in which the quark and antiquark in the rest system satisfy the free Dirac equation inside a spatial boundary. Initial and final states are then obtained by appropriate Lorentz boosts, and it is found, surprisingly, that the form factor falls as $(q^2)^{-1}$ for large momentum transfer.

In the massive quark model of Preparata, which explicitly deals with the quark confinement problem, the meson form factor is assumed to fall asymptotically as $(-q^2)^{-3/2}$, which is, as we have seen is consistent with the data. However, this result is derived by using the Drell–Yan–West relation, and assuming (from a crossing requirement and data) that $F_{2\pi}(x) \sim (1-x)^2$ for $x \sim 1$. However, as emphasized by Ezawa [114], the DYW relation should be modified in the case of spin $\frac{1}{2}$ constituent Bethe–Salpeter models, and thus there is no compelling theoretical reason for a $(q^2)^{-3/2}$ law.

In the model of Bohm and Krammer [49], quarks are always taken to have very large free mass; thus $|q^2| \ll 4M^2$. The quark–quark interaction is taken to be a four-dimensional hadronic oscillator with a $\gamma_5 \cdots \gamma_5$ Dirac structure. The assumption that the form factor can be built up by resonances leads to an excellent phenomenological fit to the pion form factor and the asymptotic falloff $F_{2\pi}(q^2) \sim -0.33\ \mathrm{GeV}^2/q^2$.

4.3.5. Dimensional counting and large-transverse momentum exclusive processes

Most of the discussion given in this section for form factors of composite systems in renormalizable theories also holds for exclusive processes in the fixed θ_{CM} limit. In general, the amplitude for the scattering of composite particles has the form

$$\mathcal{M}_{\mathrm{AB}\to\mathrm{CD}} = \int \psi^{\mathrm{A}}_{\mathrm{BS}}\, \psi^{\mathrm{B}}_{\mathrm{BS}}\, \mathcal{M}_n\, \psi^{\mathrm{C}}_{\mathrm{BS}}\, \psi^{\mathrm{D}}_{\mathrm{BS}}\, \pi\, \mathrm{d}^4 k\,, \tag{4.3.8}$$

where $\mathcal{M}_n$ is the connected amplitude for the scattering of the n elementary active constituents. If the Bethe–Salpeter wavefunctions are finite, the scaling of $\mathcal{M}_n$ at large momentum transfer controls the scaling behavior of $\mathcal{M}_{\mathrm{AB}\to\mathrm{CD}}$. With the usual state normalization $\langle p'|p\rangle = 2E\,\delta^3(\boldsymbol{p}-\boldsymbol{p}')$ the amplitude $\mathcal{M}_n$ has dimension $[\mathrm{length}]^{n-4}$. If there is no external scale and no infrared problem, then we can write at fixed angle

$$\mathcal{M}_n \sim (\sqrt{s})^{n-4}\,. \tag{4.3.9}$$

The dimensional counting/automodality results (4.2.9)–(4.2.11) thus follow. Some comparisons with experiment are presented in section 4.2.

The crucial question for the validity of the counting rules is the possible origin of infrared effects or an external scale in $\mathcal{M}_n$. The possible corrections to (4.3.9) from anomalous dimensions of the quark fields or the accumulation of logarithmic factors are not known, except that they should be small in some sense if the contributions to Bjorken scaling in deep inelastic lepton scattering are small.

The general validity of the counting rules for hadronic scattering is, however, complicated by the possible contribution of multiple-scattering Glauber-like diagrams. The importance of these diagrams, which in fact contain linear infrared divergences, was discussed by Landshoff [170].

For example in pp → pp, each quark of one proton can scatter elastically and near the mass shell on a quark of the other hadron through the same angle θ_{CM} with a finite fraction of the proton's momentum.

If the underlying quark–quark interaction for near on shell quarks is scale-invariant, then the amplitude is only suppressed by a phase-space factor,

$$A_{LAND} \sim (is^{-3/2})^{L-1}, \tag{4.3.10}$$

where L is the number of q–q scatterings. For pp scattering $L=3$ and the contribution of this diagram to the differential cross section

$$\left.\frac{d\sigma}{dt}\right|_{LAND} \sim \frac{1}{s^8} f(\theta_{CM}), \tag{4.3.11}$$

which would be expected to dominate the dimensional counting, s^{-10}, contribution. Empirically, this falloff is too slow. Explicit calculation of the Landshoff diagrams has been given by Cvitanovic [95] using Feynman parameters and by Brodsky and Farrar [63] using infinite momentum techniques. Appelquist, Coleman and Quinn [14] have shown that, in a renormalizable field theory, the Landshoff diagrams are the only ones with linear infrared divergences.

There have been numerous speculations about the possible suppression of the Landshoff diagrams. Clearly, any mechanism which eliminates scale-invariant quark–quark scattering between quarks of different hadron as empirically required by the absence of a scale-invariant term in the large p_T inclusive data, will also eliminate these multiple-scattering contributions. Polkinghorne [198] and Appelquist and Poggio [15] have proposed an on-shell infrared suppression factor and Ezawa and Polkinghorne [116] have demonstrated a simple model in which the dimensional counting rules are rigorously correct. This is discussed in detail in section 4.3. As a final empirical note, Farrar and Wu [118] have shown that the Landshoff diagram cannot account for the angular distribution in present pp elastic scattering data.

4.4. Soft gluon theories

These theories differ from the "hard" gluon theories, exemplified by the Wu–Yang model as extended by Abarbanel, Drell and Gilman [1], in that the exchange of soft gluons strongly modifies a single large t exchange (Fried, Gaisser and Kirby [126,127]). This damping effect grows with momentum transfer and actually controls the large angle behavior. There are several versions of the model which use this same basic physical picture of the large t scattering process, and they seem to be very similar but differ in calculational details. The elastic scattering amplitude for pp → pp is of the form

$$\frac{d\sigma}{dt} = \left(\frac{d\sigma}{dt}\right)_{Born} [\exp 4\gamma(f(t) + f(u) - f(4m^2 - s))], \tag{4.4.1}$$

where the nucleon form factor at large t is given by

$$G(t) \propto \exp[\gamma f(t)]. \tag{4.4.2}$$

The Born term due to the hard scattering interaction is usually taken to arise from a low spin (1 or 0) meson exchange. In the original model of Fried and Gaisser [125], γ was taken to be constant and the function $f(t)$ was shown to behave as $\ln t$. In the model of Contagouris et al. [87],

γ grows as $\ln s$. This double log behavior was shown to arise in perturbation theory by Halliday, Huskins and Sachrajda [140,141], who have clarified the basic properties required so that the above form holds. This double log was previously found to occur in the form factor in a calculation by Sudakov [219] see eq. (4.3.7) and can be related to the soft photon forms of Yennie et al. [228].

Since the effects of soft gluon damping become more important at large t, these theories can explain the large difference between the angular distributions of pp (K^+p) and $\bar{p}p$ (K^-p), for example. This is in sharp contrast to hard gluon exchange theories that require single gluon exchange to dominate at large t and hence would have the cross sections equal.

The predictions of these theories for inclusive reactions is based on the same physical picture, in which neutral vector mesons are radiated and then decay to mesons. The inclusive cross sections achieve the form

$$E \frac{d\sigma}{d^3p} = H(x_T)\, s^{-n(x_T)}, \tag{4.4.3}$$

where in the approximate calculation of Fried and Gaissner, $n = 2 + 4\gamma x_T$. This behavior is in agreement with the trends of the data, but it does not scale according to Feynman for $x_T \to 0$. (See Fried [124].)

These theories give rise to a breaking of Bjorken scaling in deep inelastic lepton scattering but this can be made undetectably small at present energies. The associated multiplicities have also been discussed by Fried et al. [129,130] and their results can be put in the general form discussed by Savit [208]. The recent work of Contagouris et al. [87] is an ambitious attempt to fit a large amount of data with the few parameters in this type of model. One of the main questions is whether a natural and simple explanation of the particle ratios in inclusive scattering can be achieved.

Perhaps the most fundamental approach is that persued by Halliday, Huskins and Sachrajda [140,141] who use perturbation theory on a vector gluon field theory to extract the asymptotic behavior extending the deep inelastic scattering work of Gribov and Lipatov [133]. The behavior of the form factor and exclusive scattering at fixed angle was found to be very similar to the above formula but the inclusive cross section was found to behave somewhat differently. At fixed x_T, it was found that many particles could be found with large p_T values, and additional logarithmic behavior arose at small x_T. The associated production was found to be widely spread in p_T, with large p_T particles produced which were not correlated strongly with or against the large p_T trigger. Again Bjorken scaling is not satisfied in these theories. In contrast to scalar ϕ^3 theories that predict a finite multiplicity, vector theories yield a multiplicity that grows like a fractional power of $\ln s$ and in general depend on the p_T of the trigger.

It must be emphasized, however, that summing only the leading (double) logarithms in perturbation theory may not be an accurate guide to the true asymptotic behavior. A skeptic could well claim that the exponential sum of double logarithms sums to a negligible contribution compared to the remaining terms. This should be contrasted with the infrared problem in quantum electrodynamics, where Yennie, Frautschi and Suura [228] demonstrated the exponentiation of all $\log \lambda$ dependence as a factor of the matrix element. A related problem occurs on the Regge behavior of the models. Halliday and Huskins [139] have shown that for $p\bar{p} \to \pi^+\pi^-$, the sum of leading logarithms gives an exponential of double logarithms times an elementary Born term (fixed pole at $j = \frac{1}{2}$). Thus the procedure does not produce a moving pole, which would be expected in the complete amplitude.

5. Phenomenology and the constituent interchange model

In sections 1 and 4 we have described the hard scattering models and their properties from a fairly general viewpoint. In order to discuss specific calculations, we now turn to the constituent interchange model which provides a definite dynamical realization of a quark parton model for hadronic reactions, and in which all of the generalized properties outlined in section 1.4 are explicitly fulfilled. These include the exclusive-inclusive connection, generalized Regge behavior, and the dimensional counting rules. From one point of view the CIM provides a covariant, but simple procedure for calculating the dynamics of duality diagrams at large momentum transfer, and thus it naturally incorporates the quark degrees of freedom of hadrons. On the other hand it is compatible with the conventional Regge and completely hadronic descriptions of low-momentum-transfer processes. Detailed discussions of the CIM may be found in the varied papers of Blankenbecler, Brodsky, Gunion, and Savit [38–46] and Landshoff and Polkinghorne [174–177]. Further calculational details are discussed by Fishbane and Muzinich [121], and M. Schmidt [211]. An introduction to calculational methods is given in Appendix B. An early comparison of calculation methods and applications of the covariant parton model and the CIM can be found in the lectures of Polkinghorne [197] and Blankenbecler [38].

5.1. The structure of the CIM

The physical structure of the CIM for both exclusive and inclusive processes at large momentum transfer is shown schematically in fig. 5.1.1. The model begins with a basic irreducible large-angle

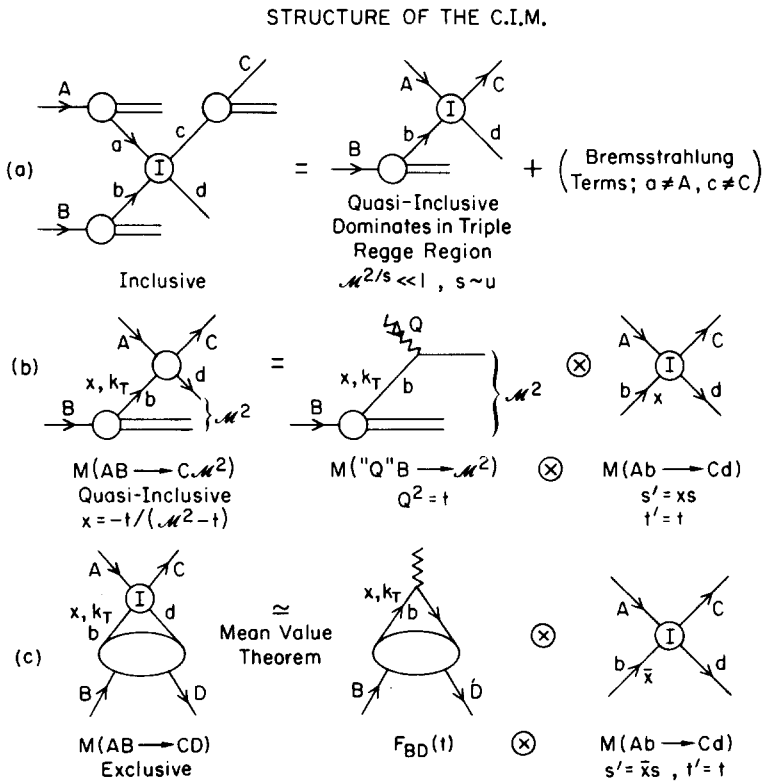

Fig. 5.1.1. Structure of CIM at large t and u.

subprocess a + b → c + d, involving quarks plus states with hadronic quantum numbers, which is then weighted by the covariant amplitudes for the fragmentation or formation of the scattering hadrons. Thus, inclusive processes at large t and u are controlled by quark–hadron scattering, and exclusive processes always involves quark interchange or quark exchange. We have already discussed in section 4.3 why scale-invariant quark–quark scattering involving quarks of different hadrons seems to be negligible or absent. The hypothesis that quark exchange processes should be dominate was originally made (Blankenbecler et al. [41,42]) to account for the difference in normalization of large angle pp → pp and $p\bar{p} \to p\bar{p}$ processes, and the fact that it accounts well for the angular structure of the exclusive processes, especially $K^+p \to K^+p$, and pp → pp. However, unless it is suppressed by kinematics, one must allow for hadronic radiation or bremsstrahlung from the initial beam particles A and B. Thus bremsstrahlung is analogous to the real and virtual radiative corrections to electromagnetic reactions and it "dresses" and reggeizes the hadronic processes. In the case of real hadronic bremsstrahlung, the effects may be incorporated into the $x \to 0$ behavior of the structure function $G_{a/A}(x)$ and $G_{b/B}(x)$, which is related to the Regge behavior of the cross sections $\sigma_{\bar{a}A}$ and $\sigma_{\bar{b}B}$ (see section 4). In the case of virtual bremsstrahlung, the coherent emission and absorption of hadrons between particles A and C moves the Regge poles $\alpha_{AC}(t)$ away from their asymptotic values at large t. This is discussed in detail by Blankenbecler, Brodsky, Gunion and Savit [45]. The virtual radiation can be neglected at large t and u, thus exposing the minimal "impulse approximation" terms which yield power law scaling laws at fixed angle. There is also the possibility of absorption corrections from Pomeron exchanges of the initial particles, which is controlled asymptotically by the S-matrix at zero impact parameter (see Blankenbecler et al. [41,42], Kane [158]). Absorptive corrections are assumed to not change the asymptotic scaling laws, but there can be residual effects reflecting the geometrical sizes of hadrons at moderate t values. The small oscillating structure in pp → pp scattering (see fig. 2.1.7) observed as a function of t by Hendry [146] and discussed by Shrempp and Shrempp [212] is thus not necessarily in conflict with the asymptotic validity of parton model ideas.

In order to examine the structure of the CIM, let us first consider the inclusive reactions A + B → C + X in a region of phase space where bremsstrahlung from particles A and C should be suppressed, for example, the "triple-Regge" region where $\mathcal{M}^2 \ll s$, and $s \gg -t$, but $|t|$ is still large. The leading CIM contribution is then quark–hadron scattering q + A → q + C, on the quarks of the target particle B. An elementary calculation, which parallels the standard parton model calculations for deep inelastic lepton scattering term gives (see fig. 5.1.1a)

$$E\frac{d\sigma}{d^3p} \cong \frac{1}{\pi}\sum_q \frac{s}{s+u}\, x\, G_{q/B}(x)\, \frac{d\sigma}{dt}(Aq \to Cq)\Big|_{\substack{s'=xs \\ t'=t \\ u'=xu}}, \tag{5.1.1}$$

where $x = -t/(s+u) = -t/(\mathcal{M}^2 - t)$, is the familiar Bjorken scaling variable. The assumptions here include the convergence of the transverse momentum integrations (i.e., the existence of the $G_{q/B}(x)$), and incoherence of the various quark contributions, and the usual neglect of the quark confinement problem.

There exists a corresponding contribution to the exclusive amplitude A + B → C + D calculated according to fig. 5.1.1c. In this case an integral over the fractional momentum (or light-cone variable) $x = (k_0 + k_3)/(p_0 + p_3)$ variable is required. Using the mean value theorem we can write the contribution from scattering on one quark

$$\frac{d\sigma}{dt}(A + B \to C + D) \cong F_{BD}^2(t)\,\frac{d\sigma}{dt}(Aq \to C + q)\Big|_{\substack{s'=\bar{x}s \\ t'=t}}, \tag{5.1.2}$$

although in fact here the quark contributions should add coherently. The central assumption in eq. (5.1.2) is that the vertex function of particles B and D converge most rapidly; in general the integral gives additional contributions where hadrons A, C, or D are treated as the target. The value of $\bar{x}$ is obtained from the mean value theorem. In practical cases $\bar{x} \sim 1$ gives the dominant region of integration. The form factor $F_{BD}(t)$ falls at the same rate as the elastic form factor.

The expressions (5.1.1) and (5.1.2) have simple analogues when we treat the coherent and incoherent scattering the nucleons of a nuclear target; the function $G(x)$ is given by the Fermi distribution, and $F_{BD}(t)$ is the "body" form factor of a nucleon in the nucleus. In the case of lepton scattering (5.1.1) and (5.1.2) are the standard parton model results. In the case of photon-scattering, (5.1.2) predicts the dominance of $J=0$ fixed pole behavior of the Compton amplitude $\gamma p \to \gamma p$ at large t, and fixed pole behavior at J below 1 for meson photo-production.

As in section 1.4, we see that the inclusive and exclusive scattering cross sections are connected and join smoothly since they have the same behavior on the kinematic variables in this limit. A calculation of the relative normalization is difficult. One difficulty is that of simply computing the inclusive cross section at a small missing mass, and another arises from the fact that the simple incoherent sum over final states used above is not justified since many of the final states become coherent at small missing mass. Therefore, one should not expect the theoretical formulas to lead to a smoother connection than expected from the above discussion. We also see that this connection will hold both at fixed t and at fixed scattering angle.

5.2. *Inclusive scattering in the CIM*

5.2.1. *Triple Regge region*

Let us now examine the triple Regge region by including the Regge effects just discussed. We now have for the basic scattering of a quark and a hadron

$$\frac{d\sigma}{dt}(Aq \to Cq) = |\gamma(t')(-u')^{\alpha_{AC}(t')} + \tilde{\gamma}(t')(-s)^{\alpha_{AC}(t')}|^2/s^2\,, \tag{5.2.1}$$

$\gamma(-\infty)$ = constant, and $\alpha_{AC}(-\infty)$ is given by the counting rules. Both terms are needed to get the angular distribution correct. The inclusive cross section arising from this basic process becomes

$$\frac{E\,d\sigma}{d^3p} = \frac{x_1^2}{(p_T^2+m^2)^{2-2\alpha(t)}}\,x G_{q/B}(x)\left[\frac{\mathcal{M}^2-t}{s}\right]^{1-2\alpha(t)} |\gamma(t) + \tilde{\gamma}(t)(-x_1)^{-\alpha(t)}|^2 + \ldots\,. \tag{5.2.2}$$

Now one can identify the expected triple Regge behavior and corrections to it when $x_1 \neq 1$ and $x \neq 0$.

5.2.2. *Central region*

In order to get particles into the central region, it is advantageous to let both incident particles A and B bremsstrahlung, lose momentum and collide at a low relative effective energy. This type of inclusive process is conveniently decomposed into peripheral interactions, hadronic bremsstrahlung and the basic irreducible process as illustrated in fig. 5.1.1. A very large class of theories including many of the statistical models can also be decomposed in this fashion. The resulting cross section is of the form (given in eq. (1.3.10))

$$\frac{E\,d^3\sigma}{d^3p}(A + B \to C + X) = \sum_{a,b} \int dx\, dy\, G_{a/A}(x)\, G_{b/B}(y) \frac{E\,d^3\sigma^I}{d^3p}(a + b \to C + d^*)\Big|_{\substack{s'=xys \\ t'=xt \\ u'=yu}}, \tag{5.2.3}$$

and

$$M_a^2 + M_b^2 + M_C^2 + M_{d^*}^2 = xys + xt + yu\ .$$

The possibility of bremsstrahlung from the final state C will be discussed shortly.

The irreducible process $a + b \to C + d^*$ (no extra hadrons are allowed to be emitted) can be conveniently separated into contributing graphs as depicted in fig. 5.2.1. The first term on the right gives the pure fixed power-behaved amplitude previously discussed while the second term gives rise to Regge behavior for the process $a + q \to C + q$. The third term corresponds to the production of a state c in the basic interaction that subsequently decays to the observed particle C.

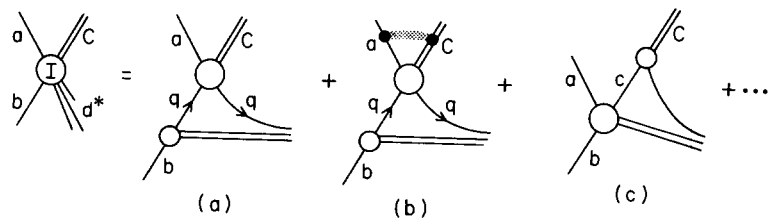

Fig. 5.2.1. Structure of the irreducible amplitude $ab \to Cd^*$.

Using the relation between the irreducible and total probability functions

$$G_{q/B}(x) = \int_x^1 \frac{dz}{z} \sum_b G^I_{q/b}\left(\frac{x}{z}\right) G_{b/B}(z)\ , \tag{5.2.4}$$

the inclusive cross section can be written in the convenient but unsymmetrical form

$$\frac{E\,d^3\sigma}{d^3p}(A + B \to C + X) = \int_{z_0}^1 dz \sum_a G_{a/A}(z) \frac{E\,d^3\sigma}{d^3p}(a + B \to C + X)\ , \tag{5.2.5}$$

where $z_0 = -u/(s+t)$ and the inclusive cross section under the integral is evaluated at $s' = zs$, $u' = u$, and $t' = zt$. Recall that in this formula, small intermediate transverse momenta have been neglected, and the required symmetrization between the particles has not been explicitly denoted. This is easily handled in any specific reaction of interest.

The general behavior of the inclusive cross section can be understood from quite simple kinematic arguments that are of course implicitly contained in the above formula. The basic (internal) process is $a + q \to C + q$ and it has an (energy)^2 of

$$s_{\text{eff}} = xys \sim \frac{x^2(-u)s}{xs + t} \geqslant 4p_T^2\ , \tag{5.2.6}$$

if the missing mass M_{d^*} is kept finite. Therefore this process is operating at a fixed angle and at an $s_{\text{eff}} \sim 4p_T^2$, and one expects the cross section to fall as $(p_T^2)^{-N}$, where N is related to the total number of constituents involved in this subreaction. Thus the p_T dependence of the inclusive cross section is related to and determined by the number of constituents involved in the basic process.

Let us further examine the central region where $p_T^2 = tu/s \cong$ constant, and $\epsilon = \mathcal{M}^2/s \cong 1$. The integral over z is easily estimated in the above formula and one finds

$$\frac{E\,d\sigma}{d^3p} = \sum_a G_a(x_L, \epsilon)(p_T^2)^{-N_a}\,, \tag{5.2.7}$$

where $N_a \equiv 2(1-\alpha_{aC}(\langle z\rangle t))$, and $\langle z\rangle$ is the average value of z involved in the integral. For large $|t|$, $\alpha_{aC} \approx \alpha_{aC}(-\infty)$ which is a number determined by counting. For example, $\alpha_{aC} = -1$ yields p_T^{-8} terms, $\alpha_{aC} = -2$ yields p_T^{-12} terms, etc. The p_T dependence reflects the fixed angle behavior of the basic process $a + b \to C + d^*$ of course.

A second interesting region is the threshold region defined by $\epsilon \to 0$. This limit should suppress the bremsstrahlung contributions and one finds that this is indeed the case. Note that the suppression works from both ends of the integral since $z_0 = 1 - \epsilon/(1+t/s) \to 1$, and also, the x variable in the inclusive process under the integral is

$$x' = -\frac{t'}{s'+u'} = \frac{(z-z_0)(s+t)}{(zs+u)}\,. \tag{5.2.8}$$

Thus in the integrand, $z \sim z_0$ is suppressed and of course $z \sim 1$ is suppressed by the explicit $G(z)$ probability function. One finds

$$\frac{E\,d\sigma}{d^3p} \cong \sum_{a,b} \epsilon^{F(a,b)}\gamma_{ab}(p_T, u/s)\,, \tag{5.2.9}$$

where

$$F(a,b) = g(a/A) + g(b/B) + 1\,, \qquad G_{a/A}(x) \sim (1-x)^{g(a/A)}, \quad \text{etc.} \tag{5.2.10}$$

Let us now examine the integral in more detail for a general contribution. We will assume that argument of $\alpha(t')$ can be replaced by a constant under the integral, that is $t' \to \langle t'\rangle = -2p_T^2(1+\langle z\rangle)^{-1}$, and assume the probability functions have the simple form $G(x) \propto (1-x)^g/x$. Finally, the basic cross section will be written in the general form

$$\frac{d\sigma}{dt}(s,z) \propto (s'+m^2)^{-N}\left(\frac{1-z}{2}\right)^{-b}\left(\frac{1+z}{2}\right)^{-a}\,, \tag{5.2.11}$$

where N, a and b may depend parametrically on p_T^2 through their dependence on $\alpha(t')$, since $N \equiv 2 - 2\alpha(\langle t'\rangle) + b$.

The integral for the inclusive cross section is

$$\frac{E\,d\sigma}{d^3p} \propto \int_{-(1-2x_1)}^{(1-2x_2)} \frac{dz}{(1-z^2)}\left(1-\frac{2x_1}{1+z}\right)^{g_A}\left(1-\frac{2x_2}{1-z}\right)^{g_B}\left(\frac{1-z^2}{4p_T^2}\right)^N\left(\frac{1-z}{2}\right)^{-b}\left(\frac{1+z}{2}\right)^{-a}\,, \tag{5.2.12}$$

where $x_1 = -u/s$, $x_2 = -t/s$. Changing variables, this can be written as

$$\frac{E\,d^3\sigma}{d^3p} = \frac{\epsilon^F f_0}{2(p_T^2+M^2)^N}\,I(x_1,x_2)\,,$$

where $M^2 \cong m^2(1-\langle z\rangle)/4$, $\epsilon = 1-x_1-x_2$, and

$$I(x_1,x_2) = \int_0^1 d\eta\,\eta^{g_A}(1-\eta)^{g_B}(x_2+\epsilon(1-\eta))^{N-1-g_B-b}(x_1+\epsilon\eta)^{N-1-g_A-a}\,. \tag{5.2.13}$$

This integral representation has several advantages. It explicitly shows the basic symmetry of the result in $x_1 \leftrightarrow x_2$ if $g_B \leftrightarrow g_A$ and $a \leftrightarrow b$. It is also in the form of the integral representation for a hypergeometric function of two variables (Bateman, HTF, Vol. 1, p. 231). The associated reduction and transformation formulae are very convenient in extracting the limiting behavior of $I(x_1, x_2)$ in a variety of regions (Pearson [193]). For example, in the singular limit of g_A or $g_B \to -1$, the integration is dominated by an endpoint behavior and one recovers the expected triple Regge formula. If the probability functions vanish at $x = 0$, extra powers of x_1 and/or x_2 occur outside the integral $I(x_1, x_2)$.

Note that if $\epsilon \to 0$ for finite x_1 and x_2, the cross section vanishes as ϵ^F. However, in the triple Regge region, where $1 \cong x_1 \gg \epsilon \gg x_2$, I is easily shown to behave as ϵ^{N-1-g_B-b}. This result can be interpreted as a triple Regge formula with an effective trajectory given by

$$\alpha_{\text{eff}}(t) = \alpha_{AC}(\langle t' \rangle) - \tfrac{1}{2}(1 + g(a/A)) , \tag{5.2.14}$$

which can be identified as a nonleading disconnected cut contribution.

We have now identified a second important correction to the triple Regge formula which should become important at large missing mass and provides the correct extrapolation into the central region. An analysis of reactions of the form $pp \to CX$, where $C = p, \pi^{\pm}, K^{\pm}, \bar{p}$, has been carried out by Chen, Wang and Wong [76]. As discussed in more detail by Blankenbecler and Brodsky [40], their results for the effective trajectory provide evidence for the type of correction we are discussing and for the quantum number dependence predicted by the above formula for α_{eff}.

In the preceding discussion, the possibility that the particle C observed at large p_T arose from the decay of a state, say c, which was produced at large p_T, was not included. We have already argued that a basic large angle scattering process produces resonances with roughly the same cross section as particles, and therefore it is important to take this into account. Generalizing the formula to this case, it is clear one has (see Appendix A)

$$\frac{E\,d\sigma}{d^3p} = \sum_{a,b,c} \int dx\, dy\, dz\, G_{a/A}(x)\, G_{b/B}(y)\, \tilde{G}_{C/c}\left(\frac{1}{z}\right) \frac{d\sigma}{dt}(ab \to cd^*)\Big|_{\substack{s'=xys \\ t'=zxt \\ u'=zyu}} \frac{xys}{\pi}\,\delta(xys + zxt + zyu) . \tag{5.2.15}$$

Since particle c must have more momentum than the detected one, C, the argument of $\tilde{G}_{C/c}$ is $1/z$, where $1/z$ is between 0 and 1. Using similar arguments as before, the threshold behavior of the cross section is given by $F = 2(n(\bar{a}A) + n(\bar{b}B) + n(\bar{c}C)) - 1$ and the p_T^2 power N depends on the basic process just as before.

Roth [204] has emphasized that since $(sE\,d\sigma/d^3p)$ arises from the discontinuity of a $3 \to 3$ amplitude, the same amplitude should describe the two processes $A + B \to C + X$ and $\bar{C} + B \to \bar{A} + X$, and they are connected by $s \leftrightarrow u$ crossing. Not all models will possess this property. In particular, those models that try to combine an exponential (statistical) final decay distribution with a power law initial state scattering amplitude cannot satisfy it.

This crossing relation must be satisfied and it leads to restrictions on the probability functions $G(z)$. In particular, from the structure of the above equation there must exist a relation between $G(z)$ and $\tilde{G}(1/z)$, and this relation for scalar particles turns out to be

$$G_{a/A}(z) = -z\, \tilde{G}_{\bar{A}/\bar{a}}\left(\frac{1}{z}\right) . \tag{5.2.16}$$

If this relation is used for both $G_{a/A}$ and $\tilde{G}_{C/c}$, and one writes

$$\frac{d\sigma}{dt}(ab \to cd^*) = \frac{1}{s^2}|M(ab \to cd^*)|^2 , \tag{5.2.17}$$

one can easily cross this relation ($s \leftrightarrow u$) and arrive at the formula

$$\frac{E\,d\bar{\sigma}}{dt} = \sum_{ab,c} \int dz\, dy\, dx\, G_{\bar{c}/\bar{C}}(z)\, G_{b/B}(y)\, \tilde{G}_{\bar{A}/\bar{a}}\left(\frac{1}{x}\right) \frac{d\sigma}{dt}(\bar{c}b \to \bar{a}d^*)\, \frac{xys}{\pi}\, \delta(zys + zxt + xyu) , \tag{5.2.18}$$

which is of the same form as the original equation.

This continuation formula for G is consistent with the integral equation satisfied by the G's. That is, if the hadron irreducible function G^I satisfies this relation, then so does the full G. Writing eq. (5.2.4) in the form

$$-z\, G_{B/A}\left(\frac{1}{z}\right) = -z \sum_a \int_{1/z}^{1} \frac{dx}{x}\, G^I_{B/a}\left(\frac{1}{xz}\right) G_{a/A}(x) , \tag{5.2.19}$$

and using the continuation formula twice on the right hand side and the change of variable $xz \to x$, one finds

$$-z\, G_{B/A}\left(\frac{1}{z}\right) = \sum_a \int_z^1 \frac{dx}{x}\, \tilde{G}_{\bar{A}/\bar{a}}\left(\frac{z}{x}\right) \tilde{G}^I_{\bar{a}/\bar{B}}(x) = \tilde{G}_{A/B}(z) , \tag{5.2.20}$$

as required, since $\tilde{G}$ satisfies the conjugate equation to (5.2.4).

It is amusing to note that a general solution of this functional equation, if one requires that $G_{B/A} = G_{A/B} = G_{\bar{A}/\bar{B}}$, is

$$G(x) = \frac{1-x}{x}(1 + x^2 - ax)\, g\left(\frac{1}{x} + x\right) . \tag{5.2.21}$$

If $a = 2$ and g = constant, this reduces to a commonly used approximate form for the nucleon's structure function. If spin one-half particles are involved, there is an extra factor of $(-1)^{f(A,B)}$, where $f^{(A,B)}$ is the total number of fermions in the state $(\bar{A}B)$. This factor arises from the associated spin traces; its effects need to be fully explored in the general case.

5.3. Exclusive scattering in the CIM

The objective of this section is to discuss several exclusive scattering processes and to extract their expected angular as well as energy dependences in the CIM. This will lead naturally into a discussion of the connection between the fixed angle and fixed t (Regge) behavior. As we shall see, this type of composite model predicts a particularly simple connection which has many experimental ramifications. A discussion of calculations of the scattering of composite systems is given in Appendix C.

The crucial result which characterizes a scattering matrix element in the CIM is

$$M_{AB \to CD}(u,t) \sim F^q_{BD}(t)\, M_{qA \to qC}(u,t) + \ldots \tag{5.3.1}$$

where $F^q_{BD}(t)$ falls in t as the B → D transition form factor and q is a constituent of particle B as illustrated in fig. 5.3.1a. The crossed diagram of 5.3.1b is also present. Direct quark–quark scattering such as in fig. 5.3.1c is neglected.

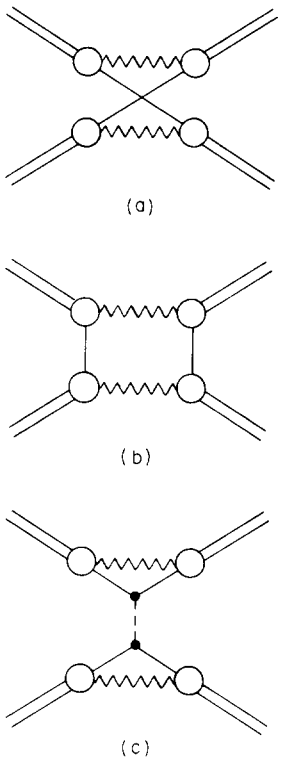

Fig. 5.3.1. (a) (ut) quark interchange contribution to hadron–hadron scattering. The wavy line represents the remaining "core" of the hadron after one quark is removed. (b) (st) quark exchange contribution to hadron–hadron scattering. (c) Gluon exchange contribution to hadron–hadron scattering.

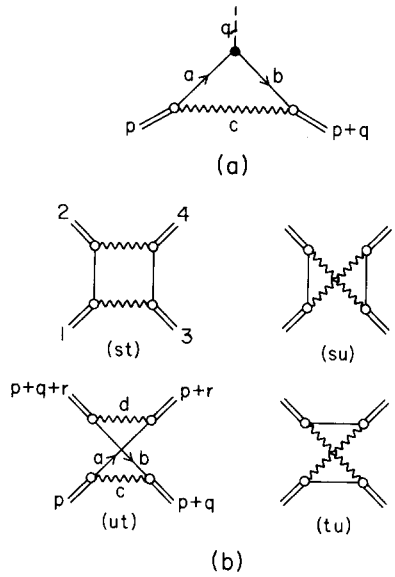

Fig. 5.3.2. Hadron form factor and scattering amplitudes in the constituent interchange amplitudes. The wavy line represents the remaining "core" of the hadron of the one quark is removed.

Let us now apply this formula to meson–baryon scattering, first ignoring spin effects. In general, the scattering amplitude is a linear combination of (ut) and (st) contributions which we will write in the form

$$M(s,t,u) = \alpha M(u,t) + \beta M(s,t)\,, \tag{5.3.2}$$

where asymptotically

$$M(u,t) \sim (-t)^{-2}(-u)^{-1}\,, \tag{5.3.3}$$

for the constituent interchange diagram of fig. 5.3.2b. The factor $(t)^{-2}$ is interpretable as a "form factor" of the nucleon as illustrated in fig. 5.3.2a, while $(-u)^{-1}$ is the quark–pion scattering amplitude.

The value of α and β for a particular reaction depends upon the quantum numbers assigned to the constituents. Pearson [193] has evaluated these coefficients in the SU(3) quark model. He further separates the terms into contributions arising from a hadronic core having quantum numbers of a $\{6\}$ and a $\{\bar{3}\}$ by writing $\alpha = \alpha(6) + \alpha(\bar{3})$ and similarly for β. The values for a selected set of reactions is given in table 5.1. Once the behavior of the M's are given, the values of α and β deter-

Table 5.1

Reaction	$\alpha(6)$	$\alpha(\bar{3})$	$\beta(6)$	$\beta(\bar{3})$
$\pi^+p \to \pi^+p$	1	1	2	0
$\pi^-p \to \pi^-p$	2	0	1	1
$\pi^-p \to \pi^0n$	$-1/\sqrt{2}$	$1/\sqrt{2}$	$1/\sqrt{2}$	$-1/\sqrt{2}$
$K^+p \to K^+p$	1	1	0	0
$K^-p \to K^-p$	0	0	1	1
$K_Lp \to K_sp$	-1	0	1	0
$\pi^+p \to K^+\Sigma^+$	0	0	-2	0
$K^-p \to \eta\Sigma^0$	$-1/\sqrt{3}$	0	$1/\sqrt{3}$	0

mine the angular distribution at large angles. In the simple quark counting model, the core is $\{6\} + 3\{\bar{3}\}$. However, the inclusion of the effects of spin (see below) modifies the expected angular distributions without changing the energy dependence at fixed angle. Absorptive corrections are assumed to affect the magnitude of M but not its large angle behavior if the absorption is smooth at short distances (as suggested by Kane [158]).

A specific model for meson–baryon scattering which included the effects of spin and assumed that the baryon was primarily a bound state of a quark and a spin one core was discussed by Blankenbecler, Brodsky and Gunion [43]. In this model, helicity is conserved asymptotically and the cross section has the form

$$\frac{d\sigma}{dt} \propto (-u/s)\,|B|^2\,, \tag{5.3.3}$$

with

$$B(s,t,u) = \alpha\, B(u,t) + \beta\, B(s,t)\,, \tag{5.3.4}$$

where

$$B(u,t) \sim (-u)^{-2}(-t)^{-2}\,, \tag{5.3.5}$$

for $|u|$ and $|t|$ large. Predictions for some typical differential cross sections in the limit of exact SU(3) are given in table 5.2, see also fig. 5.3.3.

Table 5.2

$$\frac{d\sigma}{dt} \equiv \frac{\sigma_0}{s^8}\,\frac{(1+z)}{(1-z)^4}\,R^2(z)$$

Reaction	$R(z)$
$\pi^+p \to \pi^+p$	$4\alpha(1+z)^{-2} + \beta$
$\pi^-p \to \pi^-p$	$4\beta(1+z)^{-2} + \alpha$
$K^+p \to K^+p$	$4\alpha(1+z)^{-2}$
$K^-p \to K^-p$	α

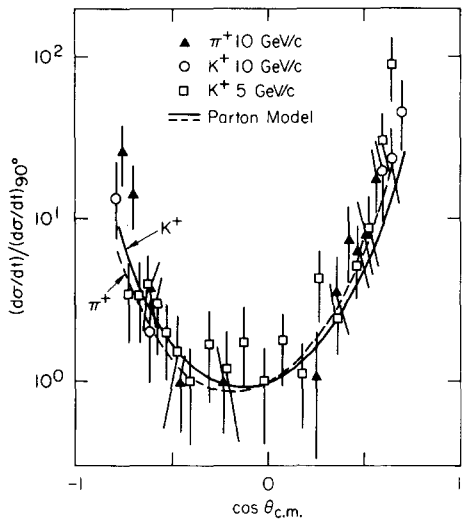

Fig. 5.3.3. Comparison with interchange model predictions for $k^+p \to k^+p$ and $\pi^+p \to \pi^+p$ elastic scattering. From Lundby [182].

The above invariant matrix element can also be used to describe the annihilation of $\bar{p}p$ into mesons by continuing to this channel by $s \leftrightarrow t$ crossing. Two results which follow from the above are

$$\frac{d\sigma}{dt}(\bar{p}p \to \pi^+\pi^-) = \frac{\sigma_a(1-z^2)}{s^8}[\alpha(1-z)^{-2} + \beta(1+z)^{-2}]^2 , \tag{5.3.6}$$

and

$$\frac{d\sigma}{dt}(\bar{p}p \to K^+K^-) = \frac{\sigma_a(1-z^2)}{s^8}[\alpha(1-z)^{-2}]^2 , \tag{5.3.7}$$

which yields the ratio

$$\frac{d\sigma}{dt}(K^-p \to K^-p)\Big/\frac{d\sigma}{dt}(\bar{p}p \to K^+K^-) = 2(1-z)^{-1} . \tag{5.3.8}$$

The above results have been confirmed by the recent calculation of Matveev et al. [184] who assume $\alpha = 2$, $\beta = 1$, and γ_5 invariance (at high energies).

In the case of nucleon–nucleon scattering, the general treatment of the angular distribution taking into account the spins of the four external baryons and the six internal quarks is extremely complicated. The proton wavefunction was treated in leading order as a quark bound to a spin-one core, and spin effects were then treated exactly in the work of Blankenbecler, Brodsky and Gunion [43]. It was found that the dominant invariant amplitudes were the vector and axial-vector ones and hence that s-channel helicity was conserved in this limit. In the paper by Matveev et al. [183] dimensional counting behavior of s^{-10} and s-channel helicity conservation were assumed. They then obtained an angular distribution that was somewhat different from Blankenbecler, Brodsky and Gunion near 90° and quite different for smaller angles. An important point here is that the lack of antiquarks in the nucleon wavefunction means that the (st) graph does not occur in leading order and the (ut) graph (with final particle symmetrization) dominates the interchange amplitude.

All of these types of models predict that the dependence on energy and angle factor into the form

$$\frac{d\sigma}{dt}(pp \to pp) \sim s^{-n}R(z) + O(s^{-n-1}) . \tag{5.3.9}$$

A check of this separation is shown in fig. 4.2.1 and fig. 2.1.8. The best fit value of n depends somewhat on the kinematic range involved. The angular dependence following from these models is also quite restricted and can be characterized by

$$R(z) = (1-z^2)^{-6}J(z) , \tag{5.3.10}$$

where $J(z)$ is slowly varying. This is again in reasonable agreement with the data. A precise calculation of $J(z)$ is very model dependent and very difficult.

A severe test of any model is to take the matrix elements and to use them in both the direct and crossed channels. It is very instructive to first consider models where a single vector meson exchange dominates the amplitude. The magnitudes of the angular distribution of pp and $\bar{p}p$ elastic scattering in this case are comparable around 90°, except for identical particle effects. If there are only neutral vector mesons then np should also be similar to $\bar{p}p$ in the backward hemisphere and have no backward peak. The data seems to rule out this scattering mechanism on both counts. Experimentally, the angular distribution of $\bar{p}p$ is strongly suppressed relative to pp and $np \to np$ has a backward peak.

In contrast the differential cross section that one gets in the CIM by crossing from eq. (5.3.10) can be characterized by the form

$$\frac{d\sigma}{dt}(\bar{p}p \to \bar{p}p) = s^{-n}(1-z)^{-6}\bar{J}(z) , \tag{5.3.11}$$

where $\bar{J}(z)$ is slowly varying. The value of $\bar{J}(0)/J(0)$ is also predicted, and we shall return to this point in the next section. Also, the CIM amplitude for $np \to np$ is found to peak in the backward hemisphere.

One of the difficult questions to answer in interchange models concerns the prediction of the absolute normalization of the scattering amplitude. A detailed model of the hadronic wavefunction is required as well as a careful calculation of all the contributing diagrams. The most careful treatment for proton–proton scattering seems to be the work of Hayashi and Yabuki [144]. They assumed the quark-core model of the nucleon and find for the scattering amplitude in the spinless case

$$\frac{d\sigma}{dt} \cong \pi^3(2m_V)^{16}m^{-4}s_0^4(1-z^2)^{-6}s^{-12}\ln^2(s/s_0) , \tag{5.3.12}$$

where m is the effective parton mass and the nucleon form factor has the behavior

$$F(q^2) \cong (m_V/q)^4 \ln(q^2/s_0) , \tag{5.3.13}$$

so that $m_V^2 \cong 0.71\ (\mathrm{GeV}/c)^2$. The value of m required to fit the data is very small and lies in the range 30–50 MeV if $s_0 = 1\ (\mathrm{GeV})^2$. An important question is whether or not the inclusion of spin and the effects of the large numbers of coherent exchanges that contribute to the process modifies this result substantially.

Finally, it should be remarked that the energy dependence at fixed angle for resonance produc-

tion is the same as for elastic scattering in this model. For example, the fixed angle cross section for $pp \to N^*p$ or N^*N^* should fall in energy at the same rate as pp elastic, and similarly for $\pi p \to \pi N^*$, ρN or ρN^*. The angular dependence for these latter processes should be different in general, and a measurement of their characteristic shape would help determine the properties of relevant wavefunctions.

5.4. Fixed-angle and Regge behavior in the CIM

We have seen that the typical basic scattering process between hadrons falls with energy at fixed angle rather rapidly in the CIM. This is true even at fixed momentum transfer unless there is a direct vector gluon force (which we have argued must be negligible). The basic scattering process can be considered as in fig. 5.4.1a. If it falls as s increases at fixed t, then the system will prefer to scatter through diagrams of the form shown in fig. 5.4.1b. In this virtual bremsstrahlung diagram, particle A converts to H with a fraction x of the incident momentum and other coherent "stuff" with momentum $(1-x)$. The basic process is thereby converted to H + B → H′ + D scattering at the reduced effective energy $s' \approx xs$. If x can be small, then this process is not suppressed much if H′ can pick up the momentum fraction $(1-x)$ and convert to C. This latter process is suppressed as t increases, so that in the large t and eventual fixed angle limit, the irreducible process (fig. 5.4.1a) will dominate. At small t, the short circuit diagram will dominate and the cross section will fall less rapidly in s. This is the typical origin of Regge behavior in this model at small t. It is dominated by the emission and absorption of the less massive hadronic states. They therefore control the long distance or small-t behavior of the amplitudes.

As discussed earlier, the amplitude for the process A + B → C + D can be separated into the form

$$M \sim \beta_{BD}(t)(-u)^{\alpha_{ac}(t)} + \beta_{BD}(t)(-s)^{\alpha_{AC}(t)} + \ldots \tag{5.4.1}$$

for fixed t as $s \to \infty$. The asymptotic behavior of the trajectory α_{AC} at large $|t|$ is controlled by the basic process which in this case (see fig. 5.3.1a) is quark–hadron scattering. It can be shown that the dominant diagrams using quark counting lead to

$$\alpha_{AC}(-\infty) = \tfrac{1}{2}(4 - n_A - n_C - n_I)\,, \tag{5.4.2}$$

$$\beta_{BD}(t) \sim \tilde{\beta}_{BD}(t) \sim (-t)^{(n_I - n_B - n_D)/2}\,, \tag{5.4.3}$$

where n_I is the minimum number of exchanged quarks.

These predictions do not automatically lead to factorization of residues as is required of t-channel singularities in Regge theory. For example, the above formula predicts that $\alpha_{\pi p}(-\infty) = -1$ and $\alpha_{pp}(-\infty) = -2$, but, of course, factorizable poles must contribute to both processes. In this case, the coupled channel T-matrix equations automatically force a cancellation between asymptotically degenerate trajectories so that the above relations are satisfied (Blankenbecler, Brodsky, Savit and Gunion [45]). It was shown that the coupled (in the t-channel) system of meson–meson and baryon–antibaryon scattering has an amplitude of the form (neglect signature)

$$M = \beta^+(t)(-u)^{\alpha_+(t)} + \beta^-(t)(-u)^{\alpha_-(t)} + \beta_0(t)(-u)^{\alpha_0(t)} + \ldots \tag{5.4.4}$$

where in the particular case studied,

$$\alpha_+(t) \sim -1 + O(-t)^{-2}, \qquad \alpha_-(t) \sim -1 + O(-t)^{-4}, \qquad \alpha_0(t) \sim -2 + O(-t)^{-2}\,, \tag{5.4.5}$$

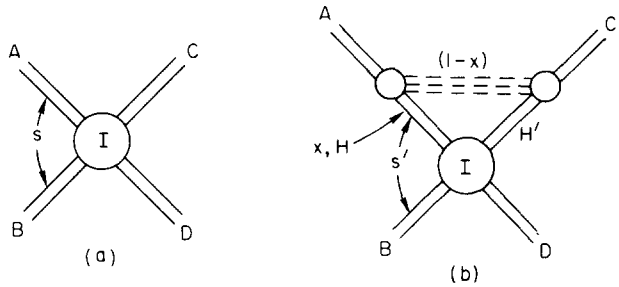

Fig. 5.4.1. (a) The irreducible contribution to hadron–hadron scattering. By definition H_0 (virtual) hadronic bremsstrahlung occurs before the interaction of A and B. (b) Virtual hadronic bremsstrahlung contribution leading to Regge behavior of the scattering amplitude.

and the β's depend on the channel involved. For meson–meson scattering, $\beta^+ \sim (-t)^{-1}$ and $\beta^- \sim -(-t)^{-4}$. Hence the fixed angle behavior is given by the first term. For meson–baryon scattering, $\beta^+ \sim (-t)^{-2}$ and $\beta^- \sim (-t)^{-2}$, and the fixed angle behavior arises from the first two terms. Finally, in the baryon–baryon case, $\beta^+ = -\beta^- \sim (-t)^{-3}$, and the first two terms tend to cancel with a remainder of the order of $(-u)^{-1}(-t)^{-5}\ln(-u) \propto s^{-6}\ln s$ at fixed angle. The third term then dominates at fixed angle since it is of order $(-u)^{-2}(-t)^{-2} \propto s^{-4}$ at fixed angle.

It should be noted that the cancellation between the two leading trajectories in baryon–baryon scattering should occur when $\alpha^+ \cong -1$, since α^- is expected to be quite flat. Now α^+ is the trajectory that dominates pion–nucleon scattering and the effective trajectory extracted from the data seems to reach (-1) for $|t| \gtrsim 2$–3 GeV^2. Thus one should expect the fixed angle power behavior s^{-10} for t's larger than this value; the behavior for smaller $|t|$ values depends in detail on the behavior of $\beta_+(t)$.

In some models, the leading trajectories for pp and πp scattering both approach the same value, but there are still degenerate trajectories at that value in order to produce the correct residues. In other models, the trajectories continue to fall logarithmically, see Baker and Coon [21].

A detailed fit to $\bar{p}p \to \pi^-\pi^+$ and K^-K^+ at low energies has been carried out by Donnachie and Thomas [100] who add the CIM term to a conventional Regge expansion with granddaughter trajectories. The CIM is important at low energies and low momentum transfer in their fit, perhaps because of the weakness of baryon exchange. Their form of the amplitude can be interpreted in terms of eq. (5.4.5), since the first term contains the ordinary Regge meson resonances on $\alpha_+(t)$ and its recurrancies. The second term is essentially a fixed pole since $\alpha_-(t) \cong -1$ for all reasonable $|t|$ and $\beta^- \cong (-t)^{-2}$ – which is exactly in the CIM form.

The counting rules determine the asymptotic behavior of exotic as well as nonexotic trajectories. For example, $\alpha_{pp}(-\infty) = -2$ whereas the exotic double baryon exchange trajectory $\alpha_{\bar{p}p}(-\infty) = -4$ and the corresponding residue is constant. Since the forces in exotic channels should be much weaker than in nonexotic ones, one might expect that $\alpha_{\bar{p}p}(u)$ remains near $\alpha_{\bar{p}p}(-\infty)$ for all u whereas the residue need not remain constant for small u. If this is the case, then $d\sigma/dt\,(\bar{p}p)$ will vary as $s^{2\alpha-2} \sim s^{-10}$ throughout the backward hemisphere; this is consistent with the present data even in the backward (exotic) peak.

It should be noted that the predicted matrix elements for a given signature are of the form $\beta(t)[(-u)^\alpha \pm (-s)^\alpha]$. This form is to be used to extract the effective trajectory from the data even

at large t, where $|u|$ is not $\cong s$ as is required in the usual Regge formula. The effective trajectories extracted from pp and $\pi^- p$ elastic data are shown in fig. 3.1.4. It is the trajectory extracted in this manner which is to be compared with the CIM predictions. This was discussed in some detail in section 3.1.

5.5. Decay distributions [40]

The functions $G_{H/A}(x)$ have been introduced to describe the fractional longitudinal momentum distribution in a Lorentz frame in which $p_A \to \infty$ (see Appendix B). It is possible in fact to determine important features of $G(x)$ by making measurements using other experimental observables which allows one to correlate decay properties of heavy systems, such as the timelike photon in e^+e^- decay with photoproduction, for example. Other examples which may be interesting to study are $\bar{N}N$ annihilation and the decay of heavy diffractively produced states.

The function $G_{H/A}(x)$ describes the breakup of A into the off-shell state H and a remainder. The decay of an unstable state A will reflect the threshold behavior of G in a new experimental context. In terms of the usual center-of-mass variable $\omega = 2E_H/M_A$, the inclusive decay $A \to H + X$ is described by

$$\frac{d\Gamma}{d\omega} \equiv d_{H/A}(\omega) . \tag{5.5.1}$$

In terms of a variable which is more like an infinite momentum frame variable, namely $x \equiv (E_H + p_H^z)/M_A$, where z is an arbitrarily chosen direction, the decay distribution is

$$\frac{d\Gamma}{dx} \equiv D_{H/A}(x) = \int_0^1 d\omega (\omega^2 - 4M_H^2/M_A^2)^{-1/2} d_{H/A}(\omega)\, \theta[\omega - x - M_H^2/xM_A^2] . \tag{5.5.2}$$

The distribution vanishes if x is too near 0 and 1 and is naturally peaked at $x = M_H/M_A$.

Using the model described in Appendix A, the momentum distribution is given by

$$G_{H/A}(x) = \frac{x}{2(1-x)} \int d^2k_T\, db^2\, \rho(b^2)\, \phi^2(xS)\, [xS]^{-2} , \tag{5.5.3}$$

where $0 < x < 1$ and

$$S(k_T, x) \equiv M_A^2 - \frac{M_H^2 + k_T^2}{x} - \frac{b^2 + k_T^2}{1-x} , \tag{5.5.4}$$

where b^2 is the (mass)^2 of the "core" and $\rho(b^2)$ is its distribution. The decay distribution is easily computed by evaluating the imaginary part of the self-energy diagram. The decay width is easily seen to be

$$\Gamma \propto \mathrm{Im} \int \frac{dy}{1-y}\, d^2k_T\, db^2\, \rho(b^2)\, \phi^2(yS)\, [yS]^{-2} . \tag{5.5.5}$$

If ϕ^2 is chosen to fall as a power of its argument, then it is easy to see that for x and ω near 1,

$$G_{H/A}(x) \sim (1-x)^{g(H/A)}, \qquad d_{H/A}(\omega) \sim (1-\omega)^{g(H/A)-1} \tag{5.5.6}$$

and hence

$$D_{H/A}(x) \sim (1-x)^{g(H/A)} . \tag{5.5.7}$$

The measurement of the decay functions $d_{H/A}(\omega)$ and $D_{H/A}(x)$ will provide independent evidence as to whether the dimensional counting rules are correct in general. An exciting possibility is to measure the threshold behavior in nuclear–nuclear collisions. The nucleons are the relevant constituents at low energies, and as the energy increases, the quark degrees of freedom should thaw and eventually become manifest. This transition would be very interesting to study – it could yield important information on the correct treatment of composite states.

5.6. *Characterization of inclusive reactions*

In this section a rough characterization of some selected inclusive cross sections in the central region will be given to illustrate the strong quantum number dependence of the predicted limiting behavior as $\epsilon \to 0$. The integral $I(x_1, x_2)$ defined in eq. (5.2.13) will be omitted in this discussion but should be included in any detailed numerical fit to the data over large ϵ range. In the previous sections we saw that the contribution of a particular basic process was described by the two numbers F and N. The value of F, the forbiddeness, measures the number of fields that must be radiated by the incident systems to arrive at the given basic process plus the number that must be radiated by c to produce the observed particle C. The value of N depends on the number of fields that are involved in the basic interaction process that produces the large angle scattering. It should be stressed at this point that the precise rules for which basic processes are allowed depend upon details of the quark confinement mechanism. Many choices are allowed within the CIM framework.

A comparison with the local effective powers F_{eff} and N_{eff} for data from ISR and FNAL as discussed by Blankenbecler, Brodsky and Gunion [44] is also given in this section. Finally, the existence of quasi-elastic peaks in the data for particle–antiparticle differences will be discussed since it can provide an important confirmation of the overall hard scattering picture.

In order to clarify the formulae to follow, consider some typical basic CIM processes and the types of states that they contribute to (M = any meson state, B = any baryon state):

$N = 4$ (6 quarks involved)	$N = 6$ (8 quarks involved)	$N = 8$ (10 quarks involved)
$M + q \to M + q$	$M + M \to M + M$	$B + M \to B + M$
$\bar{q} + q \to M + M$	$q + (qq) \to M + B$	$B + (qq) \to B + (qq)$
$q + q \to B + \bar{q}$	$B + q \to B + q$	$(qq) + (qq) \to B + q$
	$\bar{q} + (qq) \to M + q$	
	$q + \bar{q} \to B + \bar{B}$	

The case of $N = 2$, quark–quark scattering, will not be considered further.

The inclusive cross sections will be written in the standard form

$$\frac{E\,d\sigma}{d^3p}(AB \to C + X) = (p_T^2 + m_4^2)^{-4} Q_4(C, \epsilon) + (p_T^2 + m_6^2)^{-6} Q_6(C, \epsilon) + \dots , \tag{5.6.1}$$

where the dependence of the Q function on the angle has been suppressed as has the dependence

on the target, incident beam, and detected particle. Only the terms with the minimum values of F will be explicitly written. However, one should keep in mind that as the energy increases for fixed p_T, $\epsilon \to 1$, and larger F values can be expected since extra bremsstrahlung becomes more and more favored. Our discussion is not meant to be exhaustive but only to indicate the general features expected.

The most important terms in reactions of the type $pp \to CX$ where $C = \pi^{\pm,0}, K^+, \eta, \rho^{\pm,0}$, etc. are expected to involve $N = 4$ and 6 from the above table. Higher values of N may be present of course, but they should be damped by the large p_T and finite ϵ values involved in present experiments. It is straightforward to count the minimum amount of bremsstrahlung necessary and one finds

$$Q_4(\pi, \epsilon) = h_1\epsilon^9 + h_2\epsilon^{11} + h_1'\epsilon^{13} + \dots , \tag{5.6.2}$$

where the h_1' term can arise from the same processes that produce the h_1 term with the emission of an additional mesonic $(q\bar{q})$ pair. Also

$$Q_6(\pi, \epsilon) = h_3\epsilon^5 + \dots . \tag{5.6.3}$$

The "constants" h_i depend on the choice of C and depend on x_1, x_2 through the integral $I(x_1, x_2)$.

In the reaction $pp \to K^-X$, which might be termed "forbidden", the initial state has no quarks in common with those in K^- and more bremsstrahlung is required to connect them. One finds

$$Q_4(K^-, \epsilon) = h_2\epsilon^{11} + h_1\epsilon^{13} , \tag{5.6.4}$$

and

$$Q_6(K^-, \epsilon) = h_3\epsilon^9 + \dots . \tag{5.6.5}$$

Note that if the ϵ^{11} process $(q + \bar{q} \to M + M)$ dominated both the K^- and K^+ reactions, then the ratio (K^-/K^+) would be constant. In general, however, one might expect that this ratio will fall as ϵ^2 or ϵ^4 as ϵ decreases.

The reaction $pp \to pX$ is an interesting one because it involves a more complex trigger particle which is also present in the initial state. It has several new types of subprocesses that contribute to it. The basic process $q + q \to B + \bar{q}$ will ultimately produce a p_T^{-8} behavior if it is present, but one might expect that those mechanisms that dominate the exclusive scattering amplitude should be very important (that is, $q + B \to q + B$ and $(qq) + B \to (qq) + B$). These involve a large N value but should be dominant at small ϵ. There is also the (possible) basic process $(qq) + (qq) \to B + q$ that is the only one that requires double fragmentation and also contributes to leading order in the inclusive limit (s^{-10}). The cross section should be characterized by the forms

$$\begin{aligned} Q_4(p, \epsilon) &= H_1\epsilon^7 + \dots \\ Q_6(p, \epsilon) &= H_2\epsilon^3 + H_3(M)\epsilon^5 + H_4(\bar{B})\epsilon^{11} + \dots \\ Q_8(p, \epsilon) &= H_5\epsilon + H_6\epsilon^3 + H_7(\bar{B})\epsilon^{11} + \dots \\ Q_{10}(p, \epsilon) &= H_8\epsilon^3 + \dots . \end{aligned} \tag{5.6.6}$$

The term $H_3(M)$ is written so as to emphasize that an associated meson system is produced with the proton and these terms should be comparable in the two cross sections. Similarly for $H_{4,7}(\bar{B})$, so that in the antiproton cross section should look like

$$
\begin{aligned}
&Q_4 \quad \text{small} \\
&Q_6 = \bar{H}_4(\mathrm{B})\,\epsilon^{11} + \ldots \\
&Q_8 = \bar{H}_7(\mathrm{B})\,\epsilon^{11} + \ldots ,
\end{aligned}
\tag{5.6.7}
$$

where consistency demands that $\bar{H}_4(\mathrm{B})$ and $\bar{H}_7(\mathrm{B})$ are of the same magnitude as $H_4(\bar{\mathrm{B}})$ and $H_7(\bar{\mathrm{B}})$ extracted from a fit to the proton data.

It is of particular importance in understanding the basic dynamics of large p_T reactions to compare experiments with different beam particles. This degree of freedom allows one to change the predicted F value for a given N value and to check the normalization of the basic subprocesses. One important process is clearly $\pi\mathrm{p} \to \pi\mathrm{X}$ which is expected to be of the form

$$
\begin{aligned}
&Q_4(\pi, \epsilon) = k_1\epsilon^7 + k_2\epsilon^5 + k_3\epsilon^3 + \ldots \\
&Q_6(\pi, \epsilon) = k_4\epsilon^3 + k_5\epsilon + k_6(\mathrm{B})\,\epsilon^5 + \ldots .
\end{aligned}
\tag{5.6.8}
$$

The k_3 and k_5 terms do not Feynman scale but they do contribute to the exclusive limit behavior of s^{-8}. They involve the basic processes $\pi + \mathrm{q} \to \pi + \mathrm{q}$ and $\bar{\mathrm{q}} + \mathrm{p} \to \pi + (\mathrm{qq})$ respectively. The $k_6(\mathrm{B})$ term produces a recoil baryon system and it should also show up in the reaction $\pi + \mathrm{p} \to \mathrm{pX}$. Other final states can be discussed in a similar manner.

The final process to be described here is the reaction $\bar{\mathrm{p}}\mathrm{p} \to \pi\mathrm{X}$ that allows the possibilities of new types of basic processes. The cross section can be written in terms of

$$
\begin{aligned}
&Q_4(\pi, \epsilon) = K_1\epsilon^9 + K_2\epsilon^7 + \ldots \\
&Q_6(\pi, \epsilon) = K_3\epsilon^3 + K_4\epsilon^5 + K_5\epsilon + \ldots
\end{aligned}
\tag{5.6.9}
$$

where the K_3 term arises from the process $(\mathrm{qq}) + (\bar{\mathrm{q}}\bar{\mathrm{q}}) \to \pi + \mathrm{M}^*$, and K_4 from $\bar{\mathrm{q}} + (\mathrm{qq}) \to \pi + \mathrm{q}$. The K_5 term is the only one that contributes to leading exclusive behavior of s^{-8} and involves $\bar{\mathrm{p}} + (\mathrm{qq}) \to \pi + \bar{\mathrm{q}}$ and $\mathrm{p} + (\bar{\mathrm{q}}\bar{\mathrm{q}}) \to \pi + \mathrm{q}$. Without extra bremsstrahlung it does not Feynman scale. Detailed fits to data are necessary to determine which diagrams are important. Such fits can be found in the paper of Raitio and Ringland [201].

The characterizations given above emphasize that there are two distinct limits involved here which are sometimes confused in the literature. They are (1) large p_T with ϵ (or x_T) fixed in which the minimum value of N eventually dominates, and (2) $\epsilon \to 0$ with p_T fixed in which the minimum value of F dominates. This should be kept in mind since it is often stated that *the* parton model (not further defined) predicts a factorization for $x_\mathrm{L} \sim 0$:

$$
\frac{E\,\mathrm{d}\sigma}{\mathrm{d}^3p} \simeq (p_\mathrm{T}^2 + m^2)^{-N} f_N(\epsilon) . \tag{5.6.10}
$$

We see that this is correct if one sums over possible values of N in the above formula. This sum is absolutely necessary since, in general, different terms with different N values will dominate in the two limits defined above.

However, this form suggests two important and complementary ways of extracting information from data. Since $f_N(\epsilon)$ is predicted to behave as ϵ^F for sufficiently small ϵ, this provides the motivation to define effective powers $N_\mathrm{eff}(\epsilon)$ and $F_\mathrm{eff}(p_\mathrm{T})$ by the equations

$$
N_\mathrm{eff}(\epsilon) = -p_\mathrm{T}^2 \frac{\partial}{\partial p_\mathrm{T}^2} \ln\left(\frac{E\,\mathrm{d}\sigma}{\mathrm{d}^3p}\right), \tag{5.6.11}
$$

where the derivative is taken at fixed ϵ and θ_{CM}, and

$$F_{\text{eff}}(p_T) = \epsilon \frac{\partial}{\partial \epsilon} \ln\left(\frac{E\,d\sigma}{d^3p}\right), \tag{5.6.12}$$

which is calculated at fixed p_T and θ_{CM}. These two functions can be extracted directly from the data. They provide not only an immediate first test of any theory, but also a guide in determining the types of terms involving different values of N and F that are required in a detailed fit and in estimates of the masses required. The N and F values then provide clues as to what type of basic processes are important which then leads to the type of final state correlations that are to be expected. The functional dependence of N_{eff} and F_{eff} can be computed in models as per eq. (5.2.12). Because of the variation of the integral $I(x_1, x_2)$, F_{eff} can vary from F as G increases even if one term dominates.

The extractions for the BS data from the ISR and the CP data from FNAL are shown in figs. 5.6.1 and 5.6.2. Since mass corrections will affect the shape of N_{eff} at small p_T, decreasing its value there, and since N_{eff} must vanish at $p_T = 0$ if the process is to Feynman scale, the experimental results clearly show the presence of $N = 4$, 6, and 8 terms as expected and show little difference between particle-antiparticle. The F_{eff} curves, however, can be quite different for various particle types. Their values clearly tend to increase as the energy increases although the errors on F_{eff} are quite large from the ISR. The F_{eff} curves for K^- and $\bar{p}$ are higher than for the other particles, reflecting more bremsstrahlung, and are quite flat, reflecting an origin in the pionization region. The F_{eff} value for protons is quite small, especially in the FNAL range, characteristic of fragmentation and the protons presence in the initial beam. For the further details on the analysis of these curves, we refer the reader to the original paper (Blankenbecler, Brodsky and Gunion [44]).

An interesting application of how the N_{eff}, F_{eff} analysis can be used to predict correlations is provided by the reaction $\mu p \to \pi X$. Here we expect two leading contributions, (a) $N = 2$, $F = 5$ corresponding to the usual parton subprocess $\mu + q \to \mu + q$ where the large p_T of the π is balanced by the muon, and (b) $N = 3$, $F = 4$ corresponding to $\gamma q \to \pi + q$ in which the recoil momentum is taken

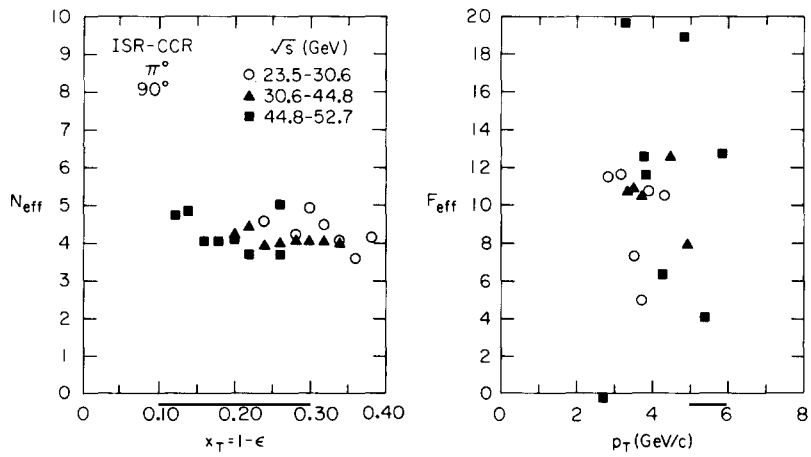

Fig. 5.6.1. Plots of N_{eff} and F_{eff} from the ISR–CCR data for the reaction $pp \to \pi^0 X$ for three energy pairs. The statistical errors are of the same size as the discrepancies from different energy pairs.

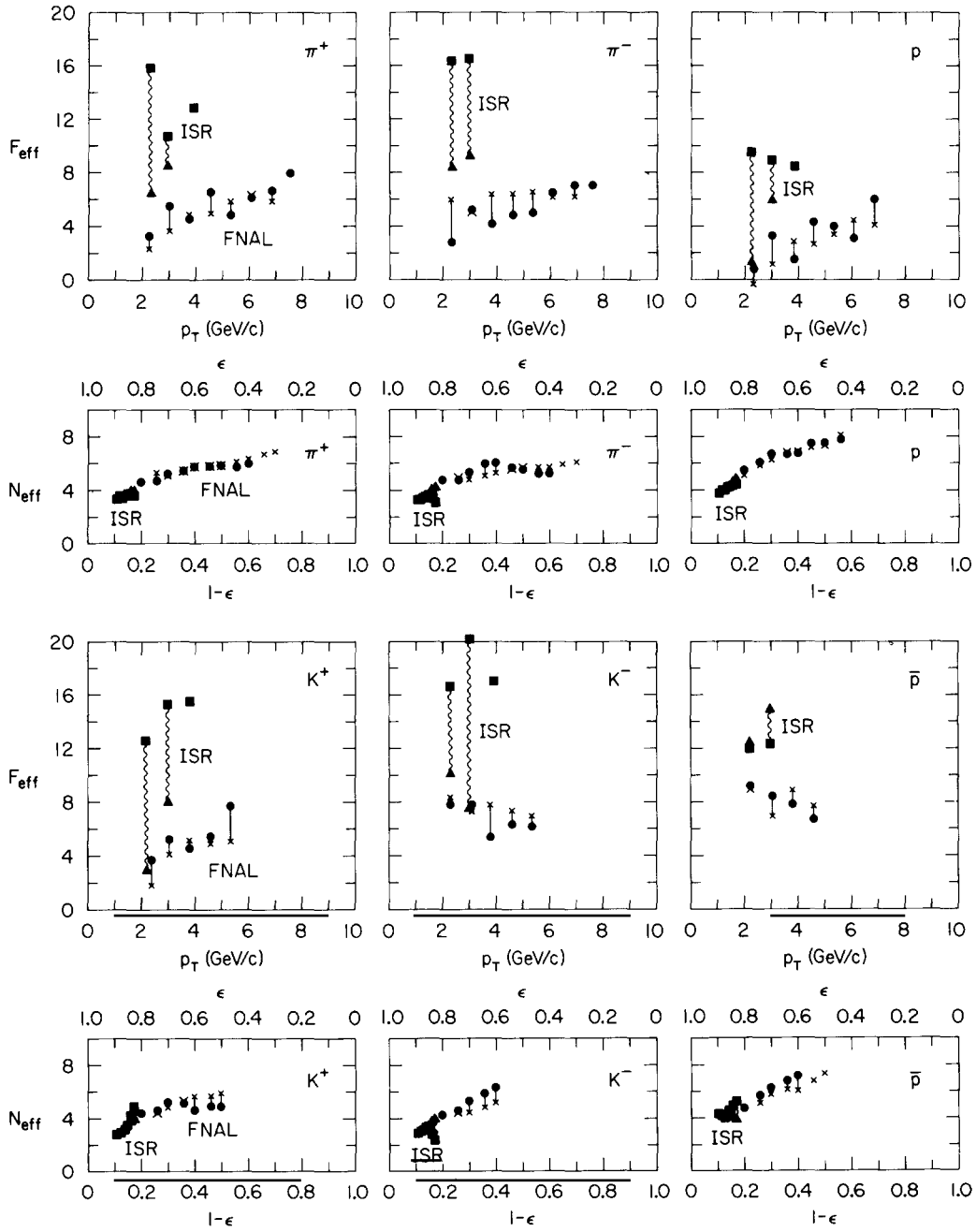

Fig. 5.6.2. Plots of N_{eff} and F_{eff} from the ISR–BS and FNAL–CP data for charged particles. The FNAL energy pairs are (19.4–23.8 GeV) marked by X's and (23.8–27.4 GeV) marked by dots.

up by a jet of hadrons. Another important application of this analysis is the process $pp \to \mu X$, since it separates the Drell–Yan $N = 2$ process from hadron-produced muons.

These F_{eff} curves also display an important feature of hard scattering models which provides

an important check of the presence of a small number of constituents. This feature is the presence of quasi-elastic peaks in the x_T distribution corresponding to the most likely momentum distribution among the constituents involved in the basic subprocess. For this configuration the cross section will peak as a function of x_T and hence F_{eff} must vanish there. This is only seen in the difference between particle and antiparticle cross sections since then the Pomeron component (which peaks at $x_T = 0$) cancels, allowing the valence part of the wave function to be observed.

The inclusive cross section can be written as an integral over z, the cosine of the C.M. scattering angle in the subprocess (neglecting final state bremsstrahlung c → C):

$$\frac{E\,d\sigma}{d^3p} \propto \int_{-(1-2x_1)}^{(1-2x_2)} \frac{dz}{(1-z^2)} F_{a/A}\left(\frac{2x_1}{1+z}\right) F_{b/B}\left(\frac{2x_2}{1-z}\right) \frac{d\sigma}{dt}\left(s' = \frac{4p_T^2}{1-z^2}, z\right), \tag{5.6.13}$$

where $F(y) = yG(y)$. Now the valence part of the probability function should be peaked at the values of y corresponding to the zero binding limit. That is, the first one should be peaked at $x_a = n_a/n_A$, where $n_A = n_a + n(\bar{a}A)$, and n_a is the number of constituents in the state a. Similarly for $G_{b/B}$. If these peaks in the integrand control the values of z, that is, if the angular dependence of $d\sigma/dt$ is sufficiently mild, then there is a peak in the integral at the value

$$x_T = \hat{x}_T \equiv 2\left[\frac{n_A}{n_a}\,\mathrm{ctn}\,\frac{\theta}{2} + \frac{n_B}{n_b}\tan\frac{\theta}{2}\right]^{-1}, \tag{5.6.14}$$

where θ is the C.M. scattering angle of C. Thus the scattering arising from the valence part of wave-

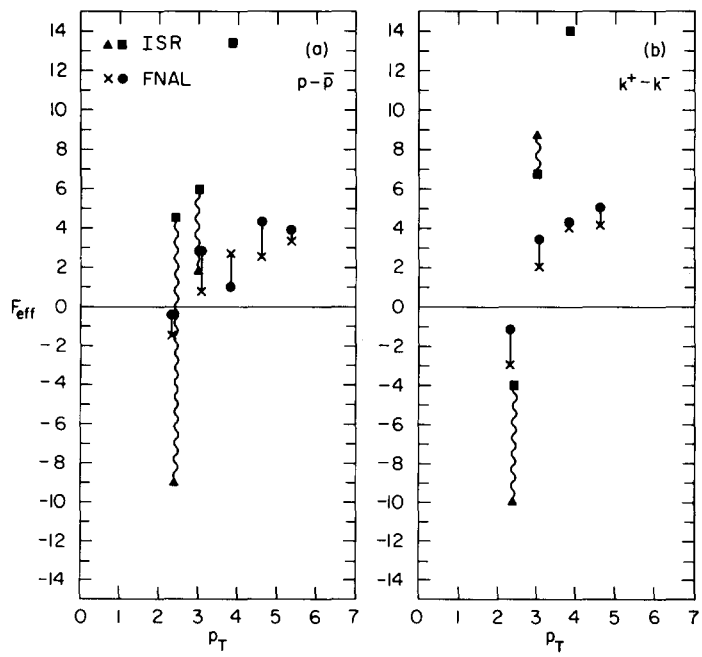

Fig. 5.6.3. F_{eff} for particle–antiparticle differences illustrating the peak in ϵ as F_{eff} vanishes.

function should have an $F_{\rm eff} = 0$ at this value of x_T (for example, at 90°, and for $n_A/n_a = 3$, $n_B/n_b \cong 5$, $\hat{x}_T \cong \frac{1}{4}$). If there is final state bremsstrahlung, the value of $\hat{x}_T$ should be multiplied by $n_C/(n_C + n(\bar{C}c))$.

The analysis for the differences $(K^+ - K^-)$ and $(p-\bar{p})$ are shown in fig. 5.6.3. The difference between π^+ and π^- is of the same size as the errors, and this analysis cannot be made in this case. We see that $F_{\rm eff}$ does seem to vanish in both the ISR (at $\hat{x}_T \sim 0.1$) and FNAL (at $\hat{x}_T \sim 0.2$) energy ranges. The relative values are consistent with the fact that larger $F_{\rm eff}$ values are found at the higher energies. The absolute values are reasonable if important small x_T Regge terms are still present in the difference of cross section.

A final simple consistency check is to examine the exclusive limit of the processes analyzed above. The exclusive limit cross section should fall as a power of s given by $N_{ex} = 1+N+F$. From the CP data, $(N_{ex})_{\rm eff}$ is estimated to be ~ 12.5 for $\pi^\pm$ and K^+, ~ 14 for K^-, ~ 13 for p and ~ 17 for $\bar{p}$. The values are higher by 1 or 2 for the BS data. These results are to be compared with the minimum possible values, which are 12, 14, 10, and 16 respectively, but a given subprocess will in general have a larger N_{ex}. The particular values are in reasonable agreement with expectations, and the relative ordering is as expected. See also the excellent paper by Jarlskog [157a].

5.6.1. Photon processes

Large transverse momentum processes onvolving photons are particularly important tests of the hard-scattering models and the counting rules (4.2.1–4.2.10) since they directly probe the point-like nature of the constituents. If the photon is counted as an elementary field, an explicit breakdown of vector dominance in the large momentum regime is predicted. The measurement of $\gamma p \to \pi p$ at fixed angle by R. Anderson et al. [11a] at SLAC gives $d\sigma/dt \sim s^{-7.3\pm0.4}$ and is consistent with the dimensional counting prediction of s^{-7}, although higher energy tests are required. Predictions for the angular distribution are given by Scott [214]. A gauge invariant parton model for photoproduction is given by Mueller-Kirsten and Hite [189]. We emphasize that Compton scattering at large t will provide a decisive test of the electromagnetic structure of hadrons. Parton model (see Brodsky, Close and Gunion [61], and Landshoff and Polkinghorne [172–174]) and light-cone analyses (see Frishman [130a]) demand the existence of a $J = 0$ fixed pole contribution to the Compton amplitude. Thus, for sufficiently large $|t|$ (where normal trajectories recede to negative values)

$$\frac{d\sigma}{dt}(\gamma p \to \gamma p) \propto \frac{1}{s^2} F^2(t), \qquad s \gg |t|, \tag{5.6.15}$$

with $F(t) \propto t^{-2}$, consistent with s^{-6} dimensional counting fixed angle prediction. Measurements of interference effects in $e^\pm p \to e^\pm p\gamma$ can test the prediction that the fixed pole contribution is independent of photon mass at fixed t. These and other related tests are discussed by Brodsky, Close and Gunion [61].

Deep inelastic Compton scattering $\gamma p \to \gamma X$ and pion photoproduction $\gamma p \to \pi X$ at large p_T are very interesting and basic inclusive tests for any parton model. The asymptotic cross section $E\,d\sigma/d^3p\,(\gamma p \to \gamma X)$ is predicted to be scale-invariant and proportional to the sum of quark charges to the fourth power (Bjorken and Paschos [37]). However present experiments are kinematically restricted in the small-t domain and thus can be expected to be sensitive to non-leading contributions in p_T. The conventional and expected contributions to $\gamma p \to \gamma X$ and $\gamma p \to \pi^0 X$ arising from (a) $\gamma + q \to \pi + q$ and $\gamma + q \to \gamma + q$ subprocesses are illustrated in fig. 5.6.4, with additional, non-

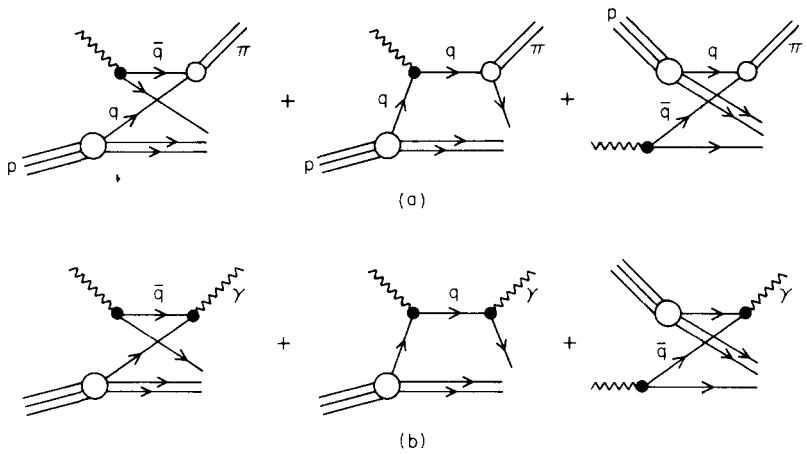

Fig. 5.6.4. The basic processes discussed in the text for inclusive (a) photoproduction and (b) Compton scattering.

leading terms arising from the subprocesses $\bar{q} + B \to \pi + (qq)$ and $\bar{q} + B \to \gamma + (qq)$. Just as in the hadronic case, the latter type of diagrams – which have a minimum number of spectator quarks – are expected to be especially important at small ϵ. It is perhaps easiest to think of these as arising from the baryon scattering off of the $(\bar{q}q)$ components of the target photon. Using the counting rules as given before, the expected cross sections are

$$\frac{E\,d\sigma}{d^3p}(\gamma p \to \pi X) = \frac{J_1\epsilon^3}{(p_T^2+m^2)^3} + \frac{J_2\epsilon^0}{(p_T^2+m^2)^6} + \ldots \tag{5.6.16}$$

and

$$\frac{E\,d\sigma}{d^3p}(\gamma p \to \gamma X) = \frac{J_1'\epsilon^3}{(p_T^2+m^2)^2} + \frac{J_2'\epsilon^0}{(p_T^2+m^2)^5} + \ldots . \tag{5.6.17}$$

The ϵ^0 terms (which also include the usual electromagnetic logarithmic factor) would be ϵ^1 if the photon were pure vector meson dominated so that it would act like a $q\bar{q}$ state rather than a fundamental field.

The photoproduction process has been analyzed by Eisner et al. [106] at $p_{LAB} = 21$ GeV/c for π^0 and they find $N_{eff} \cong 6$–7 and $F_{eff} \cong 0.5$ with $m^2 \cong 0.5$–1.2 GeV^2. Boyarski et al. [55] have analyzed $\pi^\pm$, $K^\pm$, and $p^\pm$ data at 18 GeV/c and for the charged pion case find a reasonable fit with $N_{eff} \cong 6$ and $F_{eff} \cong 1$. In the case of deep inelastic Compton scattering, the SLAC measurements of the Santa Barbara group (Eisner et al. [106]) give a fit with $N_{eff} \cong 4.5$, $F_{eff} \cong 0.5$, and $m^2 \cong 0.8$ GeV^2. Further the ratio of $\gamma p \to \gamma X$ to $\gamma p \to \pi^0 X$ does seem to be consistent with the predicted $p_T^2 + m^2$ behavior; despite the extra factor of α. The cross sections should eventually become of comparable magnitude. Note that if $\gamma p \to \gamma X$ is measured at large t, away from the edge of phase space, we still expect the scale-invariant parton model prediction to hold at large p_T. Finally, we also mention that the difference of cross sections for $e^\pm p \to e^\pm \gamma X$ at large photon mass and large p_T measures the interference of Bethe–Heitler and virtual Compton amplitudes and the sum of the cube of the parton charge (see Brodsky, Gunion, and Jaffe [64]). Because of the interference nature of this measurement, background terms of the J_2' type cannot contribute. A light-cone analysis of this process is given by Kiskis [163].

5.7. Theoretical expectations for correlations involving large p_T hadrons

Thus far, there has not yet been a great deal of theoretical work on inclusive correlations involving a large p_T hadron in spite of the fact that this area should provide fertile ground for new theoretical insights. The simple theoretical work which has been done suggests that correlations are crucial in disentangling the underlying dynamic mechanisms. The preliminary data on correlations have provided hints of unexpected phenomena. The opportunities for further progress here are many.

One aspect of the problem of correlations which has apparently caused some misunderstanding involves p_T conservation. It is important to recall that *the way* in which transverse momentum is conserved depends on the underlying dynamical mechanism so that it is not possible to isolate momentum conservation as a separate kinematic effect. The following simple example will illustrate this point. Assume that the absolute square of the matrix element for an event with $n+1$ particles can be written in the form

$$|M(p_1 \ldots p_{n+1})|^2 \propto f(p_{T1}) \ldots f(p_{T(n+1)}) \,. \tag{5.7.1}$$

This is just the assumption of the "uncorrelated jet model" (Krzywicki [165]) or transverse cutoff phase space which is often used as an example of a model without dynamical correlations. If we then trigger on an event containing a large p_T particle, we have the constraint

$$-\boldsymbol{p}_{T(n+1)} = \boldsymbol{p}_T = \sum_{i=1}^{n} \boldsymbol{p}_{Ti} \,. \tag{5.7.2}$$

If we neglect energy conservation this is the only source of correlations in transverse momentum in the model. We can see, however, that the implications of the constraint depend on the form of the $f(p_{Ti})$. If, for example, the f's are gaussian

$$f(p_{Ti}) \propto \exp(-bp_{Ti}^2) \,, \tag{5.7.3}$$

the preferred way to satisfy (5.7.2) is for each of the n particles to be clustered around the point p_T/n. In contrast, if $f(p_T)$ has a simple power falloff the preferred configuration is where one recoil particle has a large p_T and the others are near the origin. We may therefore find something like the phase space configuration found in hard collision models without assuming any underlying 2–2 hard process.

The fundamental test of an underlying 2–2 mechanism is, of course, the coplanarity of events containing large transverse momentum particles. As discussed in 2.3, this follows from the assumption that the constituents and the products of hadronic bremsstrahlung have limited transverse momentum relative to the beam direction so that the probability functions, $G_{a/A}(x, \boldsymbol{p}_T)$, eq. (A.8), in hard collision models are sharply peaked at small p_T. Gunion [134–136] has suggested that it is consistent with the spirit of hard collision models that the probability functions themselves have slow power-law-behavior in their high p_T tails so that the implied convolutions over p_T can give significantly larger deviations from coplanarity than might otherwise be expected. It has not yet been demonstrated, however, that the broad azimuthal correlations observed by the CCR group can be obtained in this manner. Also, it detracts from the conceptual simplicity of hard scattering models when all the mechanisms leading to large p_T are not explicitly isolated. One possibility is that significant contributions from inclusive generalizations of multiple-scattering diagrams are necessary to achieve the experimentally observed noncoplanarity of large p_T events. The azimuthal

correlations give an indication that while the hard scattering models may be able to explain data on large p_T production, there remains a substantial gap in our understanding. Additional data is needed.

An alternative way to approach the jet hypothesis which temporarily avoids confrontation with the fact that there be significant noncoplanarity in the events is to look for evidence of the underlying hard collision in the quantum number structure of an event. The basic idea is that the quantum numbers of the particles with large p_T should, in some statistical sense, be related to the quantum numbers of the constituents participating in the hard collision. For example, if we give up the idea of a scale-invariant quark–quark cross section but assume that quark–quark scattering is the dominant internal mechanism, we would predict that the large p_T hadrons should reflect the quantum numbers of the valence quarks of the incident beams. For pp collisions, the observed surplus of positive over negative particles at large p_T is in crude agreement with this idea.

At the level of two particle correlations, the quark–quark scattering mechanism does not lead to significant correlations between the quantum numbers of one large p_T jet and those of the jet on the opposite side. There are only the overall constraints due to charge-conservation, etc. In contrast, the constituent interchange model contains many possible internal hard-scattering mechanisms. Yet, if the model is correct, by triggering on a large p_T particle with definite quantum numbers, experiments can select the particular mechanisms that dominate. This mechanism must be consistent with the observed single particle spectrum. An example discussed by Newmeyer and Sivers [190] consists of triggering an apparatus on a large p_T proton and looking in the opposite hemisphere for p's or $\bar{p}$'s. If quark-scattering is the dominant mechanism, the opposite hemisphere jet should contain the usual surplus of baryons over antibaryons expected in the fragmentation region of a quark. In the CIM, however, triggering on a large p_T baryon may select a substantial contribution from the hard subprocess $qq \to B\bar{q}$. Here an antiquark is balancing the large p_T of the baryon and we expect a surplus of antibaryons over baryons in the opposite hemisphere jet. Simple model calculations for

$$R = \frac{\langle p \rangle - \langle \bar{p} \rangle}{\langle p \rangle + \langle \bar{p} \rangle}, \tag{5.7.4}$$

where $\langle p \rangle$ is the average number of protons and $\langle \bar{p} \rangle$ the average number of antiprotons in the hemisphere opposite a large p_T proton are shown in fig. 5.7.1 as a function of the x_T of the trigger particle. At FNAL energies, the subprocess $q + qq \to M + B$ may be important, predicting the dominance of mesons opposite a triggered baryon.

Another example of the importance of quantum number constraints involves the production of strange particles in the CIM. The tendency is for strangeness to be balanced between opposite large p_T jets. In pp collisions of a large p_T meson where the leading irreducible mechanism is $qM \to qM$, the strangeness transfer components

$$u\pi^o \to sK^+, \quad d\pi^+ \to sK^+, \quad \text{etc.} \tag{5.7.5}$$

lead to jets containing opposite strangeness. The process $uK^+ \to uK^+$, however, balances the strangeness of a jet with a particle in the fragmentation region.

Another important question is whether correlations involving large p_T hadrons are related to the clustering properties of low p_T events. In models such as the CIM the participating hadrons in the subprocess can be resonances. Since energy-momentum constraints would imply a negative correlation between two particles with large transverse momentum in the same direction if all

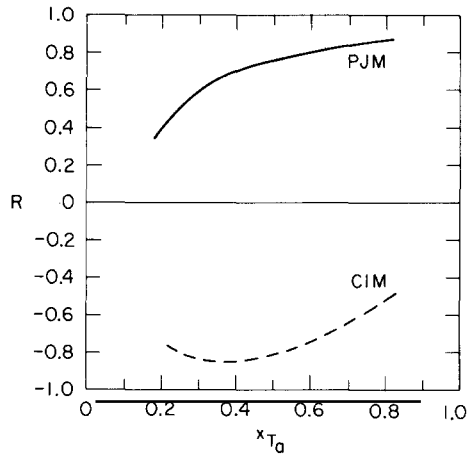

Fig. 5.7.1. The asymmetry in baryons and antibaryons (5.7.4) in a jet opposite a high p_T proton as calculated in the parton jet model (PJM) and the constituent interchange model (CIM).

hadrons were produced singly, the observation of positive same side correlations is already sufficient to guarantee that there is some clustering. It remains open whether it is intrinsically different from the clustering observed among low p_T particles. For a review of cluster models, see Ranft [203].

As emphasized by Bjorken [35] there are several relations between the invariant cross sections for clusters and the invariant cross section for their decay products in the limit where angle or rapidity is approximately conserved by the "soft" decay process. Let us assume that the invariant cross section for the production of a cluster,

$$\frac{E\,\mathrm{d}^3\sigma^{\mathrm{c}}}{\mathrm{d}^3p}(\boldsymbol{p},s) \cong \frac{1}{p_{\mathrm{T}}^n} f^{\mathrm{c}}(p/p_{\max},\theta_{\mathrm{CM}}), \tag{5.7.6}$$

approximately exhibits power law scaling and assume a scaling law (see 5.5.2)

$$\frac{\mathrm{d}N_{\mathrm{c}}}{\mathrm{d}x} = D_{\mathrm{h/c}}(x), \tag{5.7.7}$$

for the decay of the cluster into hadrons, where

$$x \cong |\boldsymbol{p}_{\mathrm{h}}|/|\boldsymbol{p}_{\mathrm{c}}| \cong p_{\mathrm{T}}^{\mathrm{h}}/p_{\mathrm{T}}^{\mathrm{c}}, \tag{5.7.8}$$

since the angles are approximately the same. We then have

$$\frac{E\,\mathrm{d}^3\sigma^{\mathrm{h}}}{\mathrm{d}^3p}(\boldsymbol{p},s) \cong \frac{1}{p_{\mathrm{T}}^n}\int_z^1 \mathrm{d}x\, x^{n-2} f^{\mathrm{c}}\left(\frac{z}{x},\theta_{\mathrm{CM}}\right) D_{\mathrm{h/c}}(x), \tag{5.7.9}$$

where $z = p_{\mathrm{T}}^{\mathrm{h}}/p_{\mathrm{T}}^{\max}$. Because the effective power of n in (5.7.6) is usually quite large it is the behavior of $D_{\mathrm{h/c}}(x)$ near $x = 1$ which determines the form of the power law scaling for the decay products

$$f^{h}(z, \theta_{CM}) \cong \int_{z}^{1} dx\, x^{n-2} f^{c}\left(\frac{z}{x}, \theta_{CM}\right) D_{h/c}(x) . \tag{5.7.10}$$

In interpreting the correlation function

$$R = \sigma_{inel} \frac{E_1 E_2 \, d\sigma/d^3p_1 \, d^3p_2}{(E_1 \, d\sigma/d^3p_1)(E_2 \, d\sigma/d^3p_2)} - 1 , \tag{5.7.11}$$

for two large p_T hadrons in approximately the same direction we see that a large amount of the p_T dependence is due to the variation of the single particle distributions. If we assume that both particles come from a cluster with momentum $\boldsymbol{p} = \boldsymbol{p}_1 + \boldsymbol{p}_2$ and $\mathcal{M}^2 = (p_1 + p_2)^2$ and then normalize that invariant cross section to the invariant cross section for a single hadron at momentum $\boldsymbol{p}$

$$\frac{E \, d\sigma/d^3p \, d\mathcal{M}^2 \, dx \, d\phi}{(E \, d\sigma/d^3p)_n} \cong \frac{R(E_1 \, d\sigma/d^3\boldsymbol{p}_1)(E_2 \, d\sigma/d^3\boldsymbol{p}_2)}{2\sigma_{inel}(E \, d\sigma/d^3\boldsymbol{p})} ,$$

with $x = E_1/E$. As pointed out by J. Bjorken, if the cross section for producing a high p_T system reflects strongly the total p_T and is not a rapidly varying function of the internal variables, this should be a slowly varying function of p_T. An estimate of the function based on CCR data on $\pi^0\pi^0$ correlations is shown in fig. 5.7.2 as a function of p_T. The fact that it is reasonably constant supports the general assumptions.

The interpretation of correlations in specific models has only now begun. Uematsu [224] has shown that the energy dependence of two particle distributions in the model of Berger and Branson [27] is quite large. Formulas for two-particle correlations in the quark scattering model are given by Ellis and Kislinger [110], and these can be readily generalized to other hard scattering models.

The correlation in θ_{CM}, or the rapidity variable $\eta = \log \tan (\theta_{CM}/2)$ between opposite side particles reflects both the angular dependence of the active subprocess and the distribution of momentum in $G_{a/A}(x)$, $G_{b/B}(x)$, $G_{C/c}(x)$, and $G_{D/d}(x)$. A subprocess with an isotropic distribution is already ruled out by the data, since it produces much too narrow an angular correlation, compared to the $\Delta\eta \sim 3.5$ correlation width measured by the Pisa–Stony Brook group at $\sqrt{s} = 52$ GeV with one particle at $\theta_{CM} = 90°$ and $p_T > 3$ GeV. Angular dependences such as $d\sigma/dt \sim t^{-4}$ or u^{-4} which might be expected in modified gluon exchange models, or the forms $d\sigma/dt \sim 1/su^3$, u/s^5, $1/s^2u^2$, which are possible for $q + \pi \to q + \pi$ are not inconsistent with the Pisa–Stony Brook data measured

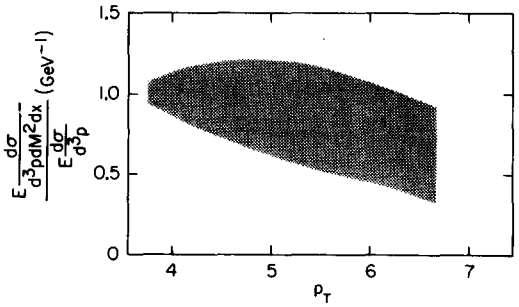

Fig. 5.7.2. The ratio of invariant cross sections for a pion pair and a single pion as a function of p_T.

at $x_T \sim 0.1$ since the data in this region are sensitive to the small-x behavior of the structure functions. However, at larger x_T, the predicted differences between the various models for $d\sigma/dt$ are very distinct. Calculations valid at large x_T have been given by Ellis [108]. Multiparticle correlations also should be able to discriminate between these models.

Recent experiments have also determined the correlation in η as a function of the CM angle of the detected large p_T particle. If two different distributions $G_{a/A}(x)$ and $G_{b/B}(x)$ occur, as in $\pi + q$, then the C.M. tends to be "thrown" in the direction of the "heavier" of the particles a and b. In the case of an isotropic $d\sigma/dt$, one expects events to have an "antiback-to-back" correlation, i.e., the particles on the opposite side of the detected high p_T particle should have the same sign of p_L^{CM}. However, if $d\sigma/dt$ (a + b → c + d) is forward or backward peaked, then the above effect can be negated, and a back-to-back correlation can occur. Future measurements of these correlations, especially at higher momentum transfers and with complete momentum determination will be very useful discriminants of the models. Generally, the features of the correlations are expected to sharpen as p_T increases. More extensive computations of the angular distributions and fits to the inclusive spectra are being carried out by Raitio and Ringland [201].

5.8. *The production of new particles and large p_T*

A very intriguing question arises concerning whether a large fraction of the observed high-transverse-momentum hadrons could be related to the production of new particles. Lederman [179] has advanced the speculation that essentially all the hadrons produced in excess of an $\exp(-6p_T)$ extrapolation are the decay products of heavy particles related to the $\psi(3100)$ and $\psi(3700)$ observed at SPEAR (Augustin et al. [18]) and at BNL (Aubert et al. [17]).

In support of this view one can note that the SPEAR data suggest the existence of a threshold at $\sqrt{s} = 3$–4 GeV resulting in the approximate doubling of the ratio $\sigma(e^+e^- \to \text{hadrons})/\sigma(e^+e^- \to \mu^+\mu^-)$. This could be translated into an effective threshold for the production of hadrons at large p_T in pp collisions. Except perhaps for the associated multiplicities of the Argo Spectrometer group (Ramanauskas et al. [202]) there is as yet no evidence for this type of threshold structure but it may emerge in careful analysis of new data. Further support of the idea can be found in the fact that

$$\frac{d\sigma}{dt}(\gamma p \to \psi p) \propto e^{at}, \qquad a \cong 2\tfrac{1}{2} - 3, \tag{5.8.1}$$

(Knapp et al. [164]). This corresponds to the general picture of the growing importance of heavy particles at large t and is consistent with the idea that the ψ's are more pointlike than ordinary hadrons.

As discussed in section 3, the most important constraint on this suggestion is the observed small and constant value of the ratio

$$\mu/\pi \cong 10^{-4}, \tag{5.8.2}$$

in pp collisions. If the leptonic/nonleptonic decay ratios of the majority of these new particles is the same as observed for the ψ's

$$\Gamma(\psi \to \mu^+\mu^-)/\Gamma(\psi \to \text{hadrons}) \cong 0.1, \tag{5.8.3}$$

then very few of the large p_T hadrons can be their decay products.

It may be that the hard subprocess in the constituent pictures we have been discussing can be effectively replaced by a sum over high-mass low-spin resonances in the direct- and crossed-channel. This new type of duality could have many implications and could perhaps lead to a correction between events with a few high p_T hadrons and those with a large multiplicity of low p_T hadrons.

It should be noted that the production of ψ's in pp collisions is suppressed in heavy quark models by the operation of "Zweig's rule" which forbids a produced quark to end up in the same hadron as its antiquark. Thus the associated production of particles which carry the new quarks bound to the usual quarks should be favored. However, in those events in which there is a ψ, arguments can be made (Sivers [217]) which indicate that there should also usually be a pair of heavy hadrons. Moreover there should be local balancing in rapidity of the number of new heavy quarks so that the momentum of a high p_T ψ should be balanced by a recoil system containing the new hadrons.

Even if there is no direct connection between the existence of the new particle and the unexpected yeild of high p_T hadrons, it is possible that large p_T physics can illuminate some of the properties of the ψ's. For example, a possible test of whether the ψ is an elementary spin-one particle or a composite $q\bar{q}$ system involves the comparison of fixed-angle scaling laws for $\gamma p \to \gamma p$ and $\gamma p \to \psi p$ or inclusive scaling laws for $\gamma p \to \gamma$ + anything and $\gamma p \to \gamma$ + anything. Note that the observation of a $J = 0$ fixed pole in ψ photoproduction,

$$\frac{d\sigma}{dt}(\gamma p \to \psi p) \propto s^{-2} f(t) , \tag{5.8.4}$$

would be dramatic proof of the elementarity of the new state since Brodsky, Close and Gunion [61] have shown that fixed-pole behavior is impossible in the photoproduction of composite systems. Whether or not these kinds of tests on the nature of the ψ are feasible, in view of the small observed cross sections, is difficult to say – the simple examples discussed here involve extremely small effects.

The production of heavy mass particles can, in principle, give us the same type of dynamical information sought in large p_T processes. An important mechanism for the production of heavy hadrons should be $q\bar{q} \to H\bar{H}$ so that the dynamics of the process may not be too different from $q\bar{q} \to K^- K^+$. This may be reflected in the scaling laws for the production processes. The production of heavy particles at large transverse momentum offers an opportunity to study how the parameter m^2, in the formula

$$\frac{E d^3\sigma}{d^3p} \sim \frac{f(\epsilon)}{(p_T^2 + m^2)^N} , \tag{5.8.5}$$

depends on the internal masses (quark masses or hadron masses) in the problem. The production of new quantum numbers implies the existence, on the average, of a greater number of spectators, so the production of heavy hadrons should be dominated by the small x_T kinematic region. Photon, lepton and meson beams offer the best opportunity for isolating the presence of the new particles because of the improved signal-to-noise ratio due to the presence of antiquarks with large x.

It is possible to dimensionally analyze the production of heavy mass systems in much the same way as in large p_T inclusive reactions. Counting rules in the CIM for lepton pair production have been derived by Sachrajda and Blankenbecler [206] which predict the behavior in mass ($\mathcal{M}$) and threshold ($1 - \mathcal{M}^2/s$) for any incident beam and choice of basic process. These include both anni-

hilation (Drell–Yan) and bremsstrahlung type contributions. The inclusive–exclusive connection was also discussed. It will be very helpful to have data of sufficient quality and quantity so that an effective power analysis can be performed. This would help distinguish between the possible basic processes that can contribute.

The presence of heavy narrow resonances offers the possibility of many interesting effects in inclusive channels. It is important to note the possibility that the anomalous energy behavior for large-angle $\bar{p}p$ elastic scattering between p_{LAB} of 5 and 6 GeV/c (Buran et al. [65]) may be due to the effect of the $\psi(3700)$ at the upper energy, $\sqrt{s} = 3.68$. The possibility that the "Ericson fluctuations" observed by Schmidt et al. [210] may really be due to a new heavy baryon coupled weakly to $\pi^{\pm}p$ is also worth considering.

The discovery of the ψ and ψ' are important in that they demonstrated both the limitations and the virtues of current theoretical approaches to hadronic phenomena. For example, we now can only expect $R = \sigma(e^+e^- \to \text{hadrons})/\sigma(e^+e^- \to \mu^+\mu^-)$ to become asymptotic at some energy regime considerably above the masses of the new particles. Efforts to explain why this ratio did not agree with simple quark model predictions in the lower energy regime did not prove too illuminating. We must keep in mind that the simple quark model rules for large p_T processes discussed here may also fail in such a way as to unmask this new dynamics. If this "thawing" is due to the opening up of new degrees of freedom, they can be included in the counting rules in an obvious manner. If not, then we will be learning about a new type of hadronic matter.

6. Summary and conclusions

The detailed study of the properties of large-transverse-momentum phenomena is now just beginning and much more experimental and theoretical work will be required before definitive conclusions are possible. It does seem appropriate, however, to make the following preliminary observations.

The kinematic regime in which large p_T data is being collected is characterized by an invariant single particle inclusive cross section which displays a falloff somewhere between $\exp(-6p_T)$ and $(p_T)^{-4}$. These two predictions may be considered extremes, the first possibly valid at low p_T and the other possibly valid at some ultra-high p_T. We do not completely understand from the quark parton picture why there is no evidence for a $(p_T)^{-4}$ component in the present kinematic regime although there are speculations, based on models for quark binding, why such a term may be absent or suppressed, see section 4.

The available data on single particle inclusives are observed to be smooth over a wide range of p_T and $\sqrt{s}$. There appears to be no sharp boundary between low p_T and high p_T regimes or between high energy and low energy dynamical mechanisms. However, we cannot be completely satisfied with this observation due to the presence of large gaps in the coverage of the high p_T, intermediate energy range. Data from SLAC, BNL, CERN–PS and Serpukhov are needed to test for this smoothness with greater precision. Data at these energies and $x_T \sim 1$ can also explore directly the connection between inclusive and exclusive cross sections.

The jet hypothesis, i.e., the assumption of an underlying hard scattering mechanism, can most easily be tested by looking at the complete phase-space structure of individual events containing a large p_T trigger. This type of data can give basic information on the internal dynamics. For example, there is speculation that the inclusive "jet cross section"

$$E_{\text{jet}}\, d\sigma/d^3(p_{\text{jet}}) \sim f(x_{\text{jet}})/(p_{\text{jet}}^{\text{T}})^4 ,$$

may display scale invariance, where $\boldsymbol{p}_{\text{jet}} = \Sigma_i p_i$ is the sum of the momenta of all particles in a given event with $p_{\text{T}i} \gtrsim \langle p_{\text{T}} \rangle$. This cross section can be measured directly, e.g., in hadronic calorimeter experiments, and the speculation should be tested. The measurements of associated multiplicities and correlations at the ISR support the idea of some sort of broad jet structure. The results of the ARGO spectrometer measurements at BNL displaying a sharp rise in the associated multiplicity as a function of p_{T} constitute, at this time, the sole exception to the rule that physical observables extrapolate smoothly between small p_{T} and large p_{T}.

Hard scattering models are consistent with a large body of data. However, the observed lack of coplanarity in the two particle inclusive data provides an important challenge to this point of view. More data on azimuthal correlations, with different particles and in different kinematic ranges, is obviously in order. It is particularly interesting to check whether the coplanarity distribution changes at higher values of x_{T}. Comparisons with correlations observed from lepton and photon induced reactions will also be significant. It is also an interesting theoretical problem to see whether hard scattering models can be generalized in some way to avoid the prediction of coplanarity. This would be, in some sense, a retreat for this model but it could be balanced against other successes. The inclusion of "hard" 2–3 internal processes might be an interesting exercise.

For completeness we also mention other important experimental constraints. Measurements of the angular dependence of inclusive reactions are of obvious importance in separating the dependence of cross sections on the distribution functions $G_{\text{a/A}}(x)$ and $G_{\text{b/B}}(x)$ and the angular dependence of the basic subprocesses. Correlation measurements between two or more large transverse momentum particles and their angular dependence will further constrain the form of the internal scattering cross sections. The distribution of momentum in the recoil system in principle can distinguish between subprocesses involving the production of jets, or systems of fixed mass.

Beams of γ's, π's, K's and $\bar{\text{p}}$'s are interesting from the quark model framework because they provide more antiquarks with a large fraction of the incident momentum. In general photon and meson beams have a larger fraction of their momentum available for high x_{T} processes compared to baryons. So far all large p_{T} experiments have been done with incident protons, but changing beams can have a dramatic effect on the large p_{T} cross sections for particles involving antiquarks. Photon experiments are valuable because γ's couple with approximately equal strength to all varieties of constituents and can provide a close connection with electroproduction data. The $J = 0$ fixed pole in Compton scattering furnishes a real test for the pointlike coupling of the photon to some internal constituent. Unified planning of experiments with these new beams is necessary to provide related measurements over a wide kinematic regime.

The flow of quantum numbers in an event containing a large p_{T} particle provides a good discriminant for different models of the internal dynamics. The quark models provide a general constraints on the quantum numbers of the irreducible hard scattering process and specific models have definite predictions. Measurements involving the differences between different beam particles, detected particles, and n or p targets are sensitive to the valence and Regge components of the distribution functions. The most critical measurements of quantum flow involve quantum number correlations. For example, in the CIM model for production in pp collisions, the detection of a K^- at sufficiently large x_{T} signals the presence of a K^+ in the opposite hemisphere. However, for different internal processes strangeness of a large p_{T} K^+ can be balanced by a K^-,

by Λ's or Σ's in the fragmentation region or by Λ's and Σ's in the opposite jet. The study of correlations with particle identification in experiments involving a variety of beams and targets is obviously an important experimental goal. The use of quantum number flow to identify the important internal subprocesses can serve as an important consistency check on the identification of the subprocesses by "effective power" analysis.

The effective powers discussed in section 5.6 can provide an important phenomenological tool. They are quantities which can summarize concisely the systematic trends of the data and which can be extracted simply from models. In combination with the quark model and constituent counting they provide important clues to the important internal mechanisms. Analysis of data from FNAL and ISR results in plateaus in N_{eff} and F_{eff} at values consistent with expectations in the CIM. Particles and antiparticles are found to have similar N_{eff}'s but, as expected, display quite different F_{eff}'s. The correlation of N_{eff} and F_{eff} with the quantum numbers of the detected particles supports the general features of the quark model. The observation of peaks in $\epsilon = \mathcal{M}^2/s$ for the difference between particle and antiparticle cross sections provides supplementary evidence of a small number of internal constituents, each with a finite fraction of the hadron's momentum. Application of this type of analysis to new data over a wide range of energies, different angles and smaller ϵ values can help probe more deeply into the basic dynamics. We also emphasize that applications of the effective power analysis can greatly clarify the physics of the deep inelastic electromagnetic processes.

The use of nuclear targets in high p_T experiments has uncovered an interesting unexplained feature incidental to the original objectives of the experiments. The dependence of the data for meson production on the nuclear target type is found to vary as $A^{1.1}$ for $p_T > 3$ GeV/c. This is distinct from both the coherent $A^{2/3}$ and the incoherent A^1 dependence expected. The explanation of this fact is uncertain although there are many theoretical suggestions. More experiments on nuclear targets at different values of p_T and $\sqrt{s}$ are obviously appropriate. The structure of the recoil system for high p_T production on various nuclear targets can clarify the role of double scattering contributions.

The expectations for fireball models as a general description of large p_T processes has not been fully exploited. If parton models run into serious snags the idea that fireball approaches can be, in some sense, supplementary to hard scattering approaches might provide new insight into the problems.

In view of the evidence from SPEAR of scaling violations associated with the production of ψ's and/or heavy charmed particles, the possibility of a connection between large p_T production and heavy particle production should be explored fully. There may be an enriched sample of new heavy particles in events in which there is a large p_T hadron. Certain of the large p_T particles (e.g. direct muons) may come from the decay of new types of particles. From a more general view, the dynamics underlying the production of massive particles may be related in structure and form to the dynamics of large p_T. Constituent models provide a framework where this type of possible connection can be easily visualized (see section 5.8).

In the area of exclusive experiments, improved high p_T data can probe several features of the strong interactions. An important test for the finite compositeness of hadrons is to check whether Regge trajectories asymptote to negative integers or continue to fall at large $|t|$. The present data is not sufficient to decide this point. It is also important to test for fixed angle scaling, $d\sigma/dt \sim s^{-N} f(\theta)$, in $2 \to 2$ processes with more data. Measurements of the ratios of the differential cross sections $\gamma B \to \gamma B$: $\gamma B \to \pi B$: $\pi B \to \pi B$: $BB \to BB$ for a fixed range of $\theta_{\text{C.M.}}$ would provide an impor-

tant check on the relative complexity of photons, mesons, and baryons. Present data agree with simple constituent counting laws but also display many features (zero structure, polarization, etc.) which are most easily understood in geometric terms. Data do not, however, display the shrinkage ($\sigma \sim \sigma(\Delta p_T \, \Delta b)$) implied by the asymptotic validity of geometric constraints. It is therefore an important question whether the geometrical features survive at higher energies. The search for Ericson fluctuations is also crucial in deciding the important question of the existence of heavy resonances.

It is also important to check the scaling laws for multiparticle exclusive processes for fixed invariant ratios such as $ep \to ep\pi$, $e^+e^- \to n\pi$, $p\bar{p} \to n\pi$, etc., and predictions for fixed angle cross sections related by crossing: $p\bar{p} \to p\bar{p} : pp \to pp$, $p\bar{p} \to \pi\bar{\pi} : \pi p \to \pi p$, etc. Another intriguing question is whether nuclear form factors and distribution functions can be predicted from constituent counting rules.

Most models that have been discussed in the text have been formulated to attempt to understand isolated features of large p_T events. It is usually very difficult to make other predictions in these models without which their overall validity cannot be tested. In contrast, the CIM models provides a unified framework to discuss exclusive reactions and inclusive processes over the entire Peyrou plot. The model is exceedingly simple in all these cases. It is consistent with the ideas tested in deep inelastic lepton scattering and hence provides a bridge between photon and hadronic processes.

At small momentum transfers, the model converts smoothly to the usual Regge – purely hadronic description of exclusive and inclusive reactions. In a sense the CIM gives a simple prescription for mapping duality diagrams to dynamics at short distances.

The predictions of the CIM can be discussed at two levels. The first level involves the general form of the cross sections and their dependence on specific kinematic variables. Thus, the exclusive differential cross sections are predicted to factorize at large angles in the form $g(s) f(\theta)$, and the form of Regge trajectories and residue functions are prescribed. At a more detailed level, the model predicts the specific functions involved for any process, and in the exclusive scattering case, $g(s) \sim s^{-N}$, where N is fixed by quark counting, and the function $f(\theta)$ is specified. Similar statements hold in the inclusive case.

Within the CIM framework, one must still specify the particular composite nature of the hadrons. For example, the nucleon can be considered to be a bound state of three equivalent quarks or of a quark and a core. These alternatives give different predictions in general for nucleon–nucleon scattering ($N = 10$ or 12 respectively). All of the constituent counting rules given in the text for inclusive scattering are based on the former model of the nucleon but the latter can be easily discussed. *Experimental information is needed to decide between these possibilities.*

Even though alternative models can do as well in describing some features of the data, the fact that there appear to be no violations of CIM predictions for form factors and exclusive or inclusive scattering is significant.

In spite of the empirical sucess of the CIM at large p_T and parton model ideas in deep electromagnetic scattering, there are important conceptual obstacles associated with the fact that quarks are assumed to be permanently bound. This must affect the treatment of strong interactions at some level, but just where and how this will occur depends on the unknown binding mechanism. It is probably necessary to understand this binding before the final state configurations in inclusive reactions can be computed. Theoretical attempts in this direction have only scratched the surface.

Acknowledgments

We wish to thank J. Alonso, J. Bjorken, G. Farrar, R. Pearson, G. Ringland, R. Ristio and D. Wright for many helpful conversations. We are particularly indebted to J. Gunion for his unlimited assistance.

Appendix A. Derivation of the hard scattering model

All of the predictions of the various hard-scattering and parton models for large-transverse-momentum inclusive processes depend on the validity of an underlying probabilistic formula. In this appendix we derive the central equation for hadronic processes in a form sufficiently general to allow for transverse momentum fluctuations. Hard scattering model for the reaction $AB \to CX$ are based on a decomposition of the form indicated in fig. 1.5 where the final state, X, consists of contributions of particles and clusters from $p(A\bar{a})$, $p(B\bar{b})$, $p(\bar{C}c)$ and $p(d)$. We write

$$d\sigma(AB \to CX) = \frac{1}{2E_A 2E_B |V_A - V_B|} |M_{AB\to CX}|^2 \, dp \,, \tag{A.1}$$

with the assumed decomposition

$$|M_{AB\to CX}|^2 = \sum_{ab,cd} \frac{\phi_A^2(p_a^2)}{(p_a^2 - m_a^2)^2} \frac{\phi_B^2(p_b^2)}{(p_b^2 - m_b^2)^2} \frac{\phi_C^2(p_c^2)}{(p_c^2 - m_c^2)^2} |M_{ab\to cd}|^2 \,, \tag{A.2}$$

and

$$\begin{aligned} dp = {} & \frac{d^4p_C}{(2\pi)^3} \delta^{(+)}(p_C^2 - m_C^2) \frac{d^4p_{A\bar{a}}}{(2\pi)^3} \delta^{(+)}(p_{A\bar{a}}^2 - m_{A\bar{a}}^2) \frac{d^4p_{B\bar{b}}}{(2\pi)^3} \delta^{(+)}(p_{B\bar{b}}^2 - m_{B\bar{b}}^2) \\ & \times \frac{d^4p_{\bar{C}c}}{(2\pi)^3} \delta^{(+)}(p_{\bar{C}c}^2 - m_{\bar{C}c}^2) \, \delta^{(+)}(p_d^2 - m_d^2) 2\pi \,. \end{aligned} \tag{A.3}$$

The absence of coherence in the decomposition can be physically motivated under the assumption that a,b are distinct "localized" constituents of A, B respectively. The ϕ's are the covariant vertex functions for one leg off-mass-shell. In the case of spin, the appropriate spin sums and traces are assumed. From the form of (A.2) and (A.3), we see that we are assuming that a,b,c,d have either well defined masses (for internal hadrons) or effective masses (for quarks, etc.). These masses are later assumed to be small in some sense so that, for example, we do not include in (A.2) an internal $2 \to 3$ process where the effective mass of the system represented by d can be arbitrarily large.

It is convenient to choose the following parametrization

$$p_b^{(+)} \equiv p_b^0 + p_b^3 = x_b p_B^{(+)}, \qquad \boldsymbol{p}_{bT} = \boldsymbol{k}_{\bar{b}T}, \qquad \boldsymbol{k}_{Tb} \cdot \boldsymbol{p}_B = 0 \,. \tag{A.4}$$

The mass-shell condition for $p_B - p_b$ then gives

$$(p_B - p_b)^2 = m_{B\bar{b}}^2 \,, \tag{A.5}$$

and one easily finds

$$p_b^2 - m_b^2 = x_b \left[M_B^2 - \frac{\boldsymbol{k}_{Tb}^2 + m_{B\bar{b}}^2}{1 - x_b} - \frac{\boldsymbol{k}_{Tb}^2 + m_b^2}{x_b} \right], \tag{A.6}$$

and

$$\int \frac{d^4 p_{B\bar{b}}}{(2\pi)^3}\,\delta^{(+)}(p_{B\bar{b}}^2 - m_{B\bar{b}}^2) = \int \frac{d^2 k_{Tb}}{(2\pi)^3} \int_0^1 \frac{dx_b}{2(1-x_b)}. \tag{A.7}$$

The limits on x_b ensure that $p_{B\bar{b}}$ is timelike and p_b is spacelike. We may then define the distribution

$$G_{b/B}(\boldsymbol{k}_{TB}, x_b) \equiv \frac{1}{(2\pi)^3}\,\frac{x_b}{2(1-x_b)}\,\frac{\phi_B^2(p_b^2)}{(p_b^2 - m_b^2)^2}, \tag{A.8}$$

which is the probability for particle b to have fractional momentum $x_b = p_b^+/p_B^+$ along the direction of particle B plus a transverse momentum $\boldsymbol{k}_{Tb}$ orthogonal to $\boldsymbol{p}_B$. The spectral sum over $m_{B\bar{b}}$ is understood in (A.8). The behavior $G_{b/B}$ at $x_b \sim 0$ is controlled by the behavior of the spectral integral at large $m_{B\bar{b}}^2$ which is, in turn, given by the high-s behavior of $\sigma_{B\bar{b}}(s)$. The existence of $G_{b/B}$ implies that b can be "found" in the wave function of particle B and its use in the hard scattering formula means that it makes sense physically to distinguish between the formation of b in this way and the subsequent interactions of this off-mass-shell "constituent".

Similarly, we can define $G_{a/A}(\boldsymbol{k}_{Ta}, x_a)$ for the distribution of momenta carried by p_a in A where, again, p_a is spacelike. Finally, we also define

$$p_c^{(+)} = y_c p_C^{(+)}, \qquad \boldsymbol{p}_{Tc} = y_c \boldsymbol{p}_{TC} + \boldsymbol{k}_{Tc}, \tag{A.9}$$

where the mass shell condition for $p_c - p_C$ implies

$$p_c^2 - m_c^2 = y_c \left[m_C^2 + \frac{\boldsymbol{k}_{TC}^2 + m_{\bar{c}c}^2}{y_c - 1} - \frac{\boldsymbol{k}_{TC}^2 + m_c^2}{y_c} \right], \tag{A.10}$$

and

$$\int \frac{d^4 p_{\bar{c}c}}{(2\pi)^3}\,\delta^{(+)}(p_{\bar{c}c}^2 - m_{\bar{c}c}^2) = \int \frac{d^2 k_{TC}}{(2\pi)^3} \int_1^\infty \frac{dy_c}{2(y_c - 1)}. \tag{A.11}$$

If we define $x_c = y_c^{-1}$, then the function

$$\tilde{G}_{C/c}(x_c, \boldsymbol{k}_{TC}) = \frac{1}{(2\pi)^3}\,\frac{1}{2(x_c^{-1} - 1)}\,\frac{\phi_c^2(p_c^2)}{(p_c^2 - m_c^2)^2}, \tag{A.12}$$

gives the probability, normalized to the multiplicity, for particle C to have a fraction x_c of the momentum along the direction of the timelike particle c and a component $\boldsymbol{k}_{TC}$ normal to this direction. The tilde indicates the parent particle c is timelike.

Without further approximation we may then write eq. (A.1) in the form

$$\frac{d\sigma(AB \to CX)}{d^3 p_C / E_c} = \sum_{ab,cd} \int d^2 k_{Ta} \int_0^1 dx_a \int d^2 k_{Tb} \int_0^1 dx_b \int d^2 k_{TC} \int_0^1 \left(\frac{dx_c}{x_c^2}\right) \tag{A.13}$$

$$\times\, G_{a/A}(\boldsymbol{k}_{Ta}, x_a)\, G_{b/B}(\boldsymbol{k}_{Tb}, x_b)\, \tilde{G}_{C/c}(\boldsymbol{k}_{TC}, x_c) \left(\frac{1}{x_a x_b\, 2E_a\, 2E_B}\right) \left(\frac{1}{|V_A - V_B|}\right) |M_{ab\to cd}|^2\, \frac{\delta_{(+)}(p_d^2 - m_d^2)}{(2\pi)^3}.$$

The next step is to assume that the off-shell continuations in the integrand of (A.13) are not important so that we can identify

$$\frac{1}{x_a x_b 2E_a 2E_b}\,\frac{1}{|V_A - V_B|}\,|M_{ab\to cd}|^2\,\frac{1}{(2\pi)^2} = \frac{s'}{\pi}\,\frac{d\sigma(ab\to cd)}{dt}\bigg|_{s't'u'}, \tag{A.14}$$

and

$$\delta_{(+)}(p_d^2 - m_d^2) \cong \delta(s' + t' + u' - m_a^2 - m_b^2 - m_c^2 - m_d^2)$$

where

$$\begin{aligned} s' &= (p_a + p_b)^2 \cong x_a x_b s - \boldsymbol{k}_{Ta}\cdot\boldsymbol{k}_{Tb} \\ t' &= (p_a - p_c)^2 \cong \frac{x_a}{x_c}\,t + \boldsymbol{k}_{Ta}\cdot\boldsymbol{k}_{TC} \\ u' &= (p_b - p_c)^2 \cong \frac{x_b}{x_c}\,u + \boldsymbol{k}_{Tb}\cdot\boldsymbol{k}_{TC} \end{aligned} \tag{A.15}$$

when the masses $m_a^2, m_b^2, m_c^2, m_d^2$ can be neglected.

The next assumption is that the structure functions

$$G_{a/A}(x) = \int d^2\boldsymbol{k}_T\, G_{a/A}(\boldsymbol{k}_T, x), \tag{A.16}$$

exist. Note, from (A.8) and (A.12) that the integrals converge even for ϕ = constant.

We then write, with $s', t' \gg \boldsymbol{k}_T^2$

$$\frac{d\sigma(AB\to CX)}{d^3p_c/E_c} \cong \sum_{ab,cd}\int_0^1 dx_a \int_0^1 dx_b \int_0^1 \frac{dx_c}{x_c^2}\, G_{a/A}(x_a)\, G_{b/B}(x_b)\, \tilde{G}_{C/c}(x_c)\, \delta(s'+t'+u')\, \frac{s'}{\pi}\,\frac{d\sigma}{dt'}(ab\to cd). \tag{A.17}$$

Comparing (A.8) and (A.12) assuming that $\phi^2(p_c^2)$ can be defined for both spacelike and timelike arguments, we get

$$G_{c/C}(x) = -x\,\tilde{G}_{C/c}(1/x), \tag{A.18}$$

which is the crossing relation discussed in section 4. This result, combined with

$$G_{\bar{c}/\bar{C}}(x) = G_{c/C}(x), \tag{A.19}$$

gives the correct crossing behavior for $AB \to CX$ to continue to $\bar{C}A \to \bar{B}X$. In the case where c and C consist of a boson and a fermion, there is an extra sign reversal in (A.18).

Appendix B. Relation betweem calculational techniques

An often perplexing feature of theoretical papers on large transverse momentum is the number of diverse, yet equivalent calculational techniques. Various authors use Bethe–Salpeter, Fock-space methods, or integral representations of scattering amplitudes to represent bound state amplitudes, and either Sudakov variables, light-cone variables, infinite momentum frame parametrizations, or standard Feynman variables to parametrize integrals. In this appendix we will discuss some of the interrelations among these techniques. Further details may be found in a paper by M. Schmidt [211] (see also Brodsky, Close and Gunion [61]).

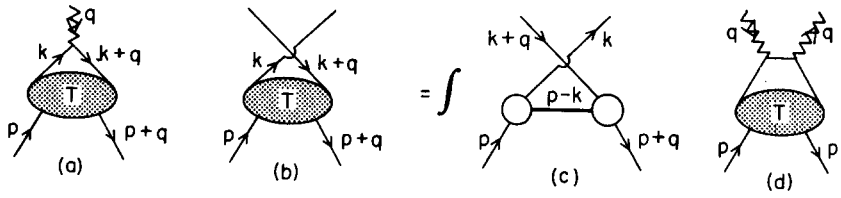

Fig. B.1. Decomposition of the form factor.

A convenient illustration of the various methods is the calculation of hadronic form factors, particularly the normalization integral since it provides a simple method to define the structure function and to relate it to a quark parton scattering amplitude.

The form factor (assuming only spinless particles are involved) corresponding to fig. B.1a is defined by

$$(2p+q)^{\mu}F(q^2) = \int \frac{\mathrm{d}^4k_{\mathrm{i}}}{(2\pi)^4} \frac{(2k+q)^{\mu}T(p,k+q\to p+q,k)}{(k^2-M^2+\mathrm{i}\epsilon)\,(k+q)^2-M^2+\mathrm{i}\epsilon}\,. \tag{B.1}$$

The relation to the off-shell scattering amplitude is indicated in fig. B.1b. Self energy insertions can also be included readily in this model.

Although the standard Feynman parametrization is useful for specific forms for T, in general it is more useful to try to reduce the k-integration. Among the many possible parametrization are

(a) Sudakov: $k = xp + yq + n, \quad n\cdot q = n\cdot p = 0\,.$ (B.2)

(b) Light-cone: $k^+ = k^0 + k^3 = x(p^0+p^3), \quad k^- = k^0 - k^3 = \dfrac{\boldsymbol{k}_{\mathrm{T}}^2 + k^2}{k^+}\,,$ (B.3)

where p is taken in the z-direction and $q^+ = 0$.

(c) Infinite momentum: one chooses

$$p = \left(P + \frac{M^2}{2P}\,, O_{\mathrm{T}}, P\right), \qquad k = \left(xP + \frac{k^2+\boldsymbol{k}_{\mathrm{T}}^2}{2xP}\,, \boldsymbol{k}_{\mathrm{T}}, xP\right), \tag{B.4}$$

where

$$P^2 \gg M^2, k^2, \boldsymbol{k}_{\mathrm{T}}^2\,.$$

Note that the light cone parametrization is exactly equivalent to the choice of frame

$$p = \left(P + \frac{M^2}{4P}\,, O_{\mathrm{T}}, P - \frac{M^2}{4P}\right), \qquad k = \left(xP + \frac{\boldsymbol{k}^2+\boldsymbol{k}_{\mathrm{T}}^2}{4xP}\,, \boldsymbol{k}_{\mathrm{T}}, xP - \frac{\boldsymbol{k}_{\mathrm{T}}^2}{4xP}\right), \tag{B.5}$$

where P may now be chosen arbitrarily. In fact $Y = \log(2P/M)$ is the rapidity of p relative to the rest frame $2P = M$. Also, $y = \log x$ is the rapidity of k relative to p. Note that y is often a useful variable, especially in multiperipheral calculations making the phase space integral $\int \mathrm{d}x/x = \int \mathrm{d}y$ uniform in rapidity. If $P\to\infty$, we have exactly the infinite momentum frame, where $x \Rightarrow k_z/p_z$ becomes the fractional longitudinal momentum.

In order to proceed further, it is convenient to assume that T can be written as a sum over its u-channel singularities (see fig. B.1c). Thus

$$T = \int \rho(\sigma^2)\, \frac{\phi_\sigma(k^2)\,\phi_\sigma[(k+q)^2]}{(p-k)^2 - \sigma^2}\, \mathrm{d}\sigma^2 \ . \tag{B.6}$$

This can be done in various ways; for example by assuming a dispersion relation, or choosing a suitable integral representation. We then have for any of the variable choices (b) $\leftrightarrow$ (d),

$$\int \mathrm{d}^4k = \int \mathrm{d}^4(p-k) = \int \mathrm{d}^2k_\mathrm{T} \int \frac{\mathrm{d}x}{2(1-x)} \int \mathrm{d}(p-k)^2 \ , \tag{B.7}$$

with

$$k^2 - m_\mathrm{q}^2 = xS(\boldsymbol{k}_\mathrm{T}, x) \ , \qquad (k+q)^2 - m_\mathrm{q}^2 = x\widetilde{S} = xS(\boldsymbol{k}_\mathrm{T} + (1-x)\boldsymbol{q}_\mathrm{T}, x) \ , \tag{B.8}$$

and we have defined

$$S(\boldsymbol{k}_\mathrm{T}, x) = M^2 - \frac{\boldsymbol{k}_\mathrm{T}^2 + m_\mathrm{q}^2}{x} - \frac{\boldsymbol{k}_\mathrm{T}^2 + \sigma^2}{1-x} \ . \tag{B.9}$$

If $x > 0$ or $x < 1$, then all of the singularities in $(p-k)^2$ are in the upper half plane and there is no contribution. For $0 < x < 1$, we can close the contour in the lower half plane and pick up the $(p-k)^2 - \sigma^2$ pole, and obtain (using the $p_0 + p_3$ component)

$$F(q^2) = \int \frac{\mathrm{d}^2k_\mathrm{T}}{(2\pi)^3} \int_0^1 \frac{\mathrm{d}x}{2(1-x)}\, x \int \mathrm{d}\sigma^2\, \frac{\phi_\sigma(x,S)}{xS}\, \frac{\phi_\sigma(x,\widetilde{S})}{x\widetilde{S}}\, \rho(\sigma^2) \ . \tag{B.10}$$

For a given single particle contribution to $\rho(\sigma^2)$, ϕ_σ can be identified with the Bethe–Salpeter wavefunction with one-leg on shell

$$\lim_{(p-k)^2 - \sigma^2 = 0} [(p-k)^2 - \sigma^2]\, \psi(k^2, (1-k)^2) = \phi_\sigma(k^2) \ . \tag{B.11}$$

Alternately, we can use Fock space wavefunctions in the $P \to \infty$ frame, and identify

$$\psi_{P\to\infty}(\boldsymbol{k}_\mathrm{T}, x) = \frac{\phi_\sigma(xS)}{S} \ . \tag{B.12}$$

Parallel results are also obtained using the Sudakov variables by using the $(p-k)^2$ pole to do the y integrations (Landshoff and Polkinghorne [173]).

Since $F(0) = 1$, we can define

$$F(x) = G_{\mathrm{a/p}}(x) = \int \frac{\mathrm{d}^2k_\mathrm{T}}{2(1-x)(2\pi)^3} \int \mathrm{d}\sigma^2\, \frac{\phi_\sigma^2(xS)}{(xS)^2}\, x \ , \tag{B.13}$$

as the normalized fractional momentum distribution. Note that x can be interpreted variously according to the parametrization (a) $\to$ (d) used above. It is easy to see that the "handbag" diagram, fig. B.1d, for forward virtual Compton scattering gives

$$\nu W_2(x) = \sum_\mathrm{a} \lambda_\mathrm{a}^2\, x f_\mathrm{a}(x)|_{x=\omega=1} \ , \tag{B.14}$$

where λ_a is the constituent charge.

Finally, we can also identify $\phi_\sigma^2(k^2)$ with the u-channel discontinuity of the virtual forward

scattering amplitude $T(k, p \to k, p)$. Thus we have

$$\nu W_2(x) = x \sum_a \lambda_a^2 \frac{1}{2x(1-x)} \int \frac{d^2k_T}{(2\pi)^3} \int d\sigma^2 \frac{\mathrm{Im}_u T(x, S, \sigma^2)}{S^2}, \tag{B.15}$$

which is the important relation obtained by Landshoff and Polkinghorne [172–174]. It is easy to see that if $\sigma_{\bar{a}p} \sim s^{\alpha-1}$, $\alpha > 0$, then $\mathrm{Im}\, T \sim (\sigma^2)^\alpha$ and $\nu W_2(x) \sim x^{1-\alpha}$ at $x \to 0$.

Appendix C. Calculations of wide-angle scattering amplitudes

One of the simplest techniques for calculating scattering amplitudes for composite systems is the "partition" method; i.e., the effective replacement of each hadron by constituents carrying finite fractions of the hadronic momentum. This is justified as follows: by definition the hadronic amplitude is given by the convolution of hadronic wave functions and n-particle amplitude integrated over relative momentum $k^\mu(i)$

$$M_{A+B\to C+D} = \int \psi^{\dagger C}_{BS} \psi^{\dagger D}_{BS} \mathcal{M}_n \psi^{A}_{BS} \psi^{B}_{BS} \prod_i d^4k_i . \tag{C.1}$$

Assuming finite hadronic binding; i.e., finite Bethe–Salpeter wavefunctions at relative $x^\mu = 0$, the leading contribution at large t and u can be obtained explicitly by iterating the kernel where ever large relative momentum are required. Thus all the wavefunctions are evaluated in their natural domain of near on-shell constituents, e.g. $p_a = x_a P_A + k_A$, with $0 < x_a < 1$, $k_a \cdot p = 0$, and k_A^2 small, and all of the hard momenta is exchanged within M_n.

Some representative contributions to M_n for meson–meson scattering are shown in fig. C.1. (Note that all of these contributions except (a) occur in positronium–positronium scattering.)

It is easy to check that each of the graphs (a)–(d) scale at fixed θ_{cm} as s^{-2} in any renormalizable theory. In these Born graphs, only the off-shell quark propagators need be counted to obtain the scaling behavior, as in ϕ^4 theory; otherwise the gluon propagator fall-off is compensated

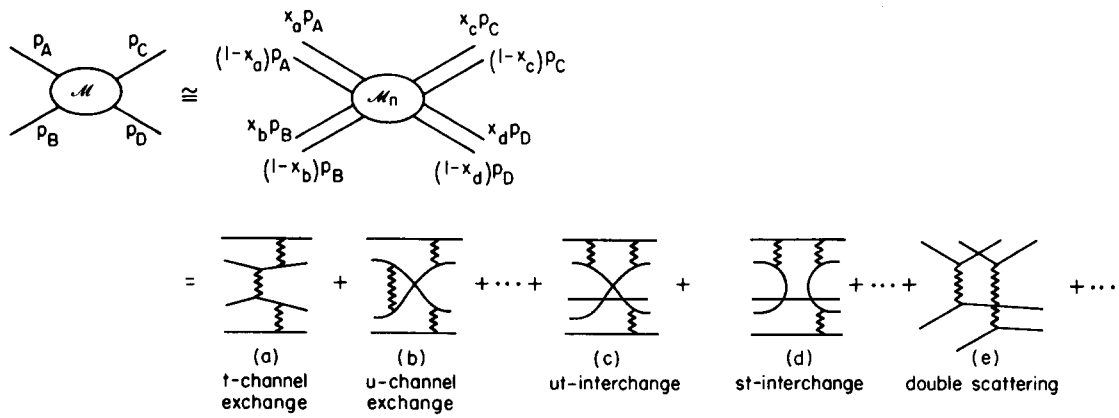

Fig. C.1. Diagrams which contribute to M_n.

by the vertex couplings -- from the convection current for spinless quarks or from the trace in the spin $\frac{1}{2}$ case. Additional, but finite, powers of $\log s$ factors appear from the $x \sim 1$ integrations, corresponding to degeneracy of routings of the large momentum transfer.

Diagram (a) is the prototype of the Wu–Yang gluon exchange model, which has been generalized by Abarbanel, Drell and Gilman [1], Fried, Gaisser and Kirby [126, 129, 130], and by Horn and Moshe [148]. Following the latter authors, we can generalize such contributions to the form

$$M_{A+B\to C+D} = F_{AC}(t)\, M_{\text{quark}}(s, t)\, F_{BD}(t) + \text{crossing contributions} . \tag{C.2}$$

If vector or axial-vector gluon exchanges are involved then this gives Regge behavior $M \sim s^{\alpha(t)}\beta(t)$ $(s \gg t)$ with $\alpha(t) \sim 1$ for all t. The phenomenological difficulties with this form are reviewed in section 5. Note that fig. C.1b gives a contribution $\sim t^{-2}$; i.e., $\alpha(t) = 0$, but is not usually taken into account in such models. We also emphasize that if gluon exchange is allowed in a composite model, then the Landshoff [170] contributions which we discuss below and in section 4.3 dominate the fixed angle amplitude so the above theories are the most consistent representation of the asymptotic amplitude. (Note, however, that in some elementary vector gluon field theory models, the Landshoff contributions cancel, see Halliday, Huskins and Sachrajda [140, 141].) Fig. C.1e contains the double-scattering (Landshoff) contribution. The matrix element scales as $is^{-3/2}$, and is dominated by the on mass shell region with $1 - x_a \sim x_b \sim 1 - x_c \sim x_d$. In general, higher order loop contributions to M_n introduce additional powers of $\log s$ in each order in perturbation theory. In accordance with Bjorken scaling, or from the various theoretical arguments advanced in section 4, it is assumed that these logarithms do not accumulate to change the overall power indicated by the lowest order contributions.

Diagrams (c) and (d) are the prototypes of the constituent interchange model, giving contributions to meson–meson scattering that survive even if gluon exchange between quarks of different hadrons are excluded. Independent of the gluon or constituent spin, one obtains the contributions

$$M_{(c)} \sim \frac{1}{u}\frac{1}{t}, \qquad M_{(d)} \sim \frac{1}{s}\frac{1}{t} \tag{C.3}$$

(modulo logarithms from the $x \sim 1$ integrations), and thus a Regge contribution at $\alpha = -1$. A natural generalization of this result for $M_{(c)}$ to meson–baryon and baryon–baryon scattering, as adopted in the original CIM paper is

$$M_{\text{CIM}}^{A+B\to C+D} = u F_A(u)\, F_C(u)\, F_D(t) . \tag{C.4}$$

This form can be justified if each composite system is effectively treated as a bound state of two particles; in particular, the proton must be regarded as a quark + core (or diquark) bound state. Using eq. (C.4) we have the interchange model prediction

$$M_{MB\to MB} \sim \alpha \frac{1}{u}\frac{1}{t^2} + \beta \frac{1}{s}\frac{1}{t^2}, \qquad \text{i.e. } \alpha(t) \Rightarrow -1 , \tag{C.5}$$

for the quark and antiquark contributions and

$$M_{BB\to BB} \sim \frac{1}{u^3}\frac{1}{t^2} ; \qquad \text{i.e., } \alpha(t) \Rightarrow -3 , \tag{C.6}$$

for the quark interchange contribution to baryon–baryon scattering in the core model. Inclusion of spin changes this result slightly. The proton core model is attractive in that (1) it can naturally

account for the anomalous behavior of $\nu W_2^p/\nu W_2^n$ at $x \to 1$, (2) the spectroscopy of baryon resonances seems to favor a diquark–quark model. The diquark state is predicted to be quasi-stable in color models (see e.g. Capps [70]). Further discussion of the use of the core model has been given by Gunion [134, 135]. Note that (C.6) predicts $d\sigma/dt\ (pp \to pp) \sim s^{-12}(1-\cos^2\theta_{cm})^{-n}$ with $n \sim 6$ which gives a good representation of the large angle data. The prediction

$$d\sigma/dt\ (K^+p \to K^+p) \sim s^{-8}(1-\cos\theta)^{-4}(1+\cos\theta)^{-1}\,, \tag{C.7}$$

from eq. (C.5) (including an extra factor of $(1+\cos\theta)^1$ from a helicity-conservation) due to u-quark interchange gives an excellent representation of the K^+p data. The core model can be simulated using a super-renormalizable field theory model for the proton couplings.

An even more convenient generalization of (C.4) for the interchange model which can be used for the case of a three quark baryon system for a ut graph is

$$M^{CIM}_{A+B\to C+D}(u,t) = M_{q+A\to q+A}(u,t)\, F_{BD}(t)\,, \tag{C.8}$$

where $F_{BD}(t)$ is assumed to be the most convergent form factor. The quark amplitude is evaluated at the appropriate kinematics. This form, which easily follows from the structure of fig. C.1, is discussed in detail in section 5.1 and is consistent with the dimensional counting rules for a three quark wave function. Logarithms from the $x \sim 1$ integration are automatically included.

The fact that different results for the CIM model can be obtained for different choices of the hadronic wavefunction was emphasized by Fishbane and Muzinich [121]. It is easy to check that this ambiguity only occurs for baryon–baryon scattering and is resolved once the basic quark-core or three quark structure is assumed.

Appendix D. Alternative theories based on parton interchange

During the past year, several other models of large angle scattering processes based on duality or "urbaryon" (i.e.: quark) rearrangement diagrams have been developed. The essential forms and assumptions used in these models are similar to those of the CIM, although there are important differences.

An interesting though heuristic formula for large angle two body exclusive processes $A+B \to C+D$ has been proposed by Kinoshita and his coworkers [161, 162]: for large t and u they propose

$$M \sim \frac{1}{s^{N_S}}\,\frac{1}{t^{N_T-1}}\,\frac{1}{u^{N_U-1}}\,; \qquad \frac{d\sigma}{dt} = \frac{1}{s^N}(1-z)^{2-2N_T}(1+z)^{2-n_U}\,, \tag{D.1}$$

where n_T is the total number of "bonds" connecting the hadrons in the t-channel (i.e., the total number of quark lines connecting A to C or B to D), etc. The overall power law agrees with dimensional counting rule $N = N_A + N_B + N_C + N_D - 2$. Although the angular dependence is derived heuristically, its form reflects the tendency of the valence quarks to persist in their direction of motion. In terms of Regge behavior, for $s \gg -t$, one has

$$\alpha_{eff}(t) = 1 - (n_S + n_U)\,\gamma(-t)\,, \tag{D.2}$$

where $\gamma(-t) \to 1$ for large negative t. Unlike eq. (C.5) $\alpha(-\infty)$ only depends on the number of exchanged quarks. Note, also that eq. (D.1) is *not* in general consistent with crossing symmetry. For

pp scattering, single quark interchange gives ($n_S = 0$, $n_T = 4$, $n_U = 2$)

$$s^{10}\frac{d\sigma}{dt} \sim (1-z)^{-6}(1+z)^{-2}, \qquad \alpha(t) \to -1, \tag{D.3}$$

and double quark interchange (as required by $t-u$ crossing)

$$s^{10}\frac{d\sigma}{dt} \sim (1-z)^{-2}(1+z)^{-6}, \qquad \alpha(t) \to -3, \tag{D.4}$$

compared with $\alpha(t) \to -2$ for the CIM using eq. (5.4.2). A novel feature of eq. (D.1) is that the "diffractive" term with zero quark exchange ($n_S = 0$, $n_T = 6$, $n_U = 0$) gives automatically an $\alpha_{eff}(t) = 1$ contribution. Kinoshita and Myozyo [161] use the sum of the above three contributions (interference and spin effects, and the u-channel diffractive term are ignored) to give a fairly good parametrization of the pp data. The small t dependence of $\gamma(t)$ can be chosen to give backward peaks (which vanish in the fixed-angle scattering limit) in K^-p and p^-p elastic reactions. A troubling feature of the suggested rule is that all $n_U = 0$ contributions vanish strongly in the backward direction in the scaling limit.

An alternative approach to the calculation of u baryon rearrangement diagrams is given by Igarashi, Nishitani, Matsuoa and Swada [150]. These authors propose the fixed angle scaling law

$$M = \frac{1}{s^{N_S-1}}\frac{1}{t^{N_T}}\frac{1}{u^{N_U}}, \qquad \frac{d\sigma}{dt} = \frac{C}{s^{N_{TOT}}}(1-z)^{-2n_T}(1+z)^{-2n_U}, \tag{D.5}$$

which differs from (D.1) by a factor of $p_T^{-4} = (tu/s)^{-2}$ in the cross section. Here N_{TOT} is the total number of fields in A, B, C, D; thus the predictions fall two powers of s faster than those based on dimensional counting, and due to mass corrections, present data must be assumed to be subasymptotic. The proposed effective trajectory $\alpha_{eff}(-t) \to -3$ power-law dependence s^{-12} for pp scattering, and phenomenological treatment of the diffractive amplitude are essentially the same as the CIM using the quark plus core model. The predictions differ for other channels, however. Again, we note the absence of crossing symmetry in the proposed rule.

Because of the freedom of mass terms, and the freedom of choice of the trajectories at lower t, a successful phenomenology of two body reactions can be based on the CIM predictions or either (D.1) or (D.5). The most decisive test will be an accurate experimental determination of the asymptotic power dependence of pp → pp. It should be emphasized that data for a large but fixed cm angular range can be used for this purpose.

Kinoshita et al. have also proposed a set of counting rules for inclusive large p_T reactions based upon u baryon rearrangement diagrams. As in the CIM, the results displaying a continuity of physics throughout the Peyrou plot, giving connections between large p_T phenomena and the triple and central Regge region of exclusive processes. However, the proposed counting rules do not recognize the importance of the subprocesses in determining the p_T^2 fall-off, and the predicted powers at fixed t/s, $\mathcal{M}^2/s$ seem unreasonable (e.g. p_T^{-2} for $\gamma B \to MX$, p_T^{-4} for $MB \to MX$, whereas p_T^{-8} for $BB \to BX$, $BB \to MX$).

References

[1] H. Abarbanel, S. Drell and F. Gilman, Phys. Rev. 177 (1969) 2458.

[2] G.W. Abshire et al., Phys. Rev. D9 (1974) 555.
[3] C.W. Akerlof et al., Phys. Rev. 159 (1967) 1138.
[4] C. Alabiso and G. Schierholz, Phys. Rev. D10 (1974) 960.
[5] J.V. Allaby et al., Phys. Letters 23 (1966) 384.
[6] J. Alonso and D. Wright, SLAC-PUB-1578 (1975).
[7] B. Alper et al., Phys. Letters 47B (1973) 75.
[8] B. Alper et al., Nuovo Cimento Letters 11 (1974) 173.
[9] B. Alper et al., CERN PRINT-74-1659 (1974).
[10] D. Amati, L. Caneschi and M. Testa, Phys. Letters 43B (1973) 186.
[11] E.W. Anderson et al., BNL-19236 (1974).
[11a] R. Anderson et al., Phys. Rev. Letters 30 (1973) 627.
[12] J.A. Appel et al., Phys. Rev. Letters 33 (1974) 719.
[13] J.A. Appel et al., Phys. Rev. Letters 33 (1974) 722.
[14] T. Appelquist, S. Coleman and H. Quinn, private communication (1974).
[15] T. Appelquist and E. Poggio, Phys. Rev. D10 (1974) 3280.
[16] T. Appelquist and J. Primack, Phys. Rev. D1 (1970) 1144.
[17] J.J. Aubert et al., Phys. Rev. Letters 33 (1974) 1404.
[18] J.E. Augustin et al., Phys. Rev. Letters 33 (1974) 1406.
[19] C. Baglin et al., Phys. Letters 47B (1973) 85.
[20] C. Baglin et al., Phys. Letters 47B (1973) 89.
[21] M. Baker and D. Coon, Phys. Rev. D4 (1971) 1234.
[22] M. Bander, R.M. Barnett and D. Silverman, Phys. Letters 48B (1974) 243.
[23] M. Banner et al., Phys. Letters 44B (1973) 537.
[24] W. Bardeen, M. Chanowitz, S. Drell, M. Weinstein and Y.-M. Yan, SLAC-PUB-1490 (1974).
[25] V. Barger, F. Halzen and J. Luthe, Phys. Letters 42B (1972) 428.
[26] R. Barnett and D. Silverman, Phys. Rev. D10 (1974) 1510.
[27] E.L. Berger and D. Branson, Phys. Letters 45B (1973) 57.
[28] S.M. Berman, J.D. Bjorken and J.B. Kogut, Phys. Rev. D4 (1971) 3388.
[29] S.M. Berman and M. Jacob, Phys. Rev. Letters 25 (1970) 1683.
[30] S.M. Berman, D.J. Levy and T.L. Neff, Phys. Rev. Letters 23 (1969) 1363.
[31] B. Betev et al., CERN PRINT-75-0019 (1974).
[32] J.D. Bjorken, Phys. Rev. D8 (1973) 4098.
[33] J.D. Bjorken, Proc. of the SLAC Institute on Particle Physics, Vol. I, ed. M. Zipf (1973).
[34] J.D. Bjorken, Talk presented at Aix-en-Provence Intern. Conf. on Elementary Physics (1973).
[35] J.D. Bjorken, Acta Physica Polonica B5 (1974) 893.
[36] J.D. Bjorken and J. Kogut, Phys. Rev. D8 (1973) 1371.
[37] J.D. Bjorken and E. Paschos, Phys. Rev. 185 (1969) 1975.
[38] R. Blankenbecler, Proc. of the Canadian Inst. of Particle Physics, McGill (1972).
[39] R. Blankenbecler, Talk presented at the IXth Balaton Symp. on Particle Physics (1974).
[40] R. Blankenbecler and S. Brodsky, Phys. Rev. D10 (1974) 2973.
[41] R. Blankenbecler, S.J. Brodsky and J.F. Gunion, Phys. Letters 39B (1972) 649.
[42] R. Blankenbecler, S.J. Brodsky and J.F. Gunion, Phys. Rev. D6 (1972) 2652.
[43] R. Blankenbecler, S.J. Brodsky and J.F. Gunion, Phys. Letters 42B (1973) 461.
[44] R. Blankenbecler, S.J. Brodsky and J.F. Gunion, SLAC-PUB-1585 (1975).
[45] R. Blankenbecler, S.J. Brodsky, R. Savit and J. Gunion, Phys. Rev. D8 (1973) 4117.
[46] R. Blankenbecler, S.J. Brodsky, R. Savit and J. Gunion, Phys. Rev. D10 (1974) 2153.
[47] R. Blankenbecler, J. Tran Thanh Van, J.F. Gunion and D. Coon, SLAC-PUB-1483 (1974).
[48] E.D. Bloom and F.J. Gilman, Phys. Rev. Letters 25 (1970) 1140.
[49] M. Bohm and M. Krammer, Phys. Letters 50B (1974) 457.
[50] G. Bonneau et al., CERN PRINT-74-0986 (1974).
[51] J.M. Borenstein, Harvard preprint (1975).
[52] M. Borghini et al., Phys. Letters 24B (1967) 77.
[53] M. Borghini et al., Phys. Letters 36B (1971) 500.
[54] A. Bouquet, J. Letessier and A. Tounsi, Phys. Letters 51B (1974) 235.
[55] A.M. Boyarski et al., to be published (1974).
[56] J.P. Boymond et al., Phys. Rev. Letters 33 (1974) 112.
[57] W.S. Brockett et al., Phys. Letters 51B (1974) 390.
[58] S. Brodsky, in: High Energy Collisions, ed. C. Quigg (American Institute of Physics, New York, 1973).

[59] S. Brodsky, SLAC Summer Institute of Particle Physics, Vol. II SLAC-179 (1974).
[60] S. Brodsky, Invited Talk, Int. Conf. on Few Body Problems in Nuclear and Particle Physics, Quebec, Canada (1974).
[61] S. Brodsky, F. Close and J. Gunion, Phys. Rev. D8 (1973) 3678.
[62] S. Brodsky and G. Farrar, Phys. Rev. Letters 31 (1973) 1153.
[63] S. Brodsky and G. Farrar, Phys. Rev. D11 (1975) 1309.
[64] S. Brodsky, J. Gunion and R. Jaffe, Phys. Rev. D6 (1972) 2487.
[65] T. Buran et al., CERN preprint (1974).
[66] F.W. Busser et al., Phys. Letters 46B (1973) 471.
[67] F.W. Busser et al., Phys. Letters 51B (1974) 306.
[68] R.F. Cahalan, K.A. Geer, J. Kogut and L. Susskind, Cornell University preprint CLNS-289 (1974).
[69] C.G. Callan and D.J. Gross, Princeton University preprint (1974).
[70] R. Capps, Purdue preprint (1974).
[71] D.C. Carey et al., Phys. Rev. Letters 32 (1974) 24.
[72] D.C. Carey et al., Phys. Rev. Letters 33 (1974) 327.
[73] A. Casher, J. Kogut and L. Susskind, Phys. Rev. D10 (1974) 732.
[74] P. Carruthers and M. Duong-Van, Phys. Rev. Letters 21 (1973) 133.
[75] F. Cerulus and A. Martin, Phys. Letters 8 (1964) 80.
[76] M.C. Chen, Ling-Lie Wang and T.F. Wong, Phys. Rev. D5 (1972) 1667.
[77] M.C. Chen and P. Zerwas, SLAC-PUB-1492 (1974).
[78] C. Chiu, Texas preprint (1972) (unpublished).
[79] A. Chodos et al., Phys. Rev. D9 (1974) 3471.
[8] A. Chodos et al., Phys. Rev. D10 (1974) 2559.
[81] J. Christenson et al., Phys. Rev. Letters 25 (1970) 1523.
[82] J. Christenson et al., Phys. Rev. D8 (1973) 2016.
[83] S.-Y. Chu and A.W. Hendry, Phys. Rev. D6 (1972) 190.
[84] S.-Y. Chu and A.W. Hendry, Phys. Rev. D7 (1973) 86.
[85] M. Ciafaloni and S. Ferrara, Scuola Normale Superiore, Pisa preprint 16 (1974).
[86] T.S. Clifford et al., Phys. Rev. Letters 33 (1974) 1239.
[87] A. Contogouris, J. Holden and E. Argyres, Phys. Letters B51 (1974) 25.
[88] D. Coon, University of Pittsburgh preprint PITT-125 (1974).
[89] J.M. Cornwall, D. Corrigan and R.E. Norton, Phys. Rev. D3 (1971) 536.
[90] R. Cottrell et al., Phys. Letters 55B (1975) 341.
[91] M. Creutz and L.-L. Wang, BNL-19078 (1974).
[92] J.W. Cronin, Proc. of the 1974 Summer Institute of Particle Physics, Vol. II, SLAC-179 (1974) p. 279.
[93] J.W. Cronin et al., Phys. Rev. Letters 31 (1973) 1426.
[94] J.W. Cronin et al., Chicago EFI preprints 74-1181 and 74-1182 (1974).
[95] P. Cvitanovic, Phys. Rev. D10 (1974) 338.
[96] P. Danysz et al., Nucl. Phys. B42 (1972) 29.
[97] P. Darriulat et al., CERN PRINT-75-0019 (1974).
[98] T. Del Prete, Invited Talk given at IXth Balaton Symp. on Particle Physics, Balatonfured, Hungary, 1974; CERN preprint.
[99] C. DeTar et al., Phys. Rev. D4 (1971) 425.
[100] A. Donnachie and P.R. Thomas, Daresbury preprint DL/P220 (1974), submitted to Nuovo Cimento.
[101] S.D. Drell and T.-M. Yan, Phys. Rev. Letters 24 (1970) 181.
[102] S.D. Drell and T.-M. Yan, Ann. Phys. (N.Y.) 66 (1971) 578.
[103] J.J. Dumont and L. Heiko, Brussels preprint IIHE-74-1 (1974).
[104] A. Eide et al., Nucl. Phys. B60 (1973) 173.
[105] G. Eilam et al., Phys. Rev. D8 (1973) 2871.
[106] A.M. Eisner et al., Phys. Rev. Letters 33 (1974) 865.
[107] S.D. Ellis, Phys. Letters 49B (1974) 189.
[108] S.D. Ellis, XVII Int. Conf. on High Energy Physics, London (1974).
[109] S.D. Ellis and P.G.O. Freund, NAL-THY 82 (1970) unpublished.
[110] S.D. Ellis and M.B. Kislinger, Phys. Rev. D9 (1974) 2027.
[111] S.D. Ellis and R. Thun, CERN preprint TH-1874 (1974).
[112] F. Elvekjaer et al., Nucl. Phys. B64 (1973) 301.
[113] T.E.O. Ericson, Ann. Phys. (N.Y.) 23 (1963) 390.
[114] Z.F. Ezawa, Nuovo Cimento 23A (1974) 271.
[115] Z.F. Ezawa and K. Nishijima, Prog. Theor. Phys. 48 (1972) 1751.
[116] Z.F. Ezawa and J.C. Polkinghorne, University of Cambridge preprint DAMTP 74/20 (1974).

[117] G. Farrar, Nucl. Phys. B77 (1974) 429.
[118] G. Farrar and C.C. Wu, CALT-68-455 (1974).
[118a] E. Fermi, Prog. Theor. Phys. (Kyoto) 5 (1950) 570.
[119] R.P. Feynman, Photon–Hadron Interactions (W.A. Benjamin, Inc., Reading, Mass., 1972).
[120] G. Finnocchiaro et al., Phys. Letters 50B (1974) 396.
[121] P. Fishbane and I. Muzinich, Phys. Rev. D8 (1973) 4015.
[122] S. Frautschi, Phys. Rev. D3 (1971) 2821.
[123] S. Frautschi, Nuovo Cimento 12A (1972) 133.
[124] H.M. Fried, Phys. Letters 51B (1974) 90.
[125] H. Fried and T.K. Gaisser, Phys. Rev. D7 (1973) 741.
[126] H. Fried, T.K. Gaisser and B. Kirby, Phys. Rev. Letters 25 (1970) 625.
[127] H. Fried, T.K. Gaisser and B. Kirby, Phys. Rev. D4 (1971) 2220.
[128] H. Fried, T.K. Gaisser and B. Kirby, Phys. Rev. D6 (1972) 2560.
[129] H. Fried, T.K. Gaisser and B. Kirby, Phys. Rev. D8 (1973) 2668.
[130] H. Fried, T.K. Gaisser and B. Kirby, Phys. Rev. D8 (1973) 3210.
[130a] Y. Frishman, XVI Int. Conf. on High Energy Physics, Batavia (1972).
[131] M. Goldberger and F. Low, Phys. Rev. 176 (1968) 1778.
[132] M. Gourdin, Phys. Reports 11C (1974) 29.
[133] V.N. Gribov and L.V. Lipatov, Sov. J. Nucl. Phys. 15 (1972) 438.
[134] J. Gunion, Phys. Rev. D10 (1974) 242.
[135] J. Gunion, Proc. APS Div. Particles and Fields (1974).
[136] J. Gunion, Proc. XVII Int. Conf. on High Energy Physics (1974).
[137] R. Hagedorn, Nuovo Cimento 56A (1968) 1027.
[138] R. Hagedorn and J. Ranft, Nuovo Cimento Suppl. 6 (1968) 109.
[139] J.G. Halliday and J. Huskins, ICTP/74/4 (1975).
[140] J.G. Halliday, J. Huskins and C.T. Sachrajda, Nucl. Phys. B83 (1974) 189.
[141] J.G. Halliday, J. Huskins and C.T. Sachrajda, Nucl. Phys. B87 (1974) 93.
[142] J. Harte, Phys. Rev. 184 (1969) 1948.
[143] J. Harte, Nucl. Phys. B50 (1972) 301.
[144] K. Hayasyi and H. Yabuki, Kyoto University preprint RIMS-175 (1974).
[145] L. Heiko, Louvain preprint (1974) unpublished.
[146] A. Hendry, Phys. Rev. D10 (1974) 2300.
[147] A.W. Hendry and G.W. Abshire (1974).
[148] D. Horn and M. Moshe, Nucl. Phys. B57 (1973) 139.
[149] R.C. Hwa and C.S. Lam, Phys. Rev. Letters 27 (1971) 1098.
[150] Y. Igarashi, T. Matsuoka and S. Sawada, Prog. Theor. Phys. 52 (1974) 618; Nagoya Univ. preprint DPNU-4 (1974); Y. Igarashi and T. Nishitani, Nagoya Univ. preprint DPNU-28 (1974).
[151] A. Jabs, Nuovo Cimento Letters 9 (1974) 570.
[152] R. Jackiw, Ann. Phys. 48 (1968) 292.
[153] R. Jackiw, Ann. Phys. 51 (1969) 575.
[154] M. Jacob, CERN preprint TH.1453 (1974).
[155] M. Jacob and R. Slansky, Phys. Rev. D5 (1972) 1847.
[156] R.L. Jaffe, MIT preprint CTP-448 (1974).
[157] P.L. Jain et al., Phys. Rev. Letters 32 (1974) 797.
[157a] G. Jarlskog, Proc. of the Tenth Rencontre de Moriond (1975).
[158] G. Kane, Proc. XVII Int. Conf. on High Energy Physics (1974).
[159] K. Kinoshita, Phys. Rev. Letters 12 (1964) 257.
[160] K. Kinoshita, Prog. Theor. Phys. 51 (1974) 1989.
[161] K. Kinoshita and Y. Myozyo, Prog. Theor. Phys. 52 (1974) 6.
[162] K. Kinoshita et al., Contributed Paper to XVII Int. Conf. on High Energy Physics (1974).
[163] J. Kiskis, SLAC-PUB-1477 (1974).
[164] B. Knapp et al., Phys. Rev. Letters (to be published, 1975).
[165] A. Krzywicki, Nuovo Cimento 32 (1964) 1067.
[166] A. Krzywicki, Proc. of the Sixth Rencontre de Moriond (1971).
[167] A. Krzywicki, Nucl. Phys. B32 (1971) 149.
[168] L.D. Landau, Izv. An. SSSR, Ser. Fiz. 17 (1953) 51.
[169] P.V. Landshoff, XVII Int. Conf. on High Energy Physics, London (1974).
[170] P.V. Landshoff, Phys. Rev. D10 (1974) 1024.

[171] P.V. Landshoff and J.C. Polkinghorne, Nucl. Phys. B52 (1971) 541.
[172] P.V. Landshoff and J.C. Polkinghorne, Nucl. Phys. B53 (1972) 473.
[173] P.V. Landshoff and J.C. Polkinghorne, Phys. Reports 5C (1972) 1.
[174] P.V. Landshoff and J.C. Polkinghorne, Phys. Letters 45B (1973) 361.
[175] P.V. Landshoff and J.C. Polkinghorne, Phys. Rev. D8 (1973) 927.
[176] P.V. Landshoff and J.C. Polkinghorne, Phys. Rev. D8 (1973) 4157.
[177] P.V. Landshoff and J.C. Polkinghorne, Phys. Rev. D10 (1974) 891.
[178] P.V. Landshoff, J.C. Polkinghorne and R. Short, Nucl. Phys. B28 (1971) 225.
[179] L. Lederman, preprint (1975).
[180] E.M. Levin and M.C. Ryskin, Leningrad preprint 12 (1973).
[181] E.M. Levin and M.C. Ryskin, Leningrad preprint 97 (1974).
[182] A. Lundby, in: High Energy Collisions, ed. C. Quigg (American Institute of Physics, New York, 1973).
[183] V.A. Matveev, R.M. Muradyan and A.N. Tavkhelidze, Lett. al Nuovo Cimento 7 (1973) 719.
[184] V.A. Matveev, R.M. Muradyan and A.N. Tavkhelidze, JINR Report E2-8048 (1974).
[185] Meng Ta-Chung, Phys. Rev. D9 (1974) 3062.
[186] P. Menotti, Phys. Rev. D9 (1974) 2767.
[187] P. Menotti, Phys. Rev. D11 (1975) 2828.
[188] P. Menotti, Scuola Normale Superiore, Pisa preprint S.N.S. 8 (1975); Phys. Letters 56B (1975) 169.
[189] H. Mueller-Kirsten and G. Hite, SLAC-PUB-1449 (1974).
[190] J.L. Newmeyer and D. Sivers, Phys. Rev. D10 (1974) 1475.
[191] K. Nishijima and M. Sato, Prog. Theor. Phys. 42 (1969) 692.
[192] J. Orear, Phys. Rev. Letters 12 (1964) 112.
[193] R. Pearson, private communication (1974).
[194] X.Y. Pham and D. Wright, SLAC-PUB-1516 (1974).
[195] S. Pokorski and L. van Hove, CERN preprint TH-1565 (1974).
[196] S. Pokorski and L. van Hove, CERN preprint TH-1930 (1974).
[197] J.C. Polkinghorne, Proc. of the Canadian Inst. of Paryicle Physics, McGill (1972).
[198] J.C. Polkinghorne, DAMTP 74/3 (1974).
[198a] A.M. Polyakov, Raporteur's talk, Lepton–Photon Symposium, SLAC (1975).
[199] G. Preparata, Nucl. Phys. B80 (1974) 299.
[200] G. Preparata, CERN preprint TH.1859 (1974).
[201] R. Raitio and G. Ringland, to be published as a SLAC preprint (1975).
[202] A. Ramanauskas et al., Phys. Rev. Letters 31 (1973) 1371.
[203] G. Ranft, CERN preprint (1974).
[204] M.W. Roth, University of Illinois preprint ILL-TH-74-10 (1974).
[205] E. Rutherford, Philosophical Magazine 21 (1911) 669.
[206] C. Sachrajda and R. Blankenbecler, SLAC-PUB-1594 (1975).
[207] S. Sakai, Prog. Theor. Phys. 50 (1973) 1644.
[208] R.S. Savit, Ph.D. Thesis, SLAC-168 (1973).
[209] L. Schiff, Ann. Phys. (N.Y.) 63 (1970) 248.
[209a] C. Schmid, in: Phenomenology in Particle Physics 1971, eds. C.B. Chiu, G.C. Fox and A.J.G. Hey (Cal. Tech., Pasadena, Calif., 1971).
[210] F. Schmidt et al., Phys. Letters 45B (1973) 157.
[211] M. Schmidt, Phys. Rev. D9 (1974) 408.
[212] B. Schrempp and F. Schrempp, Nucl. Phys. B60 (1973) 110.
[213] B. Schrempp and F. Schrempp, Phys. Letters 55B (1975) 303.
[214] D.M. Scott, Nuovo Cimento 18A (1973) 271; Phys. Letters 53B (1974) 185.
[215] S.S. Shei, Rockefeller University preprint (1974).
[216] D. Sivers, Ann. Phys. (N.Y.) to be published (1975).
[217] D. Sivers, Phys. Rev. to be published (1975).
[218] J. Stack, Phys. Rev. 164 (1967) 1904.
[219] V.P. Sudakov, JETP 3 (1956) 65.
[220] M. Teper, Phys. Letters 50B (1974) 261.
[221] M. Teper, Westfield College preprint (1974).
[222] W. Theis, Phys. Letters 42B (1972) 246.
[223] G. Tiktopolos, UCLA preprint (1974).
[224] T. Uematsu, Kyoto University preprint (1974).
[224a] M.A. Virasoro, Phys. Rev. D3 (1971) 2834.

[225] J.K. Walker, in: High Energy Collisions, ed. C. Quigg (American Institute of Physics, New York, 1973).
[226] G. West, Phys. Rev. Letters 24 (1970) 1206.
[227] T.T. Wu and C.N. Yang, Phys. Rev. 137 (1965) B708.
[228] D. Yennie, S. Frautschi and H. Suura, Ann. Phys. 13 (1961) 379.
[229] H. Yuta et al., ANL preprint (1974).